Norbert Galler

Investigation of optical pH sensors below 10 mM ionic strength

MASTER'S THESIS

for the acquisition of the academic degree "Diplom-Ingenieur"
in the field of studies "Individual Master program biotechnology:
biochemical analysis and sensor techniques"
at the

University of Technology, Graz

Supervisor:
Univ.-Ass. Dipl.-Chem. Dr. rer. nat. Torsten Mayr

2013

“I know that I know nothing.”

(Sokrates)

Danksagung

An dieser Stelle möchte ich mich als erstes bei meinen Betreuer Torsten Mayr sowie bei Ingo Klimant bedanken, die mir die Möglichkeit gegeben haben, meine beiden Abschlussarbeiten, die des Masterstudiums als auch die des Lehramtsstudiums, in ihrer Arbeitsgruppe zu verfassen, und die stets viel Verständnis für meine „besondere“ Situation zeigten.

Ein großer Dank gebührt der gesamten Arbeitsgruppe für das positive Klima, das hier vorherrscht. Ein besonderer Dank ergeht an Jan, der viel seiner Zeit mit mir in meinen Messaufbau investierte. – Die anderen erwähne ich jetzt nicht alle persönlich, aber bei jedem könnte ich mich für andere Dinge extra bedanken, hierfür ein kollektives „Danke“ an dieser Stelle!

Abseits der Arbeitsgruppe muss ich mich auch bei meinem Studienkollegen Thomas Eixelsberger bedanken, der immer für fachlichen Diskurs und Beistand zu haben ist und war. Persönlicher Dank gebührt auch meinem langjährigen Mitbewohner Josef Ehgartner und meinem ältesten Freund Ulrich Bohrn.

Bei meinen Eltern bedanke ich mich für die langjährige, vor allem auch finanzielle Unterstützung während meiner gesamten Lebens- und Ausbildungszeit.

Besonders im Fokus stand während der Zeit meiner Masterarbeit aber mein Sohn Jonathan, dem ich vor allem zwei Dinge zu verdanken habe: einerseits, um 8 Uhr 30 schon drei Tassen Kaffee intus zu haben, andererseits aber auch Glücksgefühle, die vielen in meinem Alter leider fremd sind. Die Basis, dass es schlussendlich überhaupt möglich war, mit Kind meine Arbeit hier zu verrichten, war aber die Mutter dazu, Selena, der wohl an dieser Stelle der meiste Dank gebührt.

Abstract

Measuring pH at very low ionic strengths (IS) is a great challenge but also a very important analytical area. The glass electrode as the usually used device reaches its limits when it comes to pH measurements in distilled or highly pure water for example. But optical pH sensors as another important approach for measuring pH have even bigger problems there. They do not measure activities but concentrations (1). If a solution for this limitation of optical indicators could be found, the optical approach is able to compete with the potentiometric approach as it presents several potential advantages over the glass electrode: easier to miniaturize, no electromagnetic interferences, less brittle, cheaper, better sensitivity (2).

In this thesis, the pH behavior of a pH sensitive dye showing no charge in its acidic form is investigated under very low ionic strength conditions (0.5 – 10 mM). The dye is embedded in the hydrogels D1, D4 and D7 in the concentrations 1, 2 and 4 mmol/kg. For this investigation, it was crucial not to dissolve CO_2 into the measurement solutions during the measurements to maintain the fixed pH values. Thus, a flow through system for the automated measurement of the absorption of sensor foils without air contact at constant temperatures was newly developed and installed. Finally, it was tried to work with even lower concentrations (0.1 mmol/kg) in the hydrogels D1 and polyacryloylmorpholine and measure fluorescence intensity.

D1 did not just show the best results of the D series but it could also be shown that the pH deviation due to IS decreased at a concentration as low as 0.1 mmol/kg. For the hydrogel polyacryloylmorpholine, the necessary polymerization emerged to be the crucial step. No pH sensor could have been prepared reproducibly yet. It was not even possible to achieve proper signals for the 0.1 mmol/kg concentration with the instruments used.

Kurzfassung

Die Messung des pH-Wertes bei sehr geringen Ionenstärken (IS) ist eine große Herausforderung, aber auch ein sehr wichtiges analytisches Feld. Die üblicherweise verwendete Glaselektrode erreicht ihre Grenzen, wenn es ans Messen etwa von destilliertem Wasser oder Reinstwasser geht. Aber optische Sensoren als ein weiterer wichtiger Ansatz zur pH-Messung haben dort noch größere Probleme. Sie messen Konzentrationen und keine Aktivitäten. Sollte eine Lösung für diese Limitierung der optischen Sensoren gefunden werden, kann der optische Weg zum elektrochemischen in Konkurrenz treten, nachdem er viele mögliche Vorteile gegenüber der Glaselektrode bietet: leichtere Miniaturisierung, keine elektromagnetischen Interferenzen, weniger zerbrechlich, billiger, bessere Sensitivität.

In dieser Arbeit wird das Verhalten eines pH-sensitiven Farbstoffs, der in seiner sauren Form keine Ladung aufweist, bei sehr niedrigen IS (0.5 – 10 mM) untersucht. Der Farbstoff wurde dafür in die Hydrogele D1, D4 und D7 in Konzentrationen von jeweils 1, 2 und 4 mmol/kg eingebracht. Es war von entscheidender Bedeutung für diese Untersuchung, dass sich während der Messungen kein CO_2 in die Messlösungen lösen kann, um die eingestellten pH-Werte nicht zu verändern. Dafür wurde ein neues Durchflusssystem entwickelt und aufgebaut, mit dem automatisiert Absorptionsmessungen von Sensorfolien unter Luftausschluss und bei konstanter Temperatur möglich gemacht wurden.

Schlussendlich wurde auch versucht, in den Hydrogelen D1 und Polyacryloylmorpholin mit einer noch geringeren Farbstoffkonzentration (0.1 mmol/kg) zu arbeiten und die Fluoreszenzintensität zu messen.

D1 zeigte nicht nur die besten Resultate innerhalb der D-Serie. Es konnte auch gezeigt werden, dass die IS-abhängigen pH-Abweichungen bei einer so geringen Konzentration wie 0.1 mmol/kg abnahmen. Bei Polyacryloylmorpholine war zunächst eine Polymerisierung notwendig, die sich als entscheidender Schritt herausstellte. Es konnte kein pH-Sensor reproduzierbar hergestellt werden. Abgesehen davon war es nicht möglich, mit den verwendeten Geräten für eine Konzentration von 0.1 mmol/kg ein verwertbares Signal zu bekommen.

EIDESSTATTLICHE ERKLÄRUNG

Ich erkläre an Eides statt, dass ich die vorliegende Arbeit selbstständig verfasst, andere als die angegebenen Quellen/Hilfsmittel nicht benutzt, und die den benutzten Quellen wörtlich und inhaltlich entnommenen Stellen als solche kenntlich gemacht habe.

Graz, am ....

STATUTORY DECLARATION

I declare that I have authored this thesis independently, that I have not used other than the declared sources / resources, and that I have explicitly marked all material which has been quoted either literally or by content from the used sources.

....
date

Table of contents

Introduction

The pH value is one of the most important measuring parameters in many fields of life. It is essential for almost all scientific research, in medicine, industry, biotechnology, wastewater treatment, but also in the private ranges, e.g. for aquaria (3) and cacti cultivation (4). The pH glass electrode is by far the widest spread instrument for pH determination.

Yet, there are also problems with glass electrodes limiting their range of applications. They can hardly be used close to strong electromagnetic fields, in aggressive media (such as the presence of fluoride) or at very high pH values (alkaline error). Further, potentiometric measurements always need a referencing element, which complicates miniaturization. Besides, they can hardly be used in food or in vivo applications due to their brittle nature. All these troubles can potentially be avoided by using optical indicator dyes. (2), (5), (6), (7), (8)

Problems with glass electrodes also arise when measuring waters of very low ionic strengths, such as pure or distilled water, ground water etc. These problems are mainly due to the liquid junction potential of the electrode and can hardly be avoided. The sensor response can soon get extremely slow, drifting, inaccurate, imprecise and irreproducible. Many deal with this problem but solutions presented are complicated, expensive and change the composition of the solution as mostly further salts are added. (9), (10), (11), (12), (13)

On the first look, optical sensors cannot be the perfect answer to the problem. The pH value is defined by means of electrochemistry and via the H^+ activity. In contrast to the glass electrode, indicator dyes can just measure concentrations. When ionic strength (IS) decreases strongly, this fact becomes extremely important and deviations from the real pH value get enormous. Yet, there are approaches how to minimize and compensate for this problem although the focus of these lie in the physiological IS range or higher. (7), (14), (15) Only Weidgans measured down to 2 mM (though he just describes buffer preparation down to 25 mM) but could not achieve minimal IS effects in this low IS range.

By using dissolved dyes and extrapolating calculations, accurate measurements in very low IS waters can already be performed (13). The research aim is to minimize IS dependency of optical pH sensors. Then they can compete with potentiometric methods for low IS applications too as they do not exhibit the other problems mentioned above. Of course, pH

indicator dyes also have other drawbacks such as a limited dynamic range of just 2-3 pH units. On the one hand, a higher dynamic range is not necessary for many applications and on the other hand, there are possibilities to broaden the calibration curves even for low IS applications (16), (17). Sensitivity of glass electrodes will always be around 59 mV/pH unit whereas the sensitivity of optical sensors can be adjusted, e.g. by the layer thickness (18) and is potentially better (16).

1 Theoretical background

The main references of each subchapter will be given in the title of the subchapter. Additional references will be quoted separately.

1.1 Sensors (19)

Originally, sensors can be imagined as artificial sensory organs. Basic principles indeed go along with nature. Thus, sensors can generally be divided into two groups: the one group referring to seeing, listening and touching can be called *physical sensors* as they react to physical stimuli, the other group referring to smelling and tasting can be called *chemical sensors* (CS) as they react to chemical stimuli. Yet of course, definition by comparison to physiological processes is to narrow.

There are some basic definitions for CS, which are of actual interest here, given by IUPAC:

> *A chemical sensor is a device that transforms chemical information, ranging from the concentration of a specific sample component to total composition analysis, into an analytically useful signal. The chemical information, mentioned above, may originate from a chemical reaction of the analyte or from a physical property of the system investigated.*(20)

and Wolfbeis et al.: Chemical sensors are miniaturized analytical devices consisting of a receptor element, a transducer and signal processing element to give information about the chemical concentration continuously and reversibly. (5),(21)

Thus, special characteristics and requirements have been formulated for CS:

- transduction of chemical information into electrical signals
- fast response time
- long-time stability
    - no drifts
    - long operating life
- small/miniaturizable
- specific/selective
- sensitive
- no hysteresis

- wide dynamic range
- possibility for linear calibration
- robust
- cheap

Basically, CS contain two main components: a chemical receptor element and a physicochemical transduction element. Usually, an electrical signal is received from the transducer, sometimes they are just combined in one element. This signal has to be further processed, amplified etc.; yet, this is no intrinsic characteristic of the CS any more.

If the receptor element is a biological system (enzyme, antibody, whole cell) the sensor is called a biosensor.

1.1.1 Classification

Mostly, classification of CS works via their principle of signal transduction. The two groups mentioned first are the most important ones, also for the understanding of this thesis:

- *optical sensors* using the principles of light absorption, reflexion, luminescence, refraction index, optothermic effects, light scattering etc.
- *electrochemical sensors* using principles of voltammetry, potentiometry, field effect transistors etc.
- *electric sensors* using oxidic or organic semicomductors, electrolytic conductivity sensors
- *mass selective sensors*, setups using piezoelectronics (quarz crystal microbalances (22)) or acoustic surface waves
- *thermometric (colorimetric) sensors* measuring absorption of heat or its production in a chemical reaction
- *others:* sensors mainly using absorption and emission of different kinds of radiation

1.2 Main principles of molecular spectroscopy

Many optical sensors are based on measuring absorption and photoluminescence. Both principles will be used in the experiments of this thesis. So, the following subchapters will go into some more detail describing them.

1.2.1 Absorption and photoluminescence (23), (24)

Electronic transition is the promotion of an electron from an orbital of a molecule in the ground state to an unoccupied orbital. Several ways to excite an electron are possible; the one usually considered for optical sensors is the absorption of a photon. After this absorption the molecule, thus one of its electrons, is in an excited state. The energy which would be necessary for the excitation of an electron in a σ-orbital is far too energetic to be relevant here. The transitions which are important in terms of chromophores used for optical sensors are $\pi \rightarrow \pi^*$ transitions, thus transitions from a π orbital to an antibinding π* orbital. Even the energy needed for an isolated double bound to be excited is 7 eV, which is related to 180 nm. The energy needed gets less in a conjugated π-system and furtherly less the larger this system gets. Absorption in the near UV and the visible spectrum are desired for the use in optical sensors. A conjugated π-electron system can be considered independent of the σ-bonds. A transition of the $n \rightarrow \pi^*$ is basically the one needing the least energy; n is a not-binding, a lone electron pair.

In absorption and fluorescence spectroscopy, there are two important types of orbitals considered: the highest occupied molecular orbital (HOMO) and the lowest unoccupied molecular orbital (LUMO). Both refer to the ground state of the molecule. When one of the two electrons of opposite spins (belonging to a molecular orbital of a molecule in the ground state) is promoted to a molecular orbital of higher energy, its spin is principally unchanged so that the total spin quantum number remains zero. As the multiplicities of the ground state and the excited state are both equal to 1 (M = 2S+1), they are both called *singlet state*. There is the possibility for an electron to change its spin upon transition to another state where its spin is changed. The total resulting spin quantum number is 1, the resulting multiplicity is 3 then. Such a state is called *triplet state* then having a lower energy than the singlet state of the same configuration. Each of these states consists of many vibrational and rotational sublevels.

In the Jablonski diagram (fig. 1) you can find the main principles which are important for optical sensors in an easy to understand (just a scheme!) illustration containing absorption and photoluminescence. Upon absorption of a photon, an electron is excited from the S_0 state to a vibrational level of an excited singlet state, preferably S_1. At room temperature, most of the electrons are in the lowest vibrational level of S_0 according to the Boltzmann

law. Many relaxation events can occur after excitation. In almost any case, the first effect will be vibrational relaxation (VR), a non-radiant relaxation from a higher vibrational level of a distinct state to the vibrational ground state of the distinct state basically producing heat. From the vibrational ground state, a transition is possible to a vibrational level of another state having the same energy. This is called *internal conversion* (IC) if the two states have the same multiplicity, it is called *intersystem crossing* (ISC) if the electron changes its spin and thus multiplicity changes from singlet to triplet. Transitions between electronic states of different multiplicity are spin forbidden but can still occur observably. After these transitions, VR occurs again to reach the vibrational ground level of the electronic state. Here, the electron stays more or less long before further relaxation to the ground state S_0 occurs (as long as it has not already reached it by IC and VR). Finally, photoluminescence events can occur – either from S_1 to S_0 called *fluorescence* or from T_1 to T_0 again spin forbidden) called *phosphorescence*. *Delayed fluorescence* can occur to a very little content when ISC from a triplet back to a singlet state takes place.

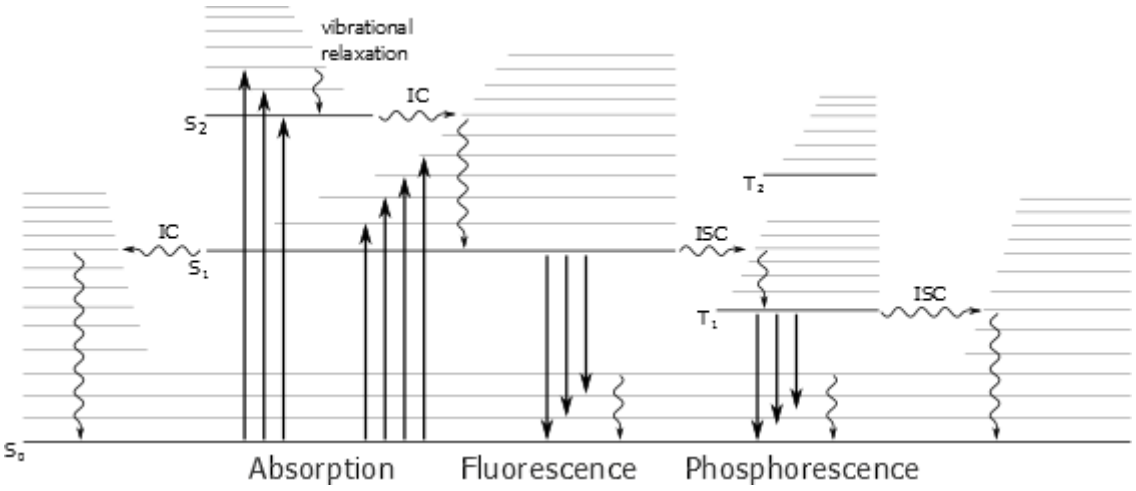

Figure 1: Jablonski diagram and possible transitions. The straight arrows give the absorption (up) or the emission (down) of a photon leading to excitation (up) or relaxation (down) of an electron. The waved arrows represent other possibilities of (radiation-free) relaxation. For these arrows going down having no label the relaxation is heat producing. S_0…singlet ground state, $S_{1,2}$…excited states (singlet), $T_{1,2}$...excited states (triplet), IC…internal conversion, ISC…inter system crossing.

The life times or durations of the states or events are quite different. Photon absorption and emission upon electron relaxation are by far faster than all the other processes with about 10^{-15} s. The lifetime of T_1 can be quite long, on the other hand, usually between 10^{-6} to 1 s, as this radiant relaxation is spin-forbidden. Table 1 gives a list of the time ranges.

event	characteristic time / s
absorption	10^{-15}
vibrational relaxation	10^{-12} - 10^{-10}
lifetime of the excited state S_1	10^{-10} - 10^{-7}
intersystem crossing	10^{-10} - 10^{-8}
internal conversion	10^{-11} - 10^{-9}
lifetime of the excited state T_1	10^{-6} - 1

Table 1: duration of photophysical processes

Spin-forbidden events can be observed when spin-orbit coupling (coupling between the orbital magnetic moment and the spin magnetic moment) is large enough. This depends on the molecule orbitals involved. If the transition is of the n → π^* type, ISC is often efficient. The presence of heavy atoms (i.e. whose atomic number is large, Br, Pb, e.g.) increases spin-orbit coupling and thus favors ISC.

Electronic transition appears vertical according to the *Franck-Condon-principle* (see fig. 2) basing on the Born-Oppenheimer approximation that during photon absorption the position of the nuclei does not change. They move slower due to their much higher weight.

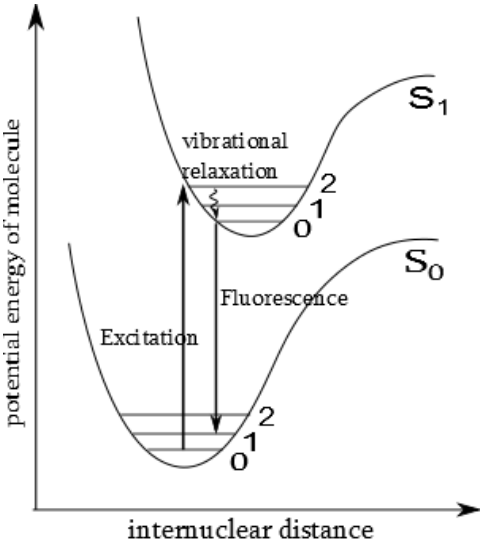

Figure 2: mechanism of absorption and fluorescence according to the Franck-Condon principle.

The absorption spectrum consists of the transition 0-1, 0-2 etc. whereas the fluorescence spectrum consists of the contrary transitions where the numbers are the vibrational levels within the electronic states of the electron (see fig. 2). Thus a fluorescence spectrum is approximately a mirror image of the absorption spectrum as the vibrational levels of both electric states resemble each other. Fluorescence is just shifted to lower energy due to VR in the excited electronic state. The absorption spectrum gives information about the excited state, fluorescence spectrum gives information about the ground state. Spectra overlap slightly. This means that a part of fluorescence is more energetic than absorption, which seems to be illogic at the first sight. But the Boltzmann law says that there is a small fraction of electrons not being excited from the vibrational level 0 but from higher levels; further, there is a small fraction of electrons relaxing directly from S_1 to the lowest vibrational level of S_0, which explains the slight overlap. 0-0 transitions should

actually appear at the same wavelength. It often does not in reality, which is due to the fact that the excited state possibly interacts with the solvent differently than the ground state.

That spectra do not consist of sharp peaks but appear more or less blurred is due to mainly two effects: homogenous and inhomogeneous band broadening. The first effect can be referred to the existence of a continuous set of vibrational sublevels in each electronic state. The other one can be attributed to the solvent and the fluctuating structure of the solvation shell of the chromophor. The distribution of solute-solvent configurations and the consequent variation in the local electric field leads to a statistical distribution of the energies of the electronic transitions. In most cases, the extent of inhomogeneous broadening is much greater than that of homogenous broadening.

The efficiency of light absorption at a wavelength λ is characterized by the a*bsorbance* A(λ) and the *transmittance* T(λ), defined as

$$A(\lambda) = \log\frac{I_0}{I} = -\log T(\lambda) \qquad \text{(Equ. 1)}$$

$$T(\lambda) = \frac{I}{I_0} \qquad \text{(Equ. 2)}$$

where I_0 is the intensity of the incident light and I the intensity of the exiting light, respectively. In many cases, the absorbance of a sample follows the *Lambert-Beer law*

$$A(\lambda) = \log\frac{I_0}{I} = \varepsilon \cdot c \cdot d \qquad \text{(Equ. 3)}$$

where ε is the molar decadic absorption coefficient (commonly expressed in L/(mol·cm), c is the concentration (in mol/L) of the absorbing species and d is the absorption path length (thickness of the absorbing medium) (in cm). Deviation from the linear dependence of the absorbance on concentration may be due to aggregate formation at high concentrations or to the presence of other absorbing species. ε is always related to the wavelength corresponding to the maximum of the absorption band of lower energy.

Various terms for characterizing light absorption can be found in literature. IUPAC recommends not to use the term optical density synonymously with absorbance. Also, the term molar absorption coefficient should be used instead of molar extinction coefficient.

Fluorescence intensity is time dependent. The concentration of excited molecules after a certain time $[^1A^*](t)$ is given by

$$[^1A^*](t) = [^1A^*]_0 \cdot \exp(-\frac{t}{\tau_S}) \qquad \text{(Equ. 4)}$$

when $[^1A^*]_0$ is the concentration of the excited molecules at time 0. The fluorescence intensity is defined as the amount of photons (in mol) emitted per unit time (s) and per unit volume of solution (L) according to

$$A^* \xrightarrow{k_r^S} A + \text{photon} \qquad \text{(Equ. 5)}$$

where k_r^S is the rate constant of the radiative transitions from S_1 to S_0. The fluorescence intensity i_F at time t after excitation by a very short pulse of light at time 0 is proportional, at any time, to the instantaneous concentration of molecules still excited $[^1A^*]$; the proportionality factor is k_r^S:

$$i_F(t) = k_r^S \cdot [^1A^*](t) = k_r^S \cdot [^1A^*]_0 \cdot \exp(-\frac{t}{\tau_S}) \qquad \text{(Equ. 6)}$$

τ_S is the lifetime of the excited state S_1 given by

$$\tau_S = \frac{1}{k_r^S + k_{nr}^S} \qquad \text{(Equ. 7)}$$

where k_{nr}^S is the rate constant for all the non radiative deactivations.

The *quantum yield* Φ_F is the fraction of the absorbed photons resulting in fluorescence. High quantum yields are desired for optical sensors. On the one hand, the dye amount needed can be reduced. On the other hand, sensitivity can be increased.

$$\emptyset_F = \frac{k_r^S}{k_r^S + k_{nr}^S} = k_r^S \cdot \tau_S$$

'Measured' luminescence intensity can be described with

$$I_F = 2.303 \cdot \Phi_F \cdot I_0 \cdot \varepsilon \cdot d \cdot c \qquad \text{(Equ. 8)}$$

to see that it is dependent from the concentration, the path length of the light, the molar absorption coefficient, the intensity of the incident light and the quantum yield. (19) The numerical value is obtained on an arbitrary scale depending on the experimental conditions and will be proportional to i_F.

I_F is proportional to the concentration only in very dilute solutions. Otherwise inner filter effects reduce it as photos from the overlap of emission and excitation spectra can be reabsorbed. Fluorimetry is up to 1000 times more sensitive than spectrophotometry. This is because I_F is measured above a low background level whereas in the measurements of low absorbances, two large signals that are slightly different are compared.

The *Stokes shift* is the gap between the maximum of the absorption band of lowest energy and the closest maximum of the fluorescence spectrum. Light detection is easier when the Stokes shift is higher. The Stokes shift for phosphorescence is higher than for fluorescence.

Lifetimes, quantum yields and Stokes shift are characteristics of major importance for luminescent dyes.

However, there are also Anti-Stokes processes. Basically, it has to be distinguished between upconversion where two or more photons are absorbed sequentially (25) and two-photon excitation where more than one photon is absorbed at the same time (26). Both of them lead to emission of photons of lower energy than the excitation photons.

1.2.2 Quenching (23), (24)

Fig. 3 shows that there are many possibilities for a molecule to deal with absorbed energy. Photoluminescence is just a fraction of it. As it causes the signal in optical sensors, it should be as high as possible for sensor applications. Other effects which are involved in de-excitation events especially those involving another substance than the luminophore (another luminophore, inorganic atoms/ions, gasses like dioxygen, solvent etc.) are called *quenching* effects as they *quench* luminescence. Such effects can be intramolecular charge transfer where it does not even need another substance but just another part in the molecule, electron transfer, proton transfer, energy transfer or the formation of excimers or exciplexes.

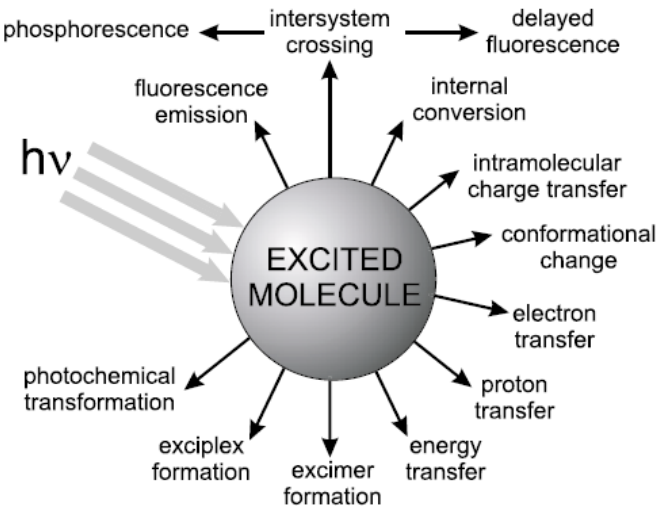

Figure 3: possibilities for a molecule how to deal with the energy of arriving photons.

Yet, these quenching events are not just bad but can intentionally be used for many sensor applications.

As a first approach to *dynamic quenching* as it appears with oxygen for example, Stern-Volmer kinetics sees the quenching constant k_q time independent. The *Stern-Volmer relation* combines quantum yields, intensities, lifetimes with and without quencher further giving a new constant, the Stern-Volmer constant K_{SV}:

$$\frac{\emptyset_0}{\emptyset} = \frac{\tau_0}{\tau} = \frac{I_0}{I} = 1 + k_q\,\tau_0[Q] = 1 + \mathrm{K}_{SV}[Q] \qquad \text{(Equ. 9)}$$

where I_0 and I are the steady-state fluorescence intensities in the absence and in the presence of quencher, respectively. The subscript 0 always means 'in the absence of quencher'. Usually, the ratio I_0/I is plotted against the quencher concentration (Stern-Volmer plot). If the plot is linear, the slope gives the Stern-Volmer constant. Then, $\mathrm{k_q}$ can be calculated if the excited-state lifetime in the absence of quencher is known.

The main difference to *static quenching* where a non-radiating complex is formed between fluorophore and quencher is that lifetime is not affected so that the relationship can be described as

$$\frac{\emptyset_0}{\emptyset} = \frac{I_0}{I} = 1 + \mathrm{K}_S[Q] \qquad \text{(Equ. 10)}$$

with the complex building constant $\mathrm{K_s}$ resembling $\mathrm{K_{SV}}$. Also other forms of quenching are known where e.g. linearity is just given via logarithm or mixtures of dynamic and static quenching.

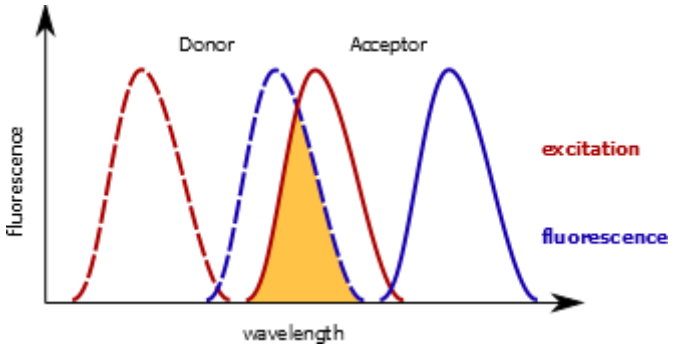

Figure 4: Resonance energy transfer

The *Förster resonance energy transfer (FRET)* is a special case of quenching (fig. 4). Energy is passed on non-radiatively from a donor to an acceptor as the emission spectrum from the donor overlaps with the absorption spectrum of the acceptor. The acceptor itself could show fluorescence then. This can be used for example to increase the effective Stokes shift in a sensor as better optical separation of the bands can be reached. Förster defined the transfer rate constant like this:

$$k_T = \frac{1}{\tau_D^0}\left(\frac{R_0}{r}\right)^6 \qquad \text{(Equ. 11)}$$

with τ_D^0 as the fluorescence lifetime of the donor molecule in absence of energy transfer, r as the distance between the molecules in resonance being close to Förster's critical radius R_0.

Corresponding to the relationship to the transfer efficiency $\emptyset_T$ described as

$$\emptyset_T = \frac{1}{1+\left(\frac{r}{R_0}\right)^6} \qquad \text{(Equ. 12)}$$

$\emptyset_T$ is 50 % when r is R_0. Typically, R_0 is in the range of 1.5 – 6 nm. Accurate measurements of distances on the molecular level are possible.

1.2.3 Methods and Referencing (5), (23)

Originally, only light intensities were measured. This brings several disadvantages as the signal is not just affected by the analyte concentration but also by the light source, the sensitivity of the photodetector, stray light, temperature, background (both from sample and the materials used) and fiber bending. Thus, referenced detection schemes are preferred.

Both to absorbing/reflecting and fluorescent/phosphorescent chemistries, two-wavelength referencing can be applied, which is simple and very effective. Two bands in the spectrum are the only necessity. Many drifts including photobleaching and leaching can be accounted for by that. Further, it is possible to add another dye. Measuring intensity thus brings the

problem that bleaching and leaching of both dyes would have to be the same. *Dual luminophore referencing (DLR, also Dual lifetime referencing* (27)*)* uses two dyes too, one analyte sensitive, the other one insensitive to it. The measurement is further based on recording phase shift rather than intensity. The phase shift is modulated by the varying contributions of the amplitude of the indicator dye to the total signal amplitude. DLR can be applied in the time domain, the frequency domain and in polarization.

The measurement of the decay time is a superb parameter but can of course just be applied to luminescent systems. There are two common methods how to measure decay time: *pulse fluorimetry (PF)* and *phase-modulation fluorimetry (PMF)*. The first technique works in the time domain the second one in the frequency domain. PF uses a very short exciting pulse of light compared to the lifetime of the fluorophore. Fluorescence intensity is built up until it reaches the value of the excitation intensity and then decreases ideally single exponentially. The time constant of this exponential decrease is the excited-state lifetime (fig. 5 b). PMF uses light sinusoidally modulated at a high frequency gives the harmonic Fourier transform of the pulse response (fig. 5 a). This response is modulated at the same frequency but phase-shifted and partially demodulated with respect to the excitation.

General relations are

$$\mathbf{I(t)} = \propto \mathbf{exp}(-\frac{\boldsymbol{t}}{\boldsymbol{\tau}}) \qquad \text{(Equ. 13)}$$

where τ is the decay time and ∝ is the pre-exponential factor or amplitude. The phase shift is related to the decay time by

$$tan\emptyset = \omega\pi \qquad \text{(Equ. 14)}$$

where ω is the angular frequency (=2πf).

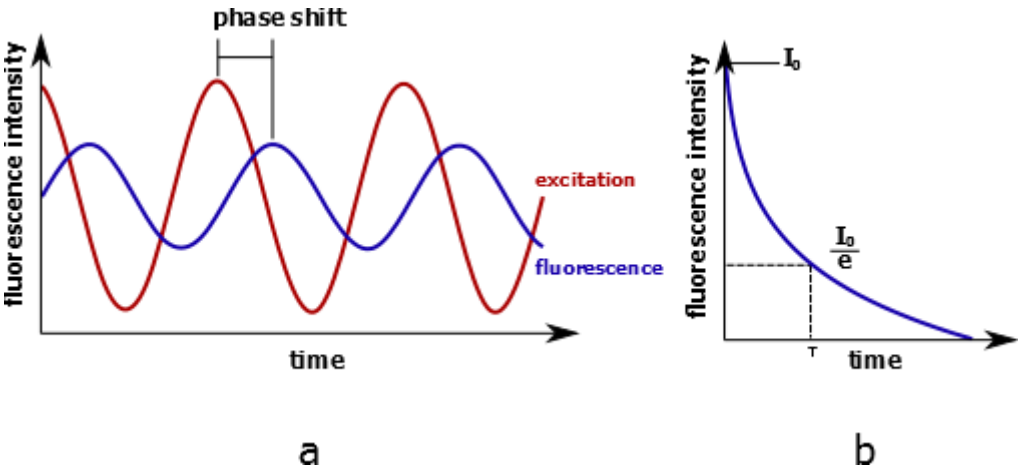

Figure 5: a) shows the principle of phase-modulated fluorimetry measuring in the frequency domain. b) shows the principle of pulse fluorimetry measuring in the time domain.

1.3 Optical sensing schemes (5)

Most optical sensors are based on layers composed of a support material and a more or less selective 'chemistry' deposited on or in them. Deposition of these layers can happen in various ways. They can be directly placed in the sample compartment, e.g. in the form of a disposable kit that can hold a blood sample. They can be placed in flow-through cells (FTC) acting as sample compartments, in disposable cuvettes, in microtiter plates and inside hollow waveguides.

The most common way for sensor materials to be deposited is in the form of a planar layer, mostly inside a FTC or a sample compartment. The sensor is then interrogated from outside through a transparent window. But sensor layers may also be deposited in or on waveguides or even form the cladding of a fiber core. Fibers can also be arranged to bundles and arrays. Organic or inorganic micro- or nanoparticles and beads are further important forms of solid supporting materials ((28), (29)).

For pH sensors, the potential of optical fiber probes was rapidly recognized. The availability of high quality fiber optic light guides facilitated the development. Principally, any sensing chemistry can be used to modify the surface or tip of a fiber optic system or integrated waveguide. Fiber optic sensors enable measurements in samples which cannot be placed into an optical meter. In analogy to electrodes, the term *optrode* was introduced (also called *optode*). In 1995, fibre optic microsensors with diameters below 50 µm were reported first.

The waveguides used either are made of plastic or glass. They are cylindrical and mainly consist of a core, a cladding and a coating impermeable for light. The refraction index of the core is higher than the one of the cladding to guide the light via total reflection through the fiber (19).

1.4 Ionic strength and thermodynamic activity (24)

The thermodynamic activity a_A of substance A can be described as its effective mole fraction x_A. The connection between these parameters is given by the activity coefficient f. So it can be said that

$$a_A = f \cdot x_A \qquad \text{(Equ. 15)}$$

For solvent A, f is approaching 1 if x_A is approaching 1. For a dissolved substance B with its mole fraction x_B, it is

$$a_B = f \cdot x_B \qquad \text{(Equ. 16)}$$

where f contains all influences that cause deviation from the ideal case. When the concentration and thus x_B approaches zero, a_B approaches zero as well. f approaches 1 then. Instead of the mole fraction, molality b_B can be used leading to the same insight

$$a_B = f \cdot \frac{b_B}{b^\theta} \qquad \text{(Equ. 17)}$$

for b^θ being the standard molality of 1 mol/kg. When it comes to ionic solutions, activities can be substituted by molalities, which is actually just an acceptable approach as long as the sum of the concentrations of all the ions in a solution is below 1 mM[1]. That ionic solutions are not ideal is due to the strength and great reach of the Coulomb interactions. A solution is neutral, but distribution of cations and anions is not uniform. Cations are more possibly close to anions and the other way round. Each ion is a central ion of a volume unit where more oppositely charged ions stay in the time average. This unit is called ion cloud. In average, the charge of the cloud is the opposite of the charge of the central ion (condition of neutrality). Energy and chemical potential of a central ion decrease because of the electrostatic interactions with its cloud. The activity coefficient is given by the Debye-Hückel law for very low concentrations:

[1] In this thesis the term M is used for both mol/L and mol/kg for practical reasons as it is always clear by the context which of those is meant.

$$\lg(f) = - |z_+ \cdot z_-| \cdot A \cdot IS^{1/2} \quad \text{(Equ. 18)}$$

where A is 0.509 for aqueous solutions at 25 °C and IS as the ionic strength of the solution:

$$IS = \frac{1}{2} \sum_i z_i^2 \frac{b_i}{b^\theta} \quad \text{(Equ. 19)}$$

Here, z_i is the number of the valence of an ion i. As it is considered squarely, it does not make any difference for the IS whether an ion is charged positively or negatively. IS sums over all kinds of ions in the solution. Formula (18) can be expanded for higher concentrations including further constants B and C. Yet, they can also be fixed for practical use as it will be shown in subchapter 1.5.3.

Table 2 shows the IS of different types of water recalculated from its correlation to electric conductivity (30).

$$EC\ (\mu S/cm) = 6.2 \cdot 10^4 \times I\ (M) \quad \text{(Equ. 20)}$$

$$IS\ (M) = 1.6 \cdot 10^{-5} \times EC\ (\mu S/cm) \quad \text{(Equ. 21)}$$

type	conductivity / µS/cm	ionic strength / mM
pure water (intrinsic conductivity)	0.055	0.0009
distilled water	0.5	0.008
rain water	5-30	0.08 – 0.48
drinking water	500-1000	8 – 16
ground water	30-2000	0.5 – 32
industrial wastewater	5000	80
seawater	54000	850

Table 2: different types of water with and there is calculated from their conductivities.(30)

1.5 pH value

1.5.1 Definition (24)

Water is amphoteric, as it can act both as an acid or a base. Thus, autoprotolysis is possible:

$$2\ H_2O \rightarrow H_30^+ + OH^- \quad \text{(Equ. 22)}$$

The law of mass action can be simplified as water is always there in excess:

$$K_w = a(H_30^+) \cdot a(OH^-) \quad \text{(Equ. 23)}$$

pK_w is defined as its decade logarithm. At 25 °C, K_w is 1.008 x 10^{-14} (pK_w = 14.00). Just a small part of water is dissociated. The used activities just accord to the molalities at very low

concentrations as it is the case in neutral water where the amount of hydronium (H_30^+) and hydroxide (OH^-) ions is the same – just 1.0 x 10^{-7} M each.

The pH value is defined as the negative decade logarithm of the H_30^+ activity:

$$pH = -\log(a_{H_3O^+}) \quad \text{(Equ. 24)}$$

Sometimes, it is useful to use the pOH scale which is correlated to the pH scale according to formulas 23 and 24:

$$pK_w = pH + pOH \quad \text{(Equ. 25)}$$

Thus, pH should be the half of pK_w in pure water, 7.00, at 25 °C. At higher temperatures, neutrality is shifted below 7, at lower temperatures above 7. Yet in practice, the pH value of pure water is not 7.00 even at 25 °C as the term 'pure' does usually not regard ubiquitous CO_2 dissolving into the water from the surrounding atmosphere, which will be discussed in the following subchapter.

Further, it has to be kept in mind that the pH value also contributes to the IS. At pH 3 and pH 11, respectively, IS already reaches 1 mM just because of the H^+ and OH^- ions and their counter ions, resp.

1.5.2 Carbon dioxide and carbonic acid (24), (31), (32), (33)

Pure water is rarely really pure in reality. There is always carbon dioxide CO_2 from the atmosphere dissolving into any aqueous solution until the solution is saturated with air. But it also results from biological decomposition processes and the dissolution of minerals. Partially, carbonic acid H_2CO_3 is formed:

$$CO_2 + H_2O \rightleftharpoons H_2CO_3 \quad \text{(Equ. 26)}$$

$$H_2CO_3 + H_2O \rightleftharpoons H_30^+ + HCO_3^- \quad \text{(Equ. 27)}$$

$$HCO_3^- + H_2O \rightleftharpoons H_30^+ + CO_3^{2-} \quad \text{(Equ. 28)}$$

The first of these equilibria is shifted far to the left side meaning that just 0.1 to 0.2 % of the dissolved CO_2 is dissolved chemically. Equilibria 26 and 27 are usually summarized to one equilibrium

$$CO_2 + 2H_2O \rightleftharpoons H_30^+ + HCO_3^- \quad \text{(Equ. 29)}$$

with a pK_a of about 6.4. The pK_a of the last equilibrium, equ. 28, is about 10.3 but of no special concern in this connection. The atmospheric CO_2 content of air – 0.03 to 0.04 % - is still enough to lower the pH value of 'pure' water to 5.4 to 5.8[2] when the water is air saturated. 1 % air saturation is enough to lower it to 6.4.

1.5.3 Buffers (34)

An easy way to describe what a buffer is and what it is good for is to call it a protection against abrupt changes in acidity and alkalinity. They cannot resist the effect but minimize it. A buffer consists of two components: If the pK_a is below 7.0, it can be called a mixture of a rather weak acid with its conjugate base; if it is above 7.0, a mixture of a weak base with its conjugate acid. A buffer is only able to buffer the pH of a solution rather close to its pK_a value; reasonably between $pK_a \pm 1$. This is how it simply works: if acid is added the H^+ ions are 'caught' by the deprotonated buffer species, if a base is added the OH^- ions are neutralized by deprotonation of the buffer's acid – the closer to the buffer's pK_a the better buffering works. The efficiency of a buffer can be calculated and expressed as the buffer capacity β. β is defined as

$$\frac{d[B]}{dpH} = \beta = 2.303 \cdot \frac{K_a \cdot c_t \cdot [H^+]}{(K_a + [H^+])^2} \qquad \text{(Equ. 30)}$$

and expresses the amount of a strong base B (NaOH, e.g.) needed to cause a certain pH change in a solution. c_t is the buffers molarity, the sum of its acidic and the basic component.

The pH of a solution can easily be calculated if the amounts of both components are known by using Henderson-Hasselbalch's equation:

$$pH = pK_a + \log\frac{[\text{base}]}{[\text{acid}]} + \log\frac{f_{A^-}}{f_{HA}} - \log(a_{H_2O}) \qquad \text{(Equ. 31)}$$

As the molarity of a buffer is the sum of the molarities of its components, it is not relevant for the defined pH but just for the current buffer capacity. The last term $\log(a_{H_2O})$ can be neglected as it will be zero in most cases of aqueous applications. However, the third term cannot be neglected. Just in very dilute solutions of IS coefficients f are close to unity.

Yet, the buffer's effective pK_a (pK_a') is not only dependent from the IS but also the temperature of a solution.

[2] Different sources present different values.

$$\log\frac{f_{A^-}}{f_{HA}} = IS_{correction} \quad \text{(Equ. 32)}$$

$$pK_a' = pK_a + IS_{correction} + T_{correction} \quad \text{(Equ. 33)}$$

In many cases, temperature dependency can be ignored, as many commonly used buffers like phosphoric acid or acetic acid do not show significant temperature dependency in contrast to the buffers of the kind Good and coworkers designed them especially for biological uses (see table 3) (35). Even over large ranges of IS, IS dependency is quite low; yet, the lower it gets the higher its influence. This can easily be calculated by using a special form of expressing Debye and Hückel's law:

$$IS_{correction} = (2z_a - 1) \cdot \frac{0.5114\sqrt{IS}}{(1+\sqrt{IS})} - 0.1 \cdot IS \quad \text{(Equ. 34)}$$

The main factor – actually the only factor – how strongly IS affects a buffer's pK_a is given by the net charge of its acidic form (which is of special importance for buffers carrying both an amine and a sulfonate group, thus for all of Good's buffers and related zwitterionic compounds). Another sign also turns the influence upside down. This extended Debye-Hückel law was determined experimentally. 0.5114 is the constant A from equ. 18 at 25 °C. In this presentation, constants B and C are already inserted too as their variation is not important for typical applications in buffer preparation.

buffer	pK_a	dpK_a/dT
Acetic acid	4.76	-0.0002
Phosphoric acid (pK_a 2)	7.20	-0.0028
MOPSO	7.01	-0.011
TAPSO	7.71	-0.02
AMPSO	9.12	n. f.

Table 3: pK_a values of buffers more or less temperature dependent. For AMPSO no value for dpK_a/dT could be found. MOPSO, TAPSO and AMPSO are buffers of the kind Good et al. investigated.

1.5.4 Measuring pH

Two important principles that can give you information about the pH value of a solution will be discussed in the following: potentiometric measurement via an H^+ sensitive electrode and optical measurement via pH sensitive dyes.

Yet, it should not be concealed that pH could also be measured by a pH sensitive ISFET (ion selective field effect transistor) as a potentiometric method (19). Further, many special

approaches exist including the use of polymers, either as pH sensitive polymers changing their color upon pH change or as hydrogels changing their refractive indices in a pH dependent way (8).

1.5.4.1Potentiometric sensor: Glass electrode (19), (24)

The glass electrode is still the most important and widest spread device to measure pH.

It is an ion sensitive electrode responding to H^+ ions. Fig. 6 shows how its composition as a combination electrode where the working and the reference electrode are combined in one glass rod. Both of the electrodes can be Ag/AgCl electrodes both dipping into a solution containing chloride ions. For the reference electrode this could just be a KCl solution, for the working electrode for example a phosphate buffer at pH 7.0. When put into a solution the electrodes are connected via the liquid junction (diaphragma) on the reference side and a glass membrane on the working side. The thin glass membrane (about 0.4 mm) at the lower part of the glass rod is the heart of this electrochemical sensor as the potential that is built up in the membrane is H^+ and thus pH dependent.

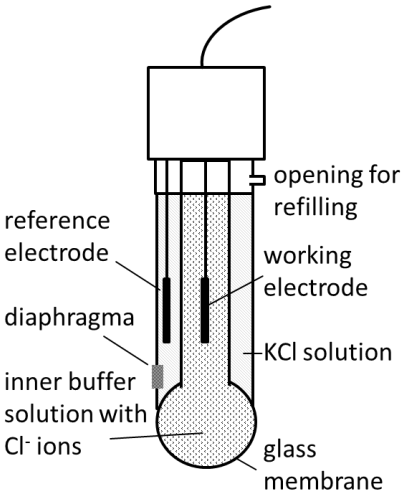

Figure 6: scheme of a pH glass electrode

The equation that is the base for the measurement is a version of Nernst's equation:

$$E = \text{const.} + 0.059 \cdot \log(a(H_30^+)) \qquad \text{(Equ. 35)}$$

When the solution whose pH should be measured is identical to the buffer surrounding the working electrode the potential should be 0. Indeed, this is not the case. The value that is reached and always has to be determined anew is called asymmetric potential. It is a collection of all not concentration dependent influences that might occur. This is because the material of the glass membrane can never be produced completely homogeneously. Also the Nernst factor of 59 mV, the slope of the linear calibration function, has to be determined anew each time before a measurement.

This glass membrane is a sodium rich silicate frame. This membrane swells upon contact with aqueous solutions, thus on both its side. On the inner side swelling is constant because

of the buffer on the outer side swelling is pH dependent. Swelling means that H^+ ions from the solution exchange with sodium ions from the glass. The potential between the inner and the outer side of the glass electrode is built up by sodium ions and lithium ions inside the membrane which is not permeable for H^+ ions.

It is obvious that these measurements depend on conductivity, thus ions, in the solution. When it is high enough and the electrode is always stored in aqueous solutions of high IS there will hardly be problems under normal measurement conditions.

Yet, problems occur when IS is very low, getting worse the fewer ions there are. It takes a long time for the potential to be built up. Responses of the sensors get slow, drifting, noisy, non-reproducible and inaccurate. So many companies developed kits to be capable of measuring pH in low ionic strength waters (high purity waters). Yet, they tend to be more complicated (flow through chambers) and/or change the composition of the solution by adding further salts, which can make impossible continuous measurements. Some standardizations even set the pH value aside. When it comes to determinations of water quality, conductivity is often used to substitute pH determination. Yet, this goes along with a loss of information as it cannot be distinguished among salts, acids or bases. Though pH measurements give more specific information, it is not sufficient to make a statement about the water's quality. These problems arise can mainly be correlated to problems with the liquid junction of the reference electrode. (9), (10), (11), (12), (13), (32)

1.5.4.2 Optical sensors: pH sensitive dyes

A pH sensor dye is a dye which changes its color in a pH dependent way. This means that the pH indicator dye must be possible of forming an acid-base pair. Thus, two equilibria exist:

$$HA \rightleftharpoons H^+ + A^- \qquad \text{(Equ. 36)}$$

$$BOH \rightleftharpoons OH^- + B^+ \qquad \text{(Equ. 37)}$$

The acid HA can also be charged, positively or more or less negatively, respectively. Spectroscopic properties of the indicator change upon this dissociation. Both, absorption of light or luminescence phenomena can be used to observe the pH change. (5)

1.5.4.2.1 Types of pH indicators and methods

There exist several types of pH indicators. The main difference is whether they show luminescence or not. Indicators suitable for pH sensing do not show significant overlap between the absorption spectra of the acid and the basic species. Further, they should possess: a) an appropriate pK_a in the range of the pH range of interest; b) strong absorption within the wavelength range 400 – 700 nm to allow the use of inexpensive optics; c) photostability and chemical stability; d) lack of toxicity; and e) the availability of functional groups suitable for covalent immobilization. In the case of fluorescence-based pH sensors, high quantum-yield, a large Stokes' shift and the lack of quenchability by oxygen and other sample constituents are desirable. (6)

Many pH dyes are known and were summarized in compendia (36). Their number is uncountable as virtually every organic compound changing its absorption spectrum in a pH dependent way can be used as a pH indicator. Nevertheless, only a few have been applied to optical sensors and intensely studied. For the physiological range, phenol red as well as bromthymol blue derivates have been considered to be useful. Bromphenol blue is useful in the pH range of 3-7 (band at 604 nm) and was used together with thymol blue which is useful for two pH ranges, namely 1-3 (at 555 nm) and 10-13 (at 600 nm). Cresol red has been studied in a fiber-optic sensor for the determination of pH in pasteurized milk. (6)

Absorption method is simple and easy to use but it is not very sensitive, which makes necessary high indicator concentrations or thick sensor layers. Fiber-optic sensors based on absorption method are difficult to miniaturize, especially for transmission mode. Reflection configuration is often employed to overcome this problem. Further, evanescent wave or attenuated total reflection modes can be used as well. In contrast, fluorescence method is more sensitive and can be used for small-size sensors and/or low indicator concentrations. (8)

Valeur (23) gives an overview over the most important fluorescent pH indicators. He counts coumarine derivatives (esp. 4.methyl-7-hydroxycoumarin), pyranine (1-hydroxypyrene-3,6,8-trisulfonic acid trisodium salt), fluorescein and its derivatives and further SNARF/SNAFL (benzoxanthene dyes) most of which are used in biological applications. There are also luminescent dyes whose excitation maxima are much higher, namely in the red range (37).

A special mechanism resulting in pH dependent fluorescence can be found in PET dyes: photoinduced electron transfer. A PET dye consists of a fluorophore, a spacer and a receptor element, e.g. an amine group, for the proton. The lone electron pair of the amine quenches fluorescence upon photo excitation but just as long as there is no H^+, the analyte, bound. The proton would “use” the lone pair hindering quenching.

Fluorescent indicators can be divided into three different groups basing on the two involved elementary processes photoinduced proton or electron transfer. There are dyes showing none of these processes (group 1 and 2), or just one of these (group 3), respectively.

1.5.4.2.2 Dye immobilization – Methods and Materials (5), (6), (8)

1.5.4.2.2.1 Methods

Immobilization of pH indicators is a key step in the development of optical and fiber-optic pH sensors, as it will have a great influence on the sensor’s characteristics. Mainly, three methods are used for immobilization of a pH indicator on/in a solid substrate:

- adsorption and intermolecular forces
- covalent binding
- physical entrapment

The first method is the simplest one as the dye is just adsorbed physically or chemically via electrostatic or hydrophobic interactions on or in a solid substrate. This is the case when e.g. a hydrophobic dye is simply dissolved in a suitable hydrophobic polymer. Insufficient solvation will lead to aggregation or crystallization of the dye. Further, the polymer will influence the dye’s pK_a (37). Besides, the method often lacks reliability due to dye leaching. A pH dye will not have the same leaching tendency in both its protonated and deprotonated form. A possibility to increase hydrophobicity of a dye and thus minimize dye leaching is introducing alkyl chains to the dye as it was shown for fluorescein (16).

Dye leaching can be abandoned by covalently linking the dye to the substrate (second method), which is usually time-consuming and complicated though. Reactive groups on both the substrate (organic or inorganic) and the dye can be converted. But linking a dye covalentely to a polymer can also be achieved by polymerization reactions. The dye has to be functionalized with a polymerizable group before it can act as a monomer in the following

copolymerization. The polymerization can be started electrochemically or photochemically followed by radical polymerisation. Photochemical initiation also makes possible direct polymerization on silanized ends of optical fibers, which can be useful if the resulting polymer is hardly soluble in any common solvent. Such an application will be used and demonstrated in the experimental part of this thesis.

In the entrapment (third) method, porous materials such as sol-gels are used to entrap the indicator. Entrapment and physical intermolecular forces go along with each other and can be combined deliberatedly. A compromise between convenience and dye leaching has to be found.

Sol-gel silica is a porous material accessible to pH indicator entrapment offering several advantages to polymeric materials: a) higher chemical, photochemical and thermal stability, as well as mechanical strength; b) optical transparency down to 250 nm; c) compatibility with various pH indicators and d) feasibility of direct coating on glass and silica fibers. However, it also suffers from several drawbacks, such as slow response, reagent leaching and aging (38). Controlled porous glass is another material suggested.

1.5.4.2.3 Basic sensor design

Several ways exist how to fabricate a pH optode depending on the field of application. There are basically two main designs: a planar one where the pH sensitive material is placed rigid and optically transparent carrier and a single-fiber design where the sensor chemistry is directly attached to the tip of an optical fiber, either at its end or at its core. The single-fiber design makes miniaturization of the sensor possible as they can be used for in vivo or in quantities which are usually considered to be too small for analysis. (6)

1.5.4.2.4 Theoretical problems and limitations

Optical pH sensors exhibit several limitations and problems that have to be overcome. The first question is if they really measure pH, which was extensively discussed by Janata (1).

He mainly focusses on the question whether optical sensors or glass electrodes perform better as both methods can measure pH precisely. The main problems in optical sensors are the solute-solvent interactions of the immobilized indicator and the relationship between the surface and the bulk value of pH and all other involved species. This problem mainly

emerges from the fact that both the analyte, H^+, as at least one form of the indicator are ions.

$$pH_{surface} = pH_{bulk} + \frac{Ne\psi}{2.3RT} \qquad \text{(Equ. 38)}$$

Ideally, the surface potential ψ should be zero.

You do not have these troubles using in glass electrodes, which really measure H^+ activity. But you will encounter other problems. The liquid junction between the reference electrode and the sample will cause problems which can be minimized by the design over a wide range of experimental conditions.

Janata basically mentions two ways to overcome the drawbacks of optical sensors, the use of two sensors with different dependency of IS to be able to finally calculate both IS and pH and second, making the sensor rather independent of the IS by immobilizing the sensor in a highly charged environment. Yet, the first 'solution' is only valid for one specific type of ion. Further, linear regression analysis is not possible at all. The second 'solution' even complicates the situation for sensors where the indicator is confined within a surface layer according to Janata.

In simple words, it can be said that pH sensors are just buffers themselves and thus, their pK_a values have the same dependency from IS as 'ordinary' buffers according to Debye-Hückel (see equ. 34). Especially for very low IS, it is hard to overcome this problem. Weidgans and coworkers presented fluorescenct pH sensors with negligible sensitivity to IS in the broad range of 25 to 500 mM by embedding lipophilic fluorescein esters carrying just one charge in their basic form in an uncharged highly proton-permeable hydrogel (D4). Another possibility of reducing IS effects is described in Weidgans' PhD thesis, namely using two indicators – one of which neutral, one of which zwitterionic in its acidic form – with contrary influence of the IS. In combination, the IS effects are partly compensated (7).

Another problem is the limited pH range of about 3 pH units. Yet, this is less crucial on the one hand because many applications (above all biological ones) mainly focus on a rather narrow pH range. Besides, the sensitivity of optical pH sensors can be varied and get very high (39). On the other hand, well working possibilities of broadening the pH range by mixing several dyes e.g. have already been suggested even with the desired linearity of the

calibration function over a pH range between 0.5 to 13.5 (17). Weidgans and coworkers even suggested a mixture of two sensors achieving a dynamic pH range of 4 pH units with a IS dependency as small as 0.1 mM between 25 and 500 mM IS (16).

1.6 Hydrogels (40), (41)

1.6.1 General definition

Hydrogels are hydrophilic polymer networks absorbing at least 10 - 20 % up to thousands of times their dry weight in water resulting in swelling of the hydrogel. They can be chemically stable or may degrade and eventually dissolve. Basically they can be divided into two groups: Physical and chemical gels. Both of them can differ in their macromolecular structures strongly.

Main fields of application are pharmaceutics, biomaterials, biotechnology. Biomedical applications such as drug delivery and using the gels as matrices for tissue engineering are of special importance.

1.6.2 Physical hydrogels

The networks of physical hydrogels are hold together by molecular entanglement or physical strengths such as ionic, H-bonding or hydrophobic forces. When a polyelectrolyte like alginate is combined with a multivalent ion of the opposite charge such as Ca^{2+} it may form a physical hydrogel known as an 'ionotropic' hydrogel, e.g. Calcium alginate. All the interactions concerning physical hydrogels are reversible and can be disrupted by changing the physical conditions such as IS, pH, temperature etc. This is why they are also calles 'reversible hydrogels'. Physical hydrogels are not homogeneous because of potential clusters and molecular entanglements or hydrophobically – or ionically – associated domains.

1.6.3 Chemical hydrogels

Chemical or permanent hydrogels consist of covalently cross-linked polymer chains. Copolymerisation of hydroxylethylmethacrylate (HEMA) with the cross-linker ethylene glycol dimethacrylate (EGDMA) was pioneer work for further interests in hydrogel research. Crosslinked hydrogels reach an equilibrium state of swelling in aqueous solutions which mainly depends on the crosslink density. Chemical hydrogels are not homogenous either, as they tend to containing regions of low water swelling and high crosslink density, clusters, dispersed within regions of high swelling and low crosslink density.

1.6.3.1 Hydrogels as a matrix for pH sensitive dyes

Different hydrogels have been used as a matrix for pH sensors to immobilize pH indicators. Hydrogels behave spongily, adsorbing a large amount of water. Thus, the surface potential will be close to zero as no discrete interface can be assumed resulting in $pH_{surface} = pH_{bulk}$, which should give the best results for the application as an pH sensor (see equ. 38) (16).

Chapter 4.1.3 will go more into detail when it comes to the choice of the hydrogels to be used for this thesis.

2 Experimental part

2.1 Introduction

This thesis studies the behavior of a pH dye in dependency of the ionic strength (IS) when it is physically immobilized in different hydrogel matrices in varying concentrations. The chosen dye is neutral in its acidic form resulting in the least possible IS dependency due to the dye itself. The three hydrogels that were investigated as matrices were D1, D4 and D7. The dye is just physically embedded by hydrophobic interactions in the hydrophobic domains of the hydrogels.

The hydrogels were tested with dye concentrations of about 1, 2 and 4 mmol per kg hydrogel (mM[3]) by absorption measurements of planar sensor foils. Four measurement series were performed for each of those nine different sensor combinations (each as triple determination): two 'titration' measurements and two 'IS scanning' experiments. The IS was kept constant at 1 mM for the one and 10 mM for the other titration measurement while pH was continuously decreased going from approx. pH 8.5 down to pH 6.0. For the two IS scanning experiments, pH was kept constant at 7.0 and 7.5, respectively, and an IS range between 0.5 mM up to about 100 mM was investigated.

The low molarities of the basic (ionic) buffer component just allowed very low buffer capacities. So, it was crucial for all the measurements to exclude CO_2 from the buffer solutions to keep the pH values of the buffers constant. For this purpose, N_2 was purged through the solutions replacing dissolved air. The effect was measured by an oxygen sensor from whose signals it was deduced to dissolved CO_2.

To reasonably perform these measurements under air exclusion, a new measurement setup was developed. Heart of this setup was a newly constructed flow through cell (FTC) combining many positive features distinguishing it from other FTCs.

The titration measurements resulted in sigmoidal pH curves. Ideally, the curves should look the same for all IS. Non-ideal behavior is described by the Debye-Hückel equation as it can be used for buffer preparation (see equ. 34). The smallest deviation that would be possible in theory can be derived from it. On the one hand, the pK_a shifts are a point of interest. On

[3] The abbreviation M is usually used for mol/L but in this context also for mol/kg.

the other hand, this is the shapes of the curves to see whether the curves are just shifted or if their slopes vary as well.

From the IS scanning measurements, you get values in dependency of the IS. After insertion of these values in a calibration function (achieved by the measurements before) you obtain pH deviations (ΔpH) in dependency of the IS.

Further experiments based on the described ones and should investigate other hydrogel/dye-concentration combinations including 0.1 mM dye concentration and polymerization of the monomer acryloylmorpholine on a glass fiber. The measurement principle was changed to fiber optic fluorescence intensity measurements.

2.2 General instrumentation and programs

Absorption measurements were performed on a Cary 50 UV-VIS spectrophotometer, Varian, Palo Alto, United States.

Fluorescence measurements and temperature control were performed using a FirestingO2, Pyroscience GmbH, Aachen, Germany[4].

For buffer preparation, a program by Thomas Eixelsberger, Institute of Biotechnology and Biochemical Engineering, Graz basing on the online buffer calculator by Beynon (42) was used.

Data processing was performed with Microsoft Excel 2010 and Origin 8.6G 64 Bit.

Instrumentation and programs as they were selected and achieved in the course of developing a new setup are described in the appropriate sections below.

2.3 Buffer preparation

All the buffers were of 1 mM IS (or 0.5 mM for one buffer of each IS scanning experiment) even when the whole IS was higher. So, the buffers' contribution to the IS was kept constant (1 mM) for better comparability of the systems (eg. 1 mM IS_{buffer} + 0 mM IS_{NaCl} vs. 1 mM IS_{buffer} + 9 mM IS_{NaCl}). The rest was adapted with NaCl.

Fig. 7 shows the structure of all the buffers used. The sodium salts of all these buffer acids were used too.

[4] In the following, it will just be referred to as 'Firesting'.

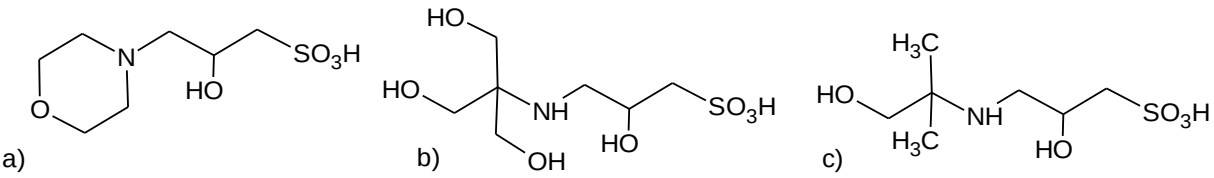

Figure 7: a) 3-(N-morpholino)-2-hydroxypropane sulfonic acid (MOPSO), b) 2-Hydroxy-3-[tris(hydroxymethyl)methylamino]-1-propanesulfonic acid (TAPSO), c) N-(1,1-Dimethyl-2-hydroxyethyl)-3-amino-2-hydroxypropanesulfonic acid (AMPSO). In solution, they all appear zwitterionic, with a protonated nitrogen atom and a deprotonated sulfonic group. MOPSO and TAPSO belong to the twenty buffers Good et coworkers investigated (35).

As pH glass electrodes are not able to measure pH at low IS fast, accurately and precisely (see chapter 1.5.4.1) the buffers' pH values were not checked by any pH electrode. Consequently, preparation was performed by weighing in both buffer components.

At first, four sets of buffers were prepared, two sets at fixed IS (1 and 10 mM) with varying pH values for titration measurements and two sets at fixed pH values (7.0 and 7.5) with varying IS for IS scanning measurements. Table 4 shows the exact pH values or IS prepared for 25.0 °C, respectively.

pH		IS / mM	
1.0 mM	**10 mM**	**pH 7.0**	**pH 7.5**
8,48*	8,44*	0,51^{+}	0,50^{+}
8,01^{+}	8,00^{+}	1,0	1,0
7,61	7,57	1,5	1,5
7,21	7,19	2,0	2,0
6,81	6,78	3,5	3,5
6,41	6,38	4,9	5,0
6,02	5,98	7,0	7,0
9,01**		10,1	10,0
10,01**		100	100
8,51**			
8,74**			
9,50**			

Table 4: MOPSO, *TAPSO, **AMPSO buffers for the absorption measurements. $^{+}$buffers were used as start solution for fluorescence titration measurements (see 3.4.2).

One buffer of each row in table 6 was used as initial point for the fluorescence measurements performed by spiking. Thus, two or three spike solutions had to be prepared for each of the four measurements, respectively. Either their acid component concentrations

(for titrations) or their NaCl concentration (for IS scannings) was much higher than in the basic solution. Their exact pH values and IS can be found in the appendix.

All the buffers were nitrogenated before the measurements to get rid of potential carbonic acid. At first, nitrogen was conducted through water in a wash bottle to have water saturated nitrogen decarbonizing the buffers without changing buffer concentration. An oxygen sensor (Firesting) was used to check the level of air saturation deducing from it to the CO_2 level.

Once a buffer was nitrogenated, it could be stored for at least a month (at about 5 °C) without significant dissolution of air (checked via O_2 again) into the buffer. This was achieved by special polybutyl plugs as they are used in the measurement setup that will be described in chapter 2.5.3.1.

2.4 Sensor preparation

2.4.1 Cocktails

A sensor cocktail consists of a polymer (hydrogel), the dye (added as a stock solution) and a solvent. Table 5 shows all the sensors used for the absorption measurements. For the stock solution, 4.70 mg of the monochloro-aza-BODYPI were dissolved in 3.4660 g (3.8944 µL) of THF which was also used as the solvent in the cocktail preparation. The resulting stock solution was 2.2 mM.

hydrogel – [dye] in mM /dry layer thickness in µm)	stock (in THF) / mg	hydrogel / mg	solvent (THF) / mg	m%	[dye] / mM	[dye] ratios among same hydrogels
D4 - 1/15	37.6	99.7	365.5	20	**0.93**	**1.0**
D4 - 2/7.5	37.7	49.8	349.8	11	**1.9**	**2.0**
D4 - 4/3.75	37.8	25.4	343.7	6	**3.7**	**3.9**
D1 - 1/15	36.8	88.3	345	19	**1.0**	**1.0**
D1 - 2/7.5	36.6	50.3	354.1	11	**1.8**	**1.7**
D1 - 4/3.75	36.2	26.4	345	6	**3.4**	**3.3**
D7 - 1/15	37.3	96.8	349.8	20	**1.0**	**1.0**
D7 - 2/7.5	37.8	53.6	370	12	**1.7**	**1.8**
D7 - 4/3.75	37.5	23.1	365.1	5	**4.0**	**4.2**

Table 5: list of pH sensor foils measured with the new setup

2.4.2 Sensor Foils

Sensors were prepared by using a 3 mil (75 µm) doctor knife to coat a polyethylene glycol terephthalate support ('Mylar' foils) which had been cleaned carefully before with acetone and lint free paper.

For the used D hydrogels, the concentration of polymer in THF was between 6 and 20 %. Solvation was possible and preparing a layer which stayed on the foil after conditioning was well possible too. Conditioning of the foils took place over nights in a buffer with an IS of 1 mM and an theoretical pH of 7.0 which was not checked but probably lower some tenth pH units because CO_2 was not excluded during conditioning as it was not crucial there.

2.4.3 Fiber Sensors

2.4.3.1Dip Coating

A glass fiber (400 µm core diameter; OFS, Specialty Photonics Division, USA) was prepared with a sensor cocktail containing D1 as the matrix. A 0.1 mM cocktail was prepared by weighing out 1.8 mg of the stock, 57.7 mg hydrogel (real molality: 0.077 mM). Here, isopropanol/H_20 (9:1 v/v; 458.8 mg) served as the solvent. The fiber was dip-coated in the cocktail. This had to be done several times (with drying in between) to reach a feasible signal. Raw signal (amplitude of fluorescence signal / mV) of the Firesting must not fall below 10 mV when it comes to the lowest point in the measurement. The settings were at their maxima with 100 % LED intensity and a 800fold signal amplification. But the Firesting's excitation and detection wavelengths (620 and 760 nm) were not ideal for the chosen dye with its absorption maximum in the hydrogel matrix at 685 nm. The created sensor tip was a

clot rather than a film, with an estimated diameter as big as 1 mm. This clot was very susceptible to mechanical harm such as nitrogen stream or even the protective cap of the sensor as the clot was too broad to be protected by it. So, work had to be performed very carefully.

2.4.3.2 Polymerization

A glass fiber (400 µm core diameter; OFS, Specialty Photonics Division, USA) was used for the cocktail with polyacryloylmorpholine as the sensor matrix. This matrix should be linked to the glass fiber covalently. The cocktail did not contain the polymer but the monomer (4-acryloylmorpholine), cross-linker (N,N'-ethylenebisacrylamide), the radical starter and the dye (see fig. 8 and table 6). The amount of cross-linker (about 1.8 %) was chosen to reach about 50 % water uptake. At first, the fiber was heat treated to get rid of possible contaminations, washed with acetone, then silanised to make the glass accessible for covalent linkage and at the end washed with acetone again. Finally, polymerization was started using UV light directly via the fiber under argon to exclude oxygen from the reaction. The cocktail resulted in an approx. 1.0 mM sensor though at first it was tried to go even further down in concentration. But with 0.1 mM no useful signal could be achieved. Even with the tenfold concentration several polymerizations had to be performed (varying polymerization time and placing of the fiber into the cocktail) to finally achieve proper signals considerably higher than 10 mV.

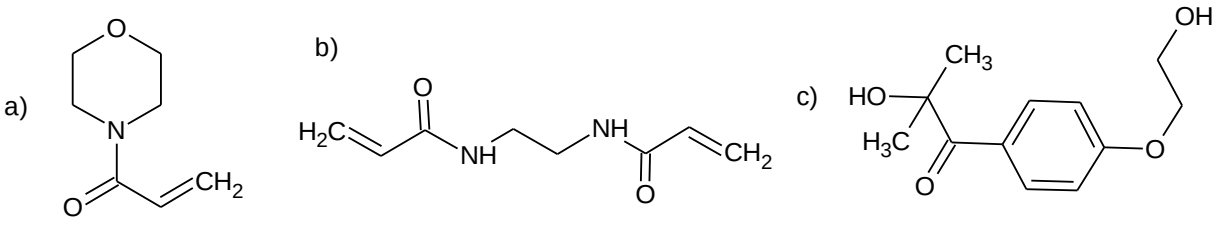

Figure 8: a) monomer: 4-acryloylmorpholine (AM), b) crosslinker: N,N'-ethylenebisacrylamide (EBA), c) radical starter: 2-hydroxy-1-[4-(2-hydroxyethoxy)phenyl]-2-methylpropan-1-one

Tapering was also tried to get a better signal. For that, a glass fiber is fixed vertically with a clamp on its end. Then, the glass is melted by a small flame so that the weight of the clamp pulls down the glass until it tears off. This results in a glass fiber with a conic ending for better light focussing resulting in a better signal.

Reasonable signals could be achieved with and without tapering. Yet, signals during the measurements were still as low as 25 to 35 mV. Another reason for the small signals could be slight damage of the glass fiber upon decladding and tapering the fiber.

polymerization cocktail	V / µL
4-acryloylmorpholine (97 %)	127
N,N'-ethylenebisacrylamide (96 %)	32
radical starter (98 %)	5
dye stock (2.2 mM)	32

Table 6: composition of the polymerization cocktail with 1 mM [dye]

As 0.1 mM dye concentration did not work, it could be changed to measuring absorption again. Yet, the FTC is designed for plastic foils.

2.5 Measurement setups

2.5.1 Absorption measurements using a flow through setup

The measurement series was performed in a newly developed automatable flow through system which is described in detail in 3.4.3.

For absorption measurements, a Mylar foil was used as a blank which was saved for all later experiments. In the course of a measurement spectra were recorded from 650 to 950 nm. Medium scan rate was chosen taking 30 seconds for one scan. One scan per minute was recorded.

2.5.2 Fluorescence via fiber optics

Fluorescence measurements were chosen as dye concentrations were decreased even further so that no absorption measurements were possible any more. These measurements were performed with fiber sensors whose preparation was described above. The sensors were connected to a Firesting. The excitation wavelength of the integrated LED was 620 nm emission was recorded at 760 nm. This is not ideal for the dye as it was mentioned above (see chapter 2.4.3.1). The settings were at its maximum (100 % LED, 800fold amplification), excitation time was 10 ms. A single data point was the average of three taken immediately one after the

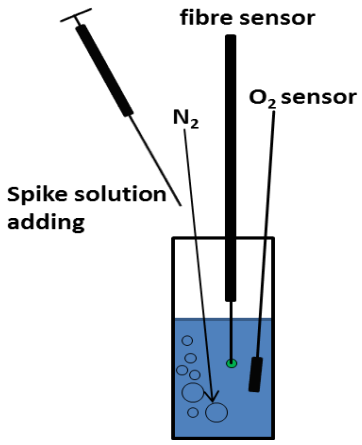

Figure 9: fiberoptic fluorescence measurements

other. The raw value (in mV), the amplitude of the intensity, was being watched.

Again, the same four measurements were performed. 10 mL of the buffer solution to begin with (see table 7) were firstly poured into a glass vessel which could maximally hold 20 mL. It was nitrogenated and the fiber sensor just dipped into the solution (see fig. 9). Care had to be taken about how to place the nitrogen and the sensor there without damaging the sensor by the nitrogen stream. Further, the signal could be very noisy due to the nitrogen (as the refraction index of the atmosphere around the setup changes with the nitrogen stream) when the decladded fiber did not dip into the solution completely. This would not have been a problem with the original plan: to close the buffer containing glass vessel, degas through the septum and then perform measurements without any nitrogen stream. But as the sensor clot was too big to be protected by its protective cap, it was not possible to get the fiber through the septum without destroying the sensitive clot. So, the septum was resigned and nitrogen flow was necessary.

Step-by-step spiking of the solution by the prepared spike solutions was performed. The spiking solution had also been purged through with nitrogen but without checking it. Via the Firesting software, the sensor response could be watched. Spiking was performed as soon as the signal reached a plateau. Spiking itself can also be followed by the oxygen signal which did increase slightly after each spiking step. Yet, there was never enough air dissolved in the measurement solutions to influence the measurements (see fig. 10). After the last spiking step temperature was checked.

Measurement	Buffer to begin with (IS/mM – pH)
Titration at 1 mM IS	1 mM – pH 8.0
Titration at 10 mM IS	10 mM – pH 8.0
IS scanning at pH 7.0	0.5 mM – pH 7.0
IS scanning at pH 7.5	0.5 mM – pH 7.5

Table 7: Buffers to begin with for fluorescence measurements

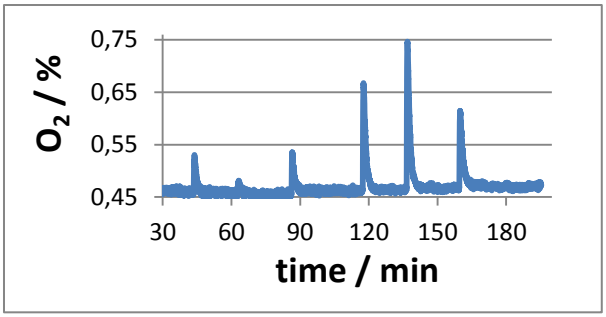

Figure 10: Each spiking step during the titration brought some new air into the solution, yet no relevant amount

Two glass syringes 'Fortuna Optima' (supplied by Carl Roth GmbH + Co. KG, Karlsruhe, Germany) with a nominal volume of 1 and 3 mL, respectively, were used to perform spiking with a steel canulla of 12 cm length. Because of the canulla, the pipetted volume was not the same as the read off volumina. No constant additional volume was assumed for the canulla. Each read off volume that was used for a spiking event was checked for its true volume seperatetly beforehand.

2.5.3 Setup for flow through absorption measurements without air contact at constant temperatures

2.5.3.1 Preceding considerations and development of the final system

The system as it is shown below in the next subchapter was a process of considerations and development. From the beginning, it was clear that the measurements have to fulfill at least these criteria:

- Totally *exclude* CO_2 during the measurement
- Contain a *flow through cell* (FTC)
- Performed at *constant temperature* (about 25,0 °C)

The first point was discussed above. The second point is necessary in terms of practicability. The last point would not definitely be necessary as long as there is temperature control and pH values could be recalculated. Yet, the dye's cross sensitivity to the temperature is not known.

As the setup should also be prototype-like, practicability and costs should be balanced.

First ideas were about developing the system from components that already existed in the institute: a metal capillary connecting the buffer and the FTC to avoid dissolving CO_2 into the buffers (freed from CO_2 beforehand) via plastic tubing and a peristaltic pump placed behind the FTC. The FTC must, of course, be insertable into the photometer. Constant temperature should be reached by placing the buffer containing bottles into a thermostatic bath big enough for all bottles at once, as the time between the buffer changes would be shorter than thermostating them one after the other. The metal capillary drawing in the buffer as well as the tube for N_2 purging and the O_2 sensor should be displaced from one bottle to the next in the course of a measurement.

Three different FTC were tried in the course of setup development. Problems and considerations about the FTC will be discussed later in the subchapter 2.5.3.2 as it is the heart of the setup.

Besides, former experiments in our group had shown that the underpressure that would be built up by the peristaltic pump being placed behind the FTC would lead to nitrogen bubbles in the FTC, which should be avoided. Other pumps, any micro dose pumps, would be a big investment, so another approach was chosen: to press the buffers through the system via overpressure of nitrogen. For that, the system has to be closed and dense. Thus, special adaptions for the setup – especially special plugs/septa and caps for the Schott bottles – were needed.

For practical reasons, the next consideration step was that sequential manual transferring of the (one) capillary and the (one) nitrogen tube is no satisfying and robust solution, especially in a closed overpressure system. Thus, decarbonization of all the buffers has to take place before the actual measurements. Step by step, all the buffers have to get inserted into the closed system right after their nitrogenation. The nitrogen stream could be splitted via a manifold, guided to the bottles via special hoses (fig. 12a) and through the plugs of the bottles via ordinary steel cannulas (fig. 12c). The steel capillaries dipping into the buffers (fig. 12 d) leave the bottles through the septa again, which leads to the next consequence of the closed system: a selector is needed connected to all the buffers via these steel capillaries which in sequence singularly selects the desired buffers going into the FTC. It was finally decided to use a selector which could even be programmed to make automation possible (fig. 12b).

Another advantage of that system would be that carbon dioxide could be excluded without purging nitrogen through the solution continuously and that the capillary and the nitrogen stream do not dip into the buffer at the same time. So, another possibility of getting nitrogen bubbles into the system is excluded.

Thus, nitrogenation of the buffers is the only manual step left. It was considered about other possibilities such as degassing by a UV bath or using a degasser as they are used in HPLC systems. Yet, no other system was convincing concerning efficiency and practicability. Thus the manual nitrogenation system was maintained.

Handiness of having a lot of glass bottles in a big water bath was questioned too, resulting in the idea of regulating temperature by helically leading a part of the capillary through a water counterflow (fig. 12g) coming from the thermostatic bath (fig. 12h) before it enters the FTC. This water flow as well as the capillary to be thermostatted should run through a simple plastic tube and be leaded back to the bath again. The problem was to get it dense on both sides. At first, it was simply tried to use two plastic T-pieces and close the sides where the steel capillary enters (leaves, respectively) the thermostating system with silicon, which did not work. Finally, steel T-pieces were achieved together with steel closing screw caps. A hole was bored into each of the caps for the capillary to go through. The system here (fig. 12i) got sealed by special ferrules and nuts (fig. 25). The residual way between thermostatisation and FTC should get isolated by foamed plastic (fig. 12j).

The FTC itself should be thermostatted too as real effects of it could be shown (see fig. 11) indeed in the way it was constructed – guided in bored lines through the FTC close to the measurement chamber. Water flow for that could have been branched off the other temperature regulation. But as another small pump (as they are used in aquaria) was at hand for leading the water from the thermostatic bath to the FTC and back, this was the first choice. The connection of the water tubes with the FTC just worked via putting the plastic tubes over small metal tubes extruding from the FTC.

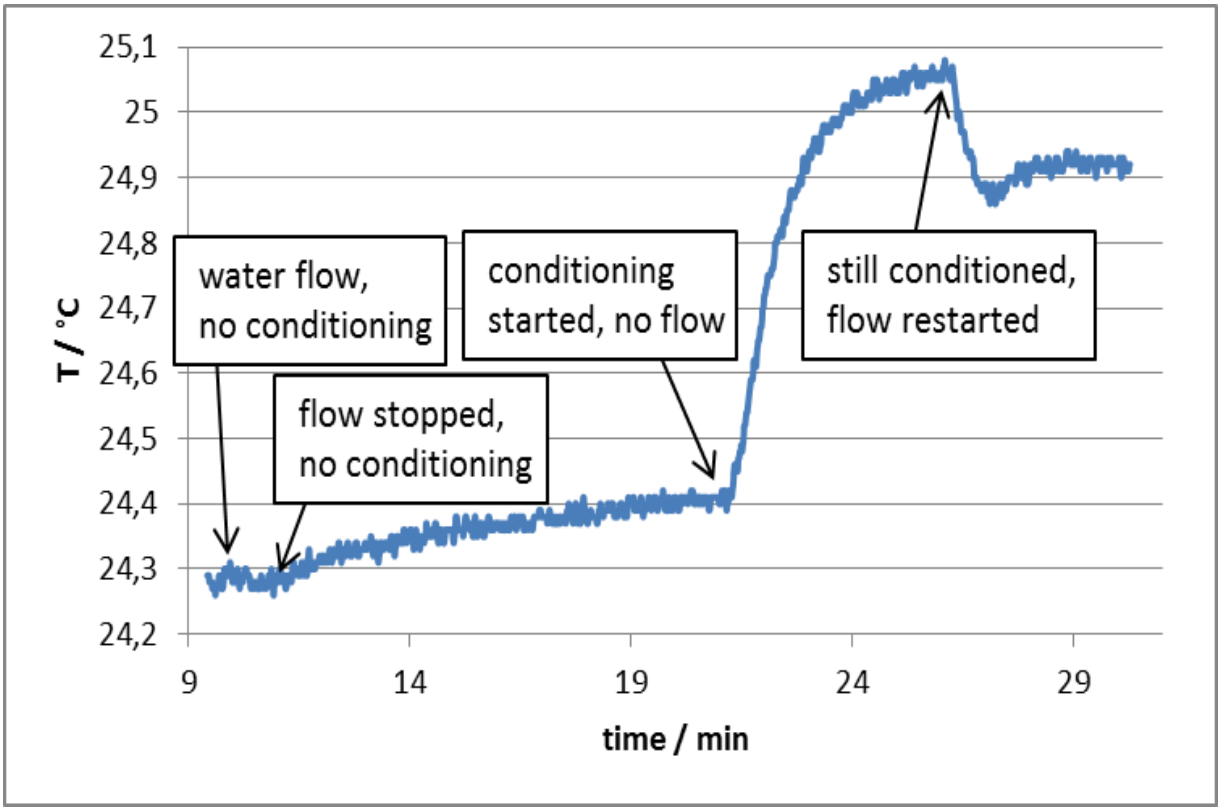

Figure 11: Temperature inside the FTC is measured. Water at 25.0 °C is guided into the FTC around the measurement chamber.

In contrast to a system with an integrated pump, flow rate now could neither be regulated via a pump nor could the flow be reversed just by pushing a button (to empty the system e.g.). The first problem could ideally be solved by a mass flow controller which would have been a too big investment for a prototype. Thus, a precision pressure regulator was inserted into the system before the buffers and a needle valve behind the selector (fig. 12e). In combination, flow rate regulation was possible. The other problem could be solved just by applying a simple plastic syringe via any suitable plastic tube at the end of the capillary leading from the FTC to the waste. However, the system is closed and under overpressure, possibly. So another three way valve had to be inserted into the system somewhere between selector and FTC (fig. 12f).

The final setup and its advantages are presented in the 'Results and Discussion' section (4.2).

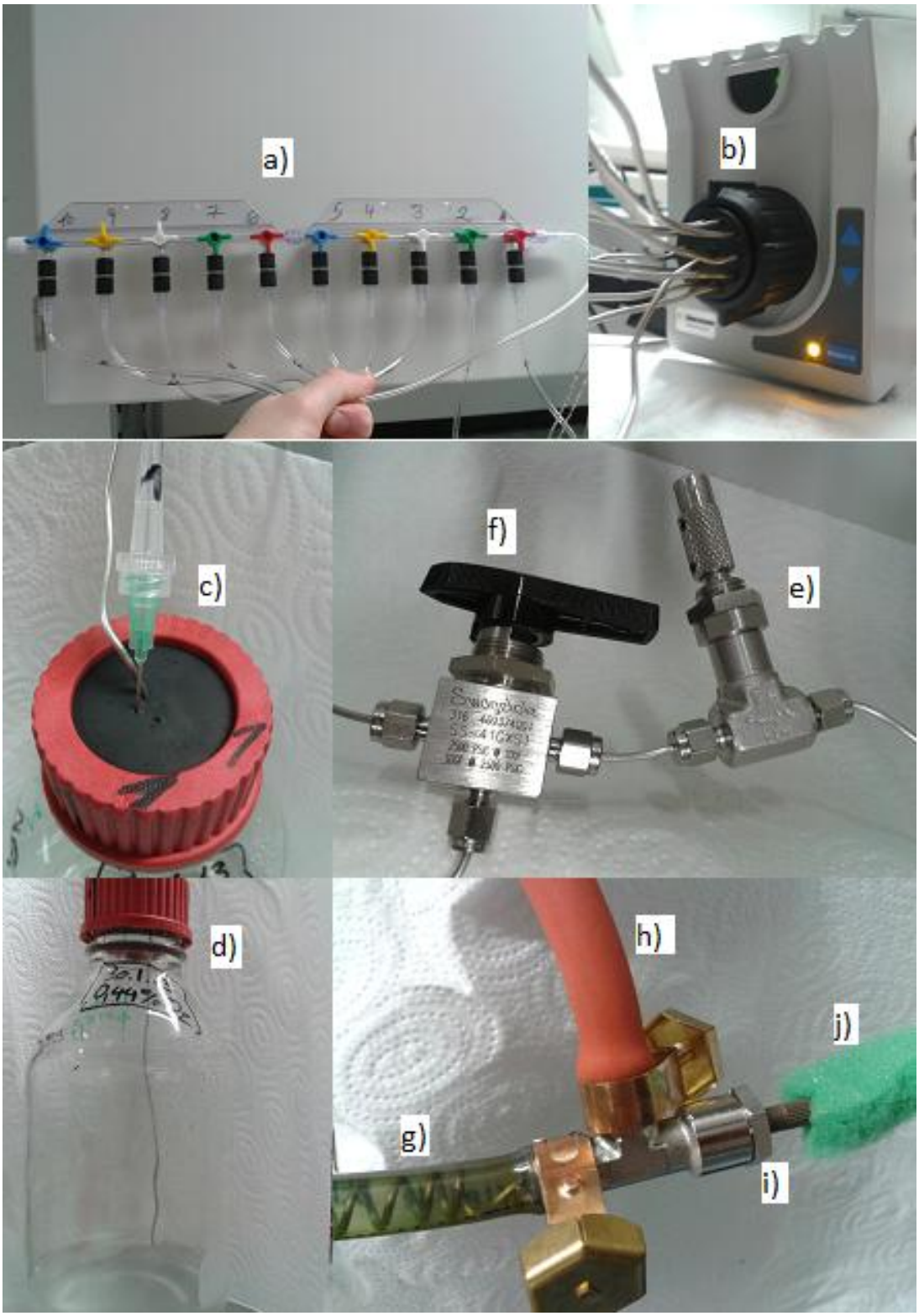

Figure 12: a) valved distribution manifold with special hoses leading to the Schott bottles b) selector c) needle entering the polybutyl plug and capillary leaving it d) Schott bottle with capillary dipping into buffer solution e) needle valve f) 3-way valve g) steel capillary helically through the thermostating water flow in a plastic tube h) connection to the thermostatic water bath i) part of the steel T-piece which has to be closed for the water flow which is reached by a cap which was bored through to screw in a ferrule and a nut j) foamed plastic isolation

2.5.3.2 Flow through cell (FTC)

Three different FTCs (fig. 13) were tried in the course of the system development. The first one (fig. 14) was at hand but there were problems with getting it fully filled and bubble free. Further, there was no handy way of exchanging the sensor and getting the system dense again. The sensor foil would have to be put between the main body of the FTC and the outer wall. Just the foil itself and an O-ring should prevent the system from leakage which is neither robust nor practical for the current application. Besides, the FTC offered temper ature control yet no temperature sensor to check it.

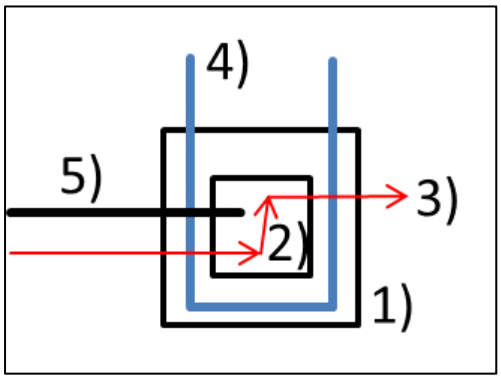

Figure 13: The scheme of a general thermostatted and temperature controlled FTC is shown. 1) FTC, 2) inner/measurement chamber, 3) [red arrows] flow of measurement solution, 4) thermostating water flow, 5) temperature sensor.

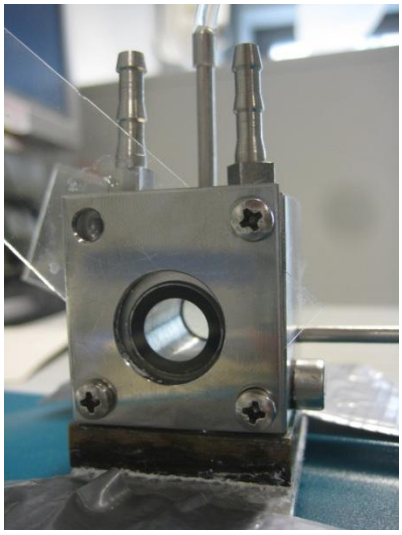

Figure 14: First FTC from the front

So, a new cell was built in the in-house handcraft. This second cell (fig. 15) fulfilled the criteria of handy sensor exchange in theory. In the wall of the cell there was a hole where a plug could be inserted. On this plug, a small piece of the sensor foil (about 1 x 1 cm) could be easily tightened by a clip system. Yet, the clip system was not optimized here as other problems evolved. The thermostating system was not dense but leaked into the inner chamber. The temperature sensor which entered the measurement chamber of the FTC by a hole in the wall as well should be fixed there by two components glue (epoxy glue). Actually, this was a dense (at first) but no robust way of fixing. It was vulnerable by mechanical strain which led to leakage.

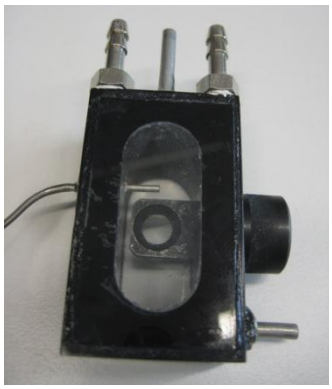

Figure 15: Second FTC from the front

Thus, a new, optimized cell was constructed (firstcut, UK)[5]. Its description is given in chapter 4.2.1, 'Results and Discussion'.

2.5.3.3 Setup Handling

A step by step instruction how to perform measurements with the new setup is given in the appendix.

2.5.3.4 Software for selector control

The software belonging to the Rheodyne selector was not very practical for the performed measurements:

- Under some conditions, it is not compatible with the Firesting software why another computer had to be used just for the selector.
- Automation is just possible partly as there are only twenty steps can be programmed. This is not enough if, for example, a three repeat measurement with more than six buffers should be started, which is not unusual.
- It is possible to change the numbers in the course of a measurement but this is not recognized by the device any more.
- Programming does not work by telling the device how long each position should be kept but times have to be added. Further, times could just be inserted in seconds leading to high numbers to be added mentally.
- During the measurement, it is neither possible to see which step is the current one nor how long the measurement will take still.

All this was compensated by a program created by Philipp Lehner (institute member).

2.5.3.5Main problems and trouble shooting

Several problems occurred in the course of the development of the system, most of which could be compensated for. A main problem was the decrease of the flow rate over time. This could have two reasons: the system was not dense on the 'nitrogen side' or clogged on the 'solution side' of the setup. The first problem distinguishes itself from the other one by observing decreasing pressure.

[5] All the design drawing was done by Jan Fischer (institute member) via Solidworks, Daussault Systèmes, GER.

- Density at all positions must be ensured.
- The setup should always be checked to be buckle-free.

Cutting the very end of the metal capillary reaching into the buffer eliminated a blockage once. It could have happened that small pieces of the polybutyl plugs get into the solutions by abrasion. The plugs should just be inserted after being wetted with water. No grease should be used. When there is a blockage, the setup has to be checked step-by-step by deconstruction and applying liquid from the 'back' of the setup.

Unfortunately, the selector provides no robust way of holding the metal capillaries. Thus, leakage is easily possible there if mechanical strength is applied to them during bottle exchange.

Even when the setup finally worked, random decrease of the flow rate could not completely be eliminated. Simple applying of a short on-off-movement to the needle valve (holding the narrowest constriction of the system) worked to remain the flow rate approximately.

2.5.4 Possible future adaptations

At first, the prototypical setup should be changed into a proper robust one. This means fixing the capillaries converging in front of the selector, fixing the connection tubing 'Heidelberg' and the distribution manifold. But also the other parts of the setup should be fixed in an own construction.

For a further use of the system, a mass flow controller or even special micro dose pumps serving as such could be inserted into the system. If air gasses do not matter at all changing to plastic tubes and to a cheap peristaltic pump is no problem. The pump can be applied then before the FTC as well and there will be less problems with bubbles due to underpressure then.

3 Data processing

Whole absorption spectra were recorded as it is exemplarily shown in fig. 16. The acidic peak lies at 685 nm, the basic one at 754 nm. The isosbestic point (IP) is at 706 nm.

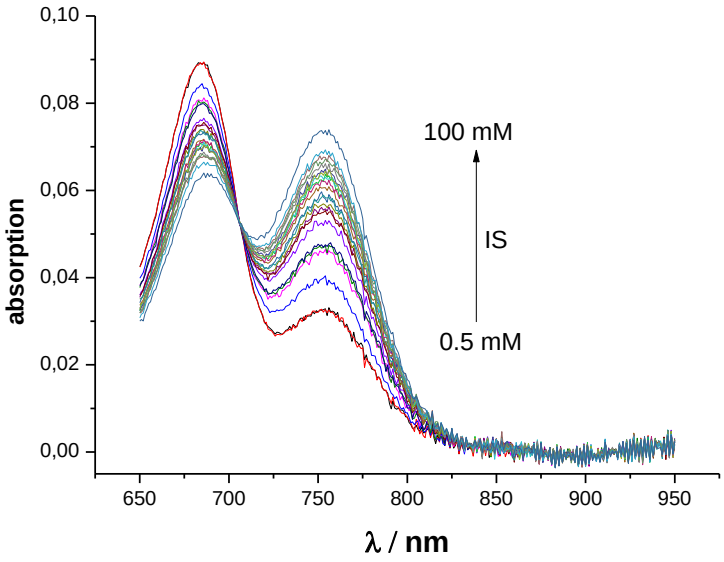

Figure 16: D1 (4 mM, 3.8 µm) – IS scanning at pH 7.0

	λ / nm
BL	880-950
E_{max}	740-760
IP	701-711

Table 8: wavelengths chosen for the mean values of BL, Emax and IP

Table 8 shows across which wavelengths raw values were taken to calculate a mean value for the baseline (BL), the absorption maximum (E_{max}) and the IP. The mean values were taken for further calculations. E_{max} and IP were baseline corrected by simple subtraction of the baseline. The final values which were used then were the corrected E_{max} values normalized (divided) by the corrected IP value as it is shown it equ. 39.

$$E_{max,normalized} = \frac{E_{max}-BL}{E_{IP}-BL} \qquad \text{(Equ. 39)}$$

Those values were plotted against time resulting in steps as it is exemplarily shown in fig. 17 for a titration measurement and 18 for an IS scanning experiment.

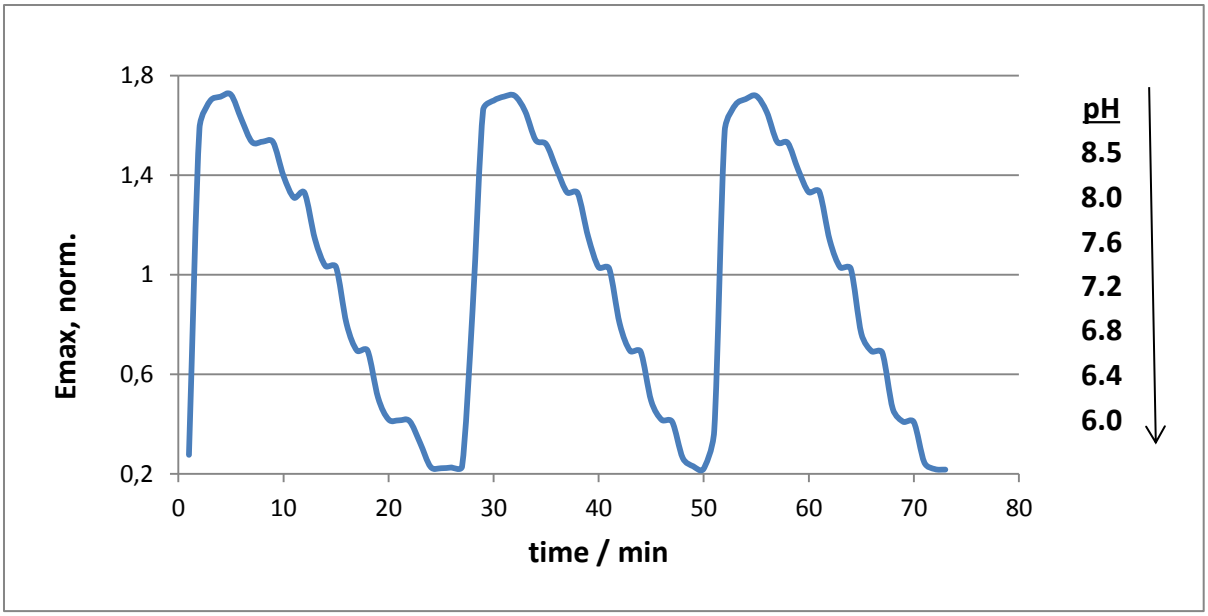

Figure 17: performed raw data of D1 (2 mM, 7.5 µm) – titration at 1 mM IS

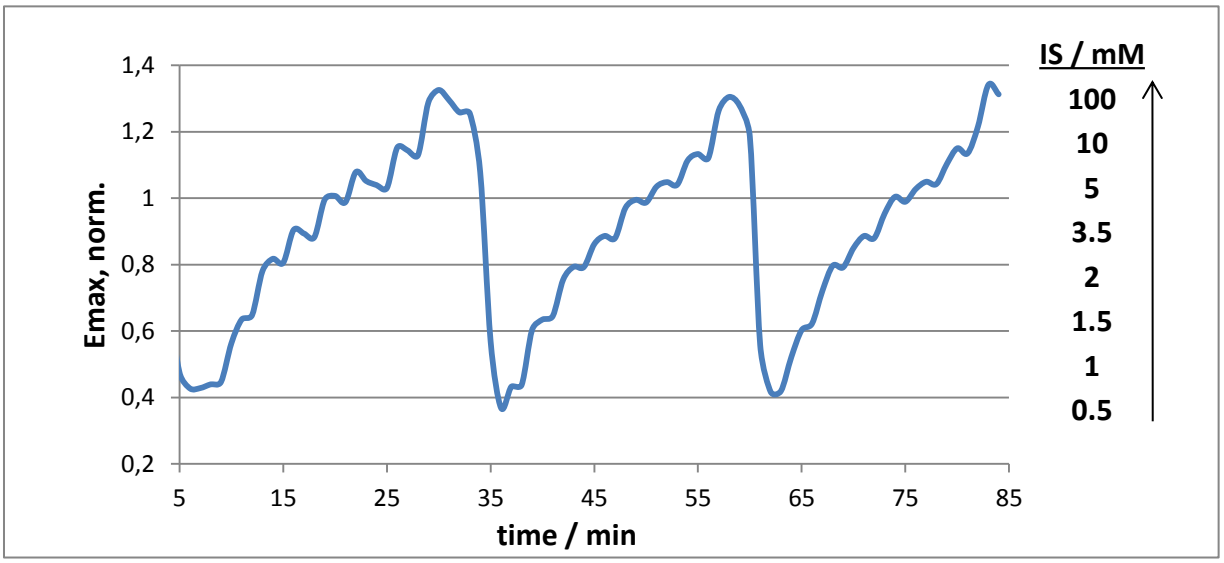

Figure 18: performed raw data of D1 (4 mM, 3.8 µm) - IS scanning at pH 7.0

For each of the shown steps one data point was used for further data processing – the one coming from the spectrum that was recorded right before the next buffer was selected. Some change in the flow rate in the moment of the buffer change could be the reason that fig. 18 rather shows slight waves instead of steps. Mean values and standard deviations were calculated from the three determinations.

Fluorescence measurements directly leaded to graphs which were called 'performed raw data' above. Examples are shown in fig. 19 and 20. Data was plotted in Origin and the plateaus of the steps (ca. last value of each step) were determined there. Not for all the

measurements mean values and standard deviations could be calculated although triple determination had been performed because the pipetting scheme was not identical.

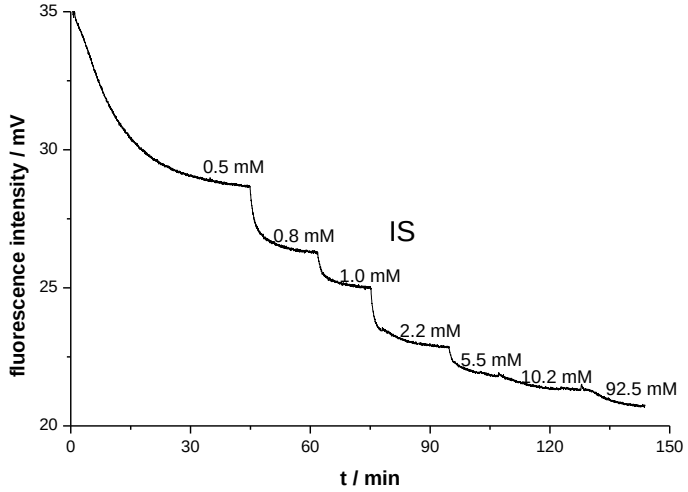

Figure 19: raw data of a titration measurement of the fluorescence measurements.

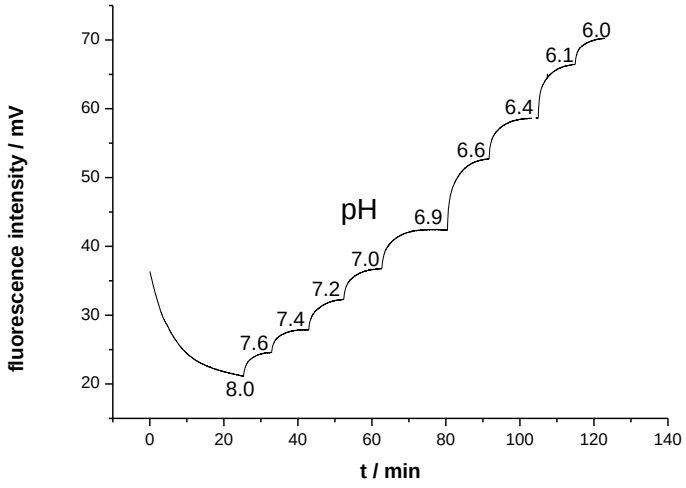

Figure 20: raw data of an IS scanning experiment of the fluorescence measurements.

3.1 How to achieve sigmoidal pH curves from the titration measurements

The values received from the titration measurements were plotted against their corresponding pH values. Fitting in Origin led to sigmoidal pH curves. The underlying equation is the Boltzmann equation

$$y = A2 + \frac{A1-A2}{1 + exp^{(x-x0)/dx}} \qquad \text{(Equ. 40)}$$

where y represents the normalized extinction ratios (for the absorption measurements; fluorescence intensity for the fluorescence measurements), A1 and A2 the two asymptotes of the curve, x_0 the pK_a, x the pH values and dx represents the width of the fit, a value indirectly correlated to the slope in x_0; the steeper the curve the smaller dx. It should never be looked at isolatedly but always together with the whole shape of the sigmoidal curve for reasonable interpretation.

Normalization was not performed overall. But as the raw values from the repeat measurements at 1 mM IS (sensor 2: D1, 0.1 mM [dye]) were apart from each other drastically, normalization to the highest value (at pH 6.0) was necessary for averaging over the values. The fits of each single determination were compared to each other and to sensor 1 to check admissibleness of the normalization.

3.2 How to achieve pH deviation curves from the IS scanning experiments

For the calculation of the pH deviations, calibration functions were needed. The Boltzmann equation as they could be derived from the fits of the 10 mM IS titration measurements delivered the needed values for x_0, A1, A2 and dx. For further calculations and results, it made no significant difference whether the values were taken from the sigmoidal curve arising from mean values of a triple determination or if the values were taken from each single determination and averaged afterwards. The second method was used for the current calculations.

The variables x and y are missing still: x values are the values achieved from the IS scanning experiments by data processing as it was described in the subchapter before representing extinction (E_{max}) or an fluorescence intensity value, resp. These values each refer to a pH value (y). These pH values would be the results of pH measurements in these solutions using the current sensor and the current calibration function. They were subtracted from the real pH values of the buffers resulting in ΔpH values. These values were further normalized to the value at 10 mM IS which should be zero by definition (simply subtracting the value at 10 mM IS from all values) but more or less slightly deviated from zero in reality.

$$\Delta pH = pH_{real} - pH_{calculated} \quad \text{(Equ. 41)}$$

$$\Delta pH_{normalized,i} = \Delta pH_i - \Delta pH_{10mM} \quad \text{(Equ. 42)}$$

The normalized ΔpH values were finally plotted against IS. So, the resulting plot gives the ΔpH in dependency of the IS (shown in the following subchapter).

4 Results and discussion

4.1 Choice of materials

For the experiments of this work just one fluorescent pH dye and mainly one buffer was used. The dye was immobilized in a hydrogel forming the sensor. Which dye, buffers and hydrogels were chosen and why will be discussed here. A list summarizing all used chemicals is given in the appendix.

4.1.1 Sensor dye

Previous experiments had shown that one form of the pH sensor dye has to be neutral for IS cross sensitivity to be as low as possible (see fig. 21) according to equation 38.

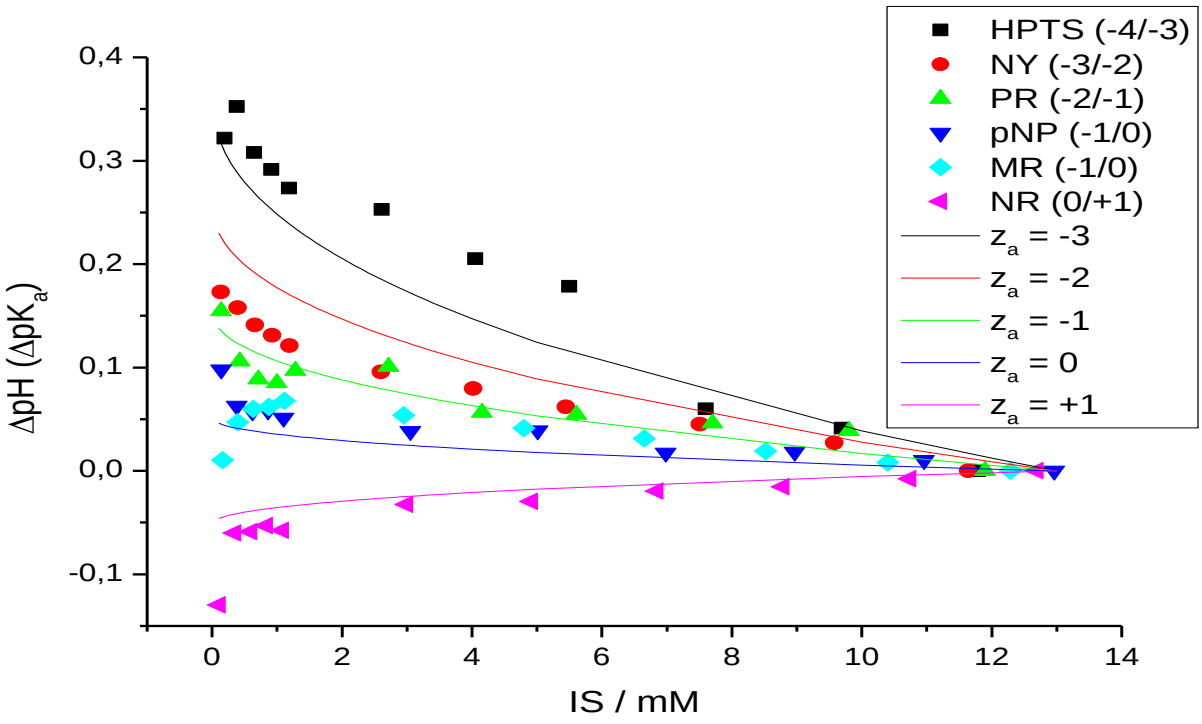

Figure 21: Previous experiments showed that the deviation a pH sensitive dye shows when IS decreases gets lower the lower its own charge gets. The legend shows the abbreviations of the used dye and the charges for its basic and acidic component in bars. z_a is the charge of the charge of the acidic component of a buffer. The lines represent the theoretical behavior of a buffer – its deviation from the thermodynamic pK_a – according to the Debye-Hückel equation (38).

Recently, Jokic and coworkers also presented a group of fluorescent pH probes: a series of new BF_2-chelated tetraarylazadipyrromethane dyes (aza-BODIPYs) (37). All of these dyes show high molar absorption coefficients of around 80 000 M^{-1} cm^{-1}, good quantum yields

and are highly photostable. Their absorption maxima lie between 660 and 710 nm, their emission maxima between 680 and 740 nm.

Fig. 22 shows the dye chosen for the current applications. It is the monochloro-aza-BODIPY whose pK_a value in absorption measurements was around the neutral pH range on which the current experiments should focus. Its absorption and fluorescence spectra are shown in fig. 22 as well, just the acidic component is fluorescent. Absorption spectra of the basic form and emission spectra of the acidic form show a great overlap. So, when using fluorescence intensity for pH titrations, the signal does not get smaller just because of decreasing concentration of the emissive component but also because the increasing basic component takes up the energy (Forster resonance energy transfer, FRET).

It can be seen that the chosen dye exhibits a very distinct isosbestic point. Further, both of its components show absorption peaks of almost the same height. As most of the current experiments based on absorption measurements, this was important: The basic form could be chosen where the peak is almost going down to zero in the acidic. So, distinguishing between different pH values can happen even more distinctly.

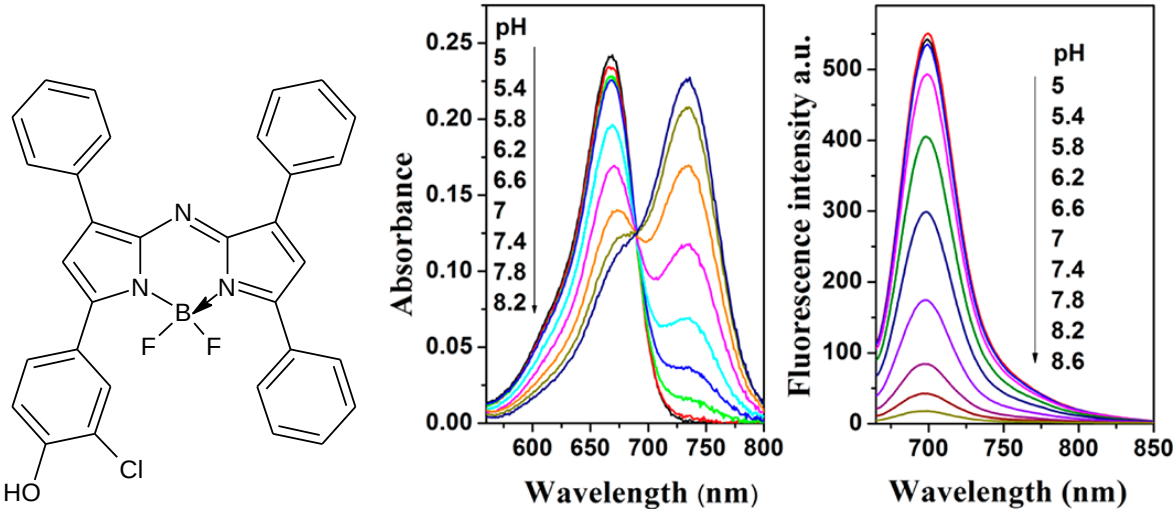

Figure 22: structure (left), absorption spectra (middle; left peak: acidic form; right peak: basic form), emission spectrum of acidic form (37).

Ongoing work tries to add polymerisable groups to these dyes to make them accessible to covalent immobilization in polymer matrices, which is another reason why this dye is chosen for the current experiments.

4.1.2 Buffers

A buffer was used covering the same pH range as the chosen dye. A common buffer like the phosphate buffer (pK_a = 7.20) would not be a good choice for this application as one component is even charged twice. Its contribution to the IS of a solution is much higher than for a buffer where one of the components is uncharged. When IS gets as low as 1 mM and you want to prepare 1 L of a puffer at pH 8.0 you would need less than 10 mg of the acidic component of the phosphate buffer. This was to be avoided for working precisely. As Good's buffers (and related ones) had already been used for preceding experiments and a buffer of that kind fulfilled the desired conditions, the buffer of choice was MOPSO with a pK_a of 7.01 under thermodynamic conditions (34). Yet, this pH range was not enough and further buffers were needed. For higher pH values than 8.0, TAPSO (pK_a=7.71 (34)) and AMPSO (pK_a=9.12[6]) were used. The references from where the pK_a values were chosen were not the same for all the buffers anymore. This could lead to some inaccuracies using them in combination within one course of measurement.

Further, it has to kept in mind that the temperature dependency of those buffers is much higher than for usual buffers as acetic acid or phosphoric acid (see table 3). This is another reason why temperature should be kept constant during the measurements. Actually, this should be done anyways as the temperature cross sensitivity of the chosen dye is not known yet.

In the current work, the buffers' purpose is to define pH values rather than buffering the solutions. Due to the low IS buffer capacities would be too low to 'protect' the solution from dissolving CO_2. Further, its contribution to the IS must not be neglected. Exact knowledge of both parameters is necessary.

4.1.3 Hydrogels

4.1.3.1D-series

Weidgans and coworkers already used D hydrogels for pH sensors with negligible influence of IS. Further, the polyurethane based D4 is stable under varying conditions of pH conditions and uncharged. It is well soluble in 90 % ethanol, but not in water. It consists of hydrophilic and hydrophobic blocks, so that the lipophilic dye can be immobilized there without

[6] Literature ((42)) gives 9.00 for 100 mM, the used pK_a was counted back to a IS of 0 mM.

covalent linkage.(16) As it does not have alkaline properties, the protonated form of the pH indicator is stable inside the membrane. Abel and coworkers used the same series of hydrogels – D1, D4 and D7 – for their ammonia sensor (43). Jokic and coworkers used D4 for characterizations of the dye series of which the currently used dye was chosen leading to good results as well (37). The water absorption of the chosen hydrogels is 70 % for D1, 50 % for D4 and 30 % for D7 according to the manufactures' information (44).

4.1.3.2 PolyHEMA

PolyHEMA and its copolymerisates are widely used hydrogels too. Its mechanical, chemical and thermal stability is excellent. It is transparent, biocompatible and exhibits good proton permeability. It could further be copolymerized with a suitable dye (45). Its nonpolar characteristics could be tuned by copolymerizing HEMA with ammonia or sulfonate groups as there is reference that the IS dependency could also decrease by using a highly charged matrix (6).

Yet, PolyHEMA did not work: The polymer did not stay on the Mylar foil after swelling in water. It was tried to prepare the plastic foil via plasma etching for five minutes at maximum performance. At a first try, fixation of the polymer layer still did not work and the foil completely lost its color in the same conditioning buffer in which the other foils were conditioned. At another try, fixation did work. Still, the sensor became stainedly whitish. Nevertheless, recording spectra was tried but no reasonable one could be achieved anymore.

Further several tries to copolymerize HEMA with monomers carrying a charge were undertaken. Yet, no product soluble in any common solvent or solvent mixture could be achieved. So, polyHEMA left beside and was not even tested as a matrix for the current application.

4.1.3.3 Polyacryloylmorpholine

IS in the current experiments is very low. An influence of the dye concentration being in the same range as the IS itself can be assumed. Thus, polyacryloylmorpholine – which water absorption potential is dependent from the grade of copolymerized cross-linker – is alternatively chosen as it could perform better than the D hydrogels because of more uniform dye distribution.

4.2 Final flow through setup

How the whole flow through setup finally looks like is structurally shown in fig. 23. After a short description of the work flow the advantages of the new system are lined out. The used components are listed in table 9 and table 10 divided into consumables/small parts and main parts. Teflon tape was used for all screwing parts which had to get dense.

Short description of work flow:

After inserting the bottles containing already decarbonized buffers into the system, the system is closed. Nitrogen overpressure is applied to all of the bottles and controlled by a pressure reduction valve. One of the capillaries allocated to one of the buffers is actuated by the selector, so that the selected buffer is pressed through the system if the needle valve and the 3-way valve are set open. The buffer is thermostatted before the FTC by helically going through a water counter flow for about half a meter. The rest of the capillary right before the buffer enters the FTC is isolated by foamed plastic. In the FTC further thermostatisation and, besides, temperature control takes place as well as the actual absorption measurement. After leaving the cell, the buffer goes to the waste.

The newly developed setup holds several advantages:

- closed system to ideally avoid solvation of CO_2 into the measuring solutions during the measurements
- no nitrogen bubbles anymore because of overpressure instead of underpressure on the one hand and because the nitrogen stream and steel capillaries leading to the FTC are not next to each other in any situation on the other hand.
- no glass bottles in water baths for temperature regulation
- online temperature control inside the measurement chamber
- two temperature regulations close to where the actual measurements take place
- during the measurements no manual operations on the setup necessary any more
- automation possible

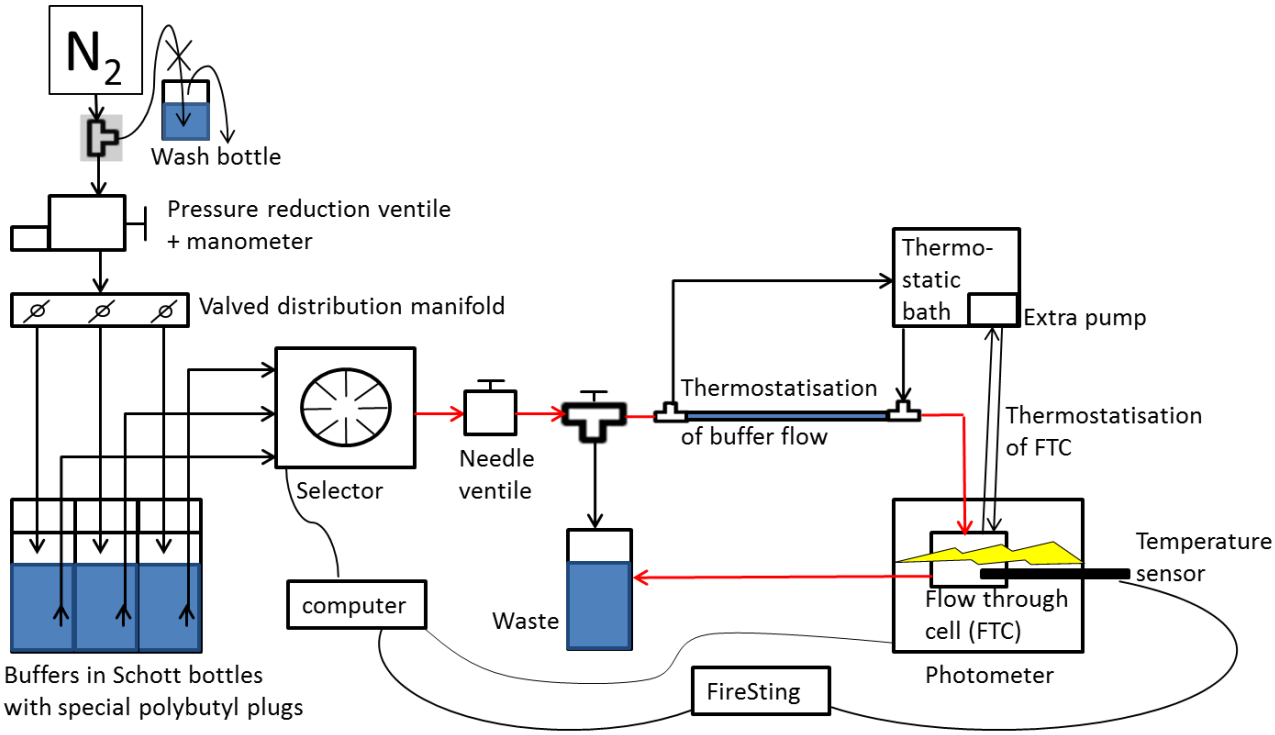

Figure 23: The whole setup for automated flow through absorption measurements under air exclusion and with temperature control is shown. The cross in front of the wash bottle signalizes that this part of the setup is not a part of the actual measurement procedure. It is just used for buffer preparation. The red line symbolizes the way any buffer usually takes during a measurement.

device	Supplier	Product number
Teflon tape		
Canullas (12 cm)		
Glass slides (1 mm thickness)		
Aquarium pump		
Pressure tubing	Festo AG & Co. KG, GER	
T piece pressure tubing connector		
manometer	Aircom, GER	MA6302-01
Valved distribution manifold	Medizintechnik Hauser, AUT	A-304050
Connection hose 'Heidelberg'		A-302380
LUER-LOCK adapter (2x male)	Vieweg, GER	990074-K
LUER-LOCK adapter (Luer-Lock female/G1/8)		990063-1/8PP
Closing plug (stainless steel, G1/4)	Esska, GER	962250010002
T piece (brass, 1 x IG/2 x AG, nickel plated, PN 16)		LTE14MSV0000
TitanEX Ferrule, 1/16	Abimed, GER	7770-044
steel capillaries (1/ 16" x 1,00 mm)	Medchrom, GER	625-40
Flangeless Ferrules		P-221
Headless Flangeless Nut		P-286
Screw in temperature sensor (M4 - 200°C - 2 m FEP/SIL)	Alfamerit, GER	PT100
O-rings (6+19 mm, 70 shore)	Steyr-Werner, AUT	
corrosion free wire	dental laboratory Johann Vinzenz Klug, AUT	

Table 9: Consumables and Small Parts of the new setup

device	supplier	Product number
Varian Cary 50 photometer		
Julabo Thermostatic bath		
Firesting	Pyroscience, GER	
FTC	firstcut, UK	
precision pressure regulator	Aircom, GER	R216-02FP
Polybutyl plugs (GL 45)	Ochs, GER	444704
Hole caps (GL 45)	Ochs, GER	222710
Screw neck bottles DURAN® -pressure plus ('Schott')	Roth, GER	H995.1
Rheodyn multi position selector (11 ports)	Abimed, GER	MXX778-605
3-way ball valve	Vaust, AUT	SS-41GXS1
Swagelok needle valve (1/16)	Vaust, AUT	SS-SS1

Table 10: Main parts of the new setup

4.2.1 Flow through cell (FTC)

Heart of the whole final setup was the optimized FTC:

The inner chamber volume is minimized to a final volume as low as 2.8 mL reaching an exchange volume at the end (including death volume of the capillaries) of just about 9 mL with the chosen conditions. This is just about a quarter of what could be reached with the second cell (35-50 mL depending of the flow rate). So, the buffer consumption during measurements could be minimized and there was no necessity of considering circular flow of the buffer to save buffer e.g.

The FTC was planned in a way that makes deconstruction and cleaning easily possible too in contrast to the second cell. Fig. 24 shows all its parts separately and the whole cell as one piece which could again be easily inserted into the photometer, of course. The almost oval form made it possible that bubbles could almost be avoided as the flow would enter at the FTC lowest and exit at its highest part.

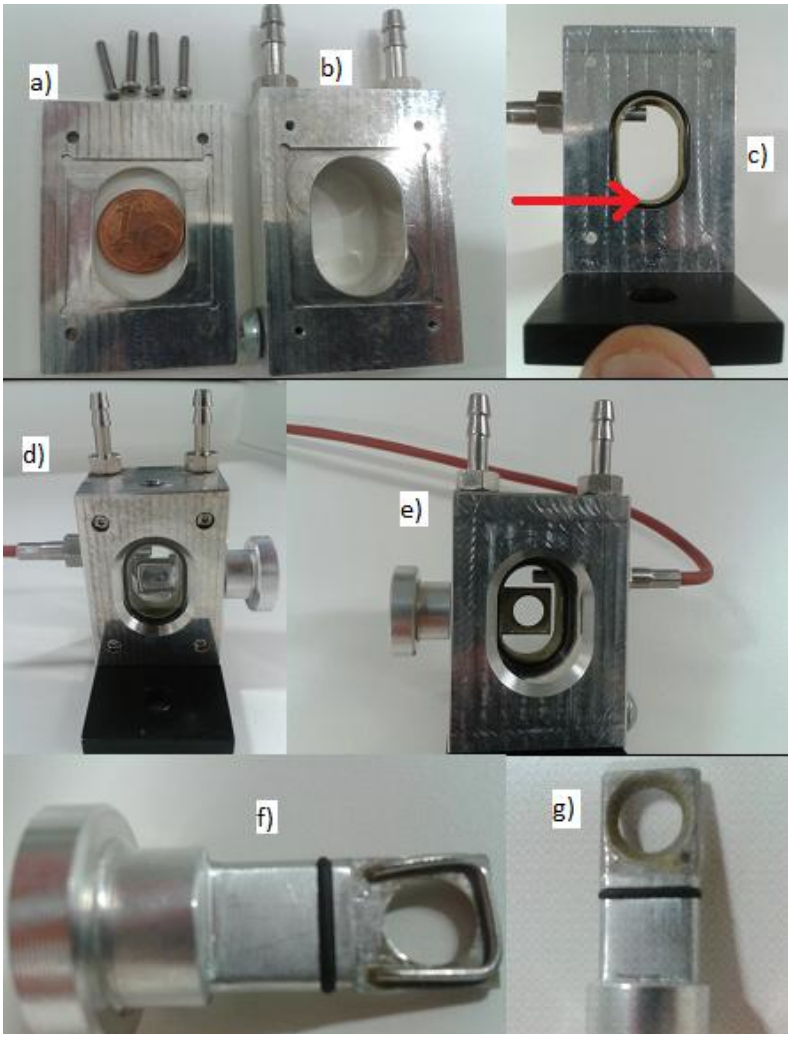

Figure 24: a) front part of the FTC with a cavity for a 1 mm glass slide. b) back part of the FTC with the same cavity as in a) + extruding connections for the thermostating water. c) middle part of the FTC to which the other parts a) and b) are fixed by screwing. The temperature sensor is penetrating into the inner chamber of the FTC. An O-ring is fixed on both sides. The middle part is fixed on a plate which can be inserted into the photometer. The red arrow shows where the liquid flow will enter the inner chamber. d) the assembled FTC with the plug from the front. The hole on top is the exit for the liquid running through the cell. Such a hole is also below the temperature sensor for liquid entering. Both connections – entrance and exit – are sealed by screwing with a nut and a ferrule (see fig. 25). e) the assembled FTC with the plug from the back f) the plug for simple sensor foil changing and sealing the system from the front with its clipping system; in black: the O-ring. g) the plug from the back.

Parts a) and b) are to be screwed onto part c). They contain cavities for glass slides (1 mm thickness) which have to be cut to the appropriate dimensions (18 x 16 mm). The cell gets dense just by screwing the parts with the glass in between together. It should be worked carefully not to break the glass. But it just has to be done once and not upon each single sensor change. Changing the sensor foil is done somewhere else lacking any tricky knack.

Figure 25: brown ferrule with colorless nut

For thermostatisation, channels are bored through part c). The two steel tubes extruding make a simple connection with the plastic tubes for the water flow possible. The temperature sensor is fixed by screwing into part c) this time instead of sticking.

Heart of the FTC is the plug (see fig. 24 f) and g)) which can be simply inserted into and taken out from the FTC without creating any leakiness. The plug consists of a circular part for simple handling and a flat bar with a hole at its front for the light beam to go through. The sensor foil can easily be fixed over the hole. The wire for the clipping system was tooled till optimal insertion and fixation of the sensor foil without scratching it were given at the same time.

4.2.2 Temperature control

As the temperature sensor in the inner chamber of the FTC just had a two-wire configuration temperature was checked by an external sensor after a night of conditioning the chamber to the room temperature. Figure 26 shows the temperature difference of 0.5 °C. Temperature measurements were automatically corrected by that value.

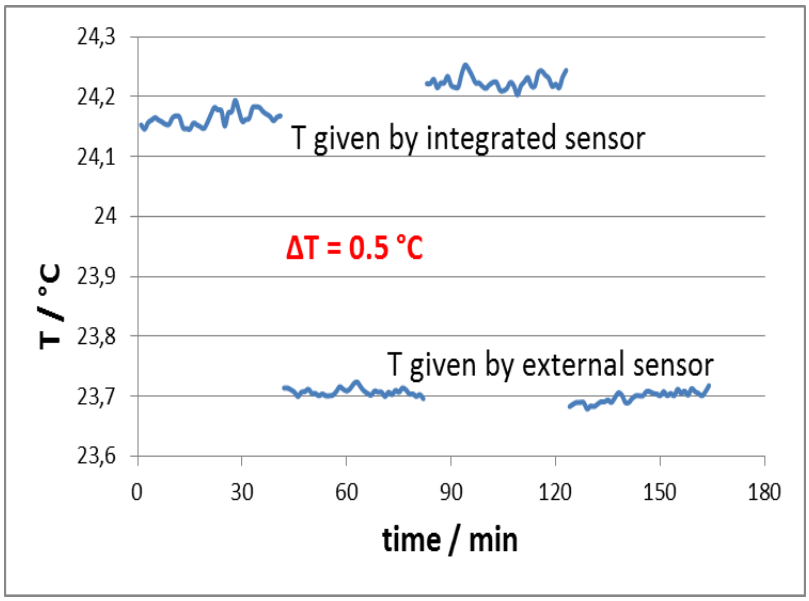

Figure 26: testing of the sensors outside and inside the FTC for the calculation of a temperature offset.

The temperature of the thermostatic bath providing the water for temperature conditioning has to be set to 24.1 °C to reach a temperature of 25.0 °C (already compensated value) in the measurement chamber.

By the thermostating system, temperature could be kept constant at 25.0 ± 0.1 °C during all of the measurements.

4.2.3 Flow control

The flow rate could be controlled by a combination of the applied pressure and the opening grade of the needle valve (see fig. 27).

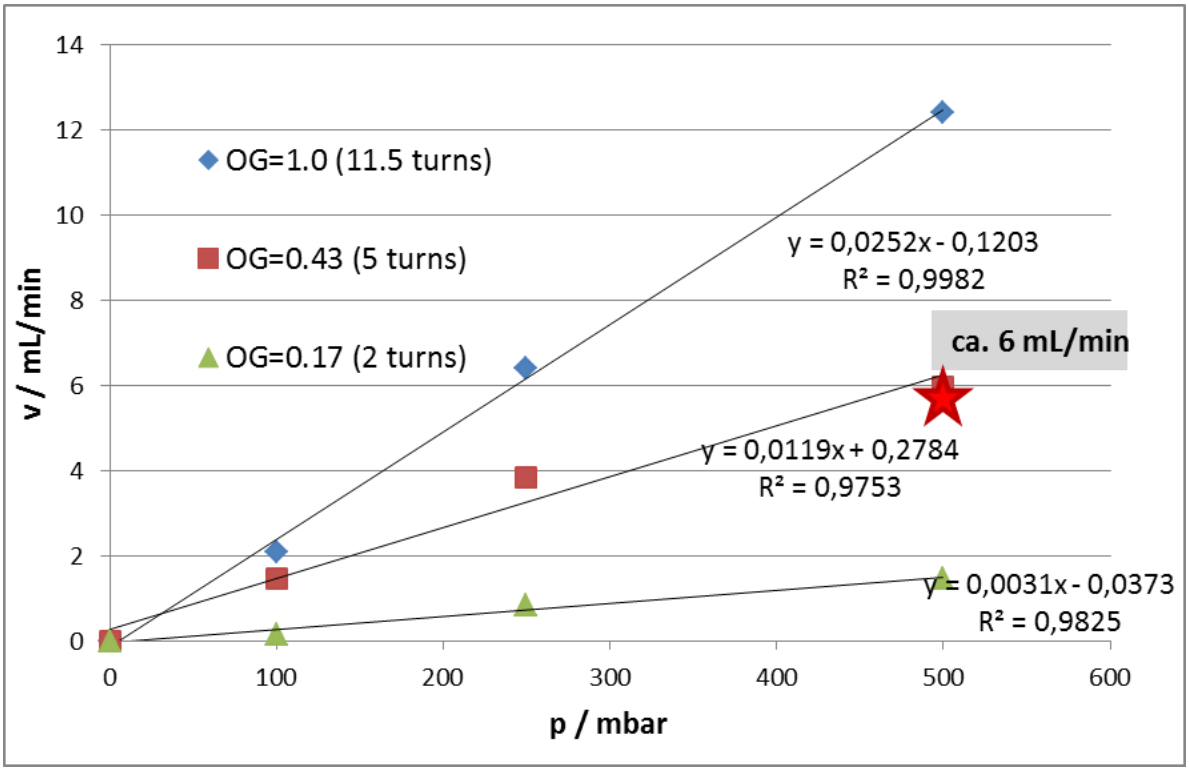

Figure 27: Flow rate in dependecy of the applied pressure and the opening grade (OG) of the needle valve. Testing was performed using fluorescein. The current measurements were performed at a flow rate of about 6 mL/min (red star).

4.3 Absorption measurements

In the following, the final graphs will be presented containing some data as well which characterize the curves: ΔpH, the shift between 10 mM and 1 mM IS, and (if possible) Δdx. Δdx will not be presented ('n.p.' meaning 'not possible') for those curves where the fit did not give reasonable results obviously. dx was fixed then at 0.50 and the fit was recalculated. So, ΔpH values are presented there too. Which values had to be recalculated will be shown

in the concluding table where all the data will be summarized. One reason for the bad fits was that the pK_a shifts were so large that the prepared buffers did not cover the whole range anymore which would be necessary for good fits of sigmoidal curves. New buffers were prepared with other buffer substances for the extension of the investigated pH range. This resulted in even worse fits probably because buffers did not perfectly match. A reason for that could be the fact that the pH values were calculated and not measured/checked relying on pK_a values from the literature. Still, the blank curves are actually enough to see if a hydrogel is a good matrix or not. For this interpretation, numeric values are not essential.

The presented graphs contain the connected raw values of the titration measurements and not the fits. The graphs showing the pH deviation in dependency of the IS contain small tables giving the real dye concentrations and the corresponding numeric pH deviation between 1 and 10 mM IS.

Five graphs in a row belong to one hydrogel in the following order: titration curve for the dye concentrations of 1 mM, 2 mM and 4 mM followed by the pH deviation curves for pH 7.0 and pH 7.5. These five graphs will be presented for D1, then for D4 and finally for D7. Table 11 summarizes data at the end of the chapter, concludingly. The reader should keep in mind that the nominal dye concentrations (used in the legends) can differ from the real concentrations (used in the tables).et al.

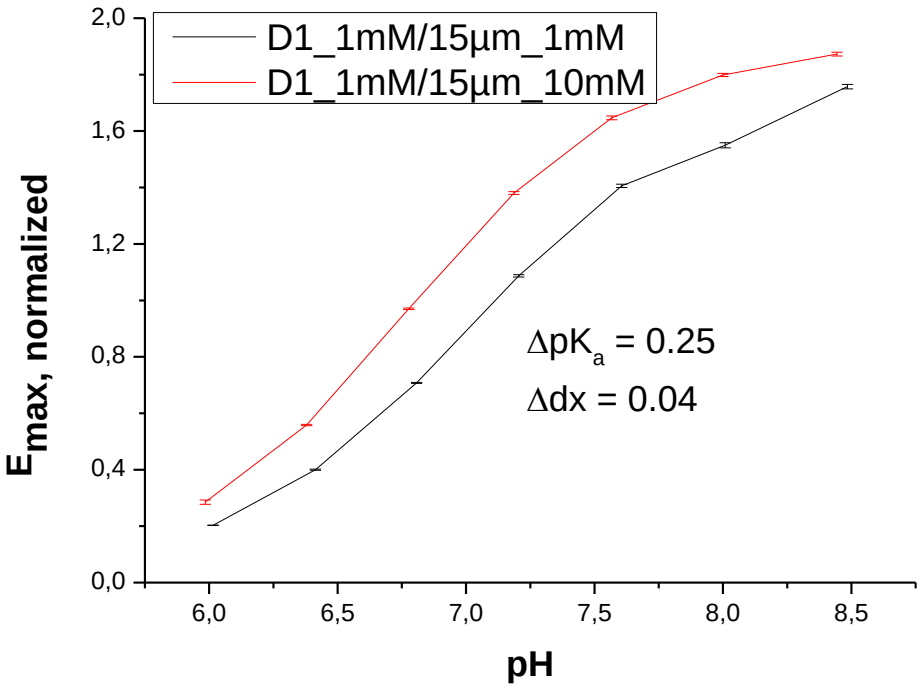

Figure 28: D1, 1 mM [dye] - titration measurements at 1 and 10 mM IS.

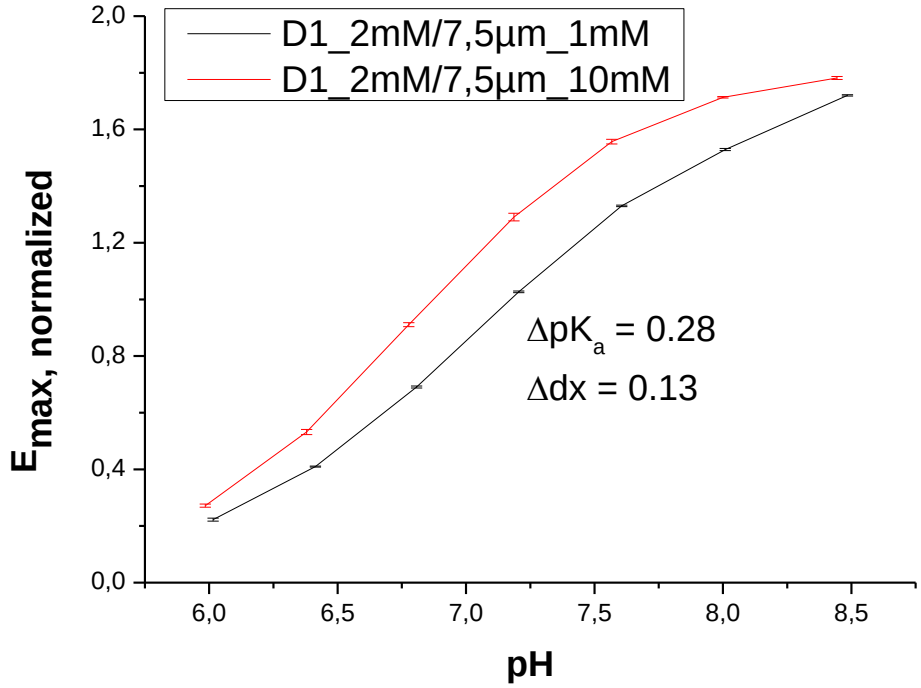

Figure 29: D1, 2 mM [dye] - titration measurements at 1 and 10 mM IS.

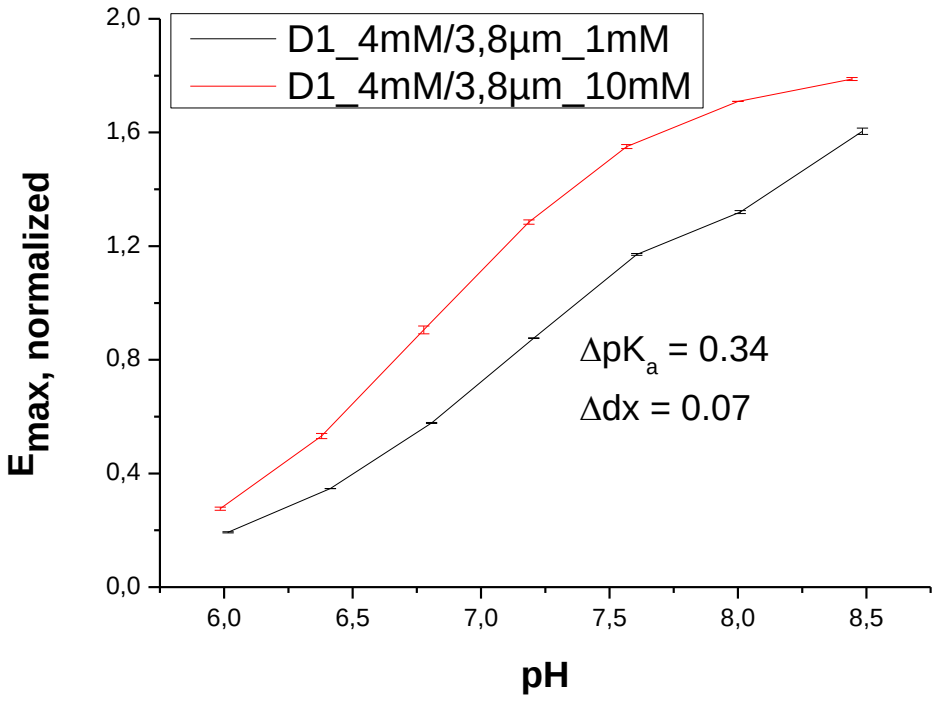

Figure 30: D1, 4 mM [dye] - titration measurements at 1 and 10 mM IS.

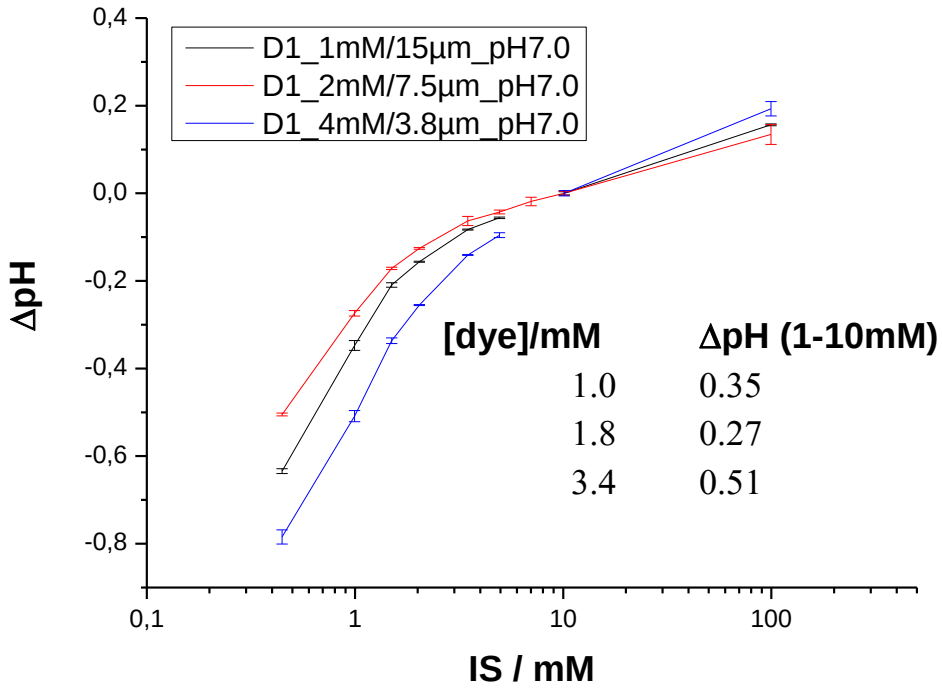

Figure 31: D1, pH7.0 – IS scanning experiments for all [dye].

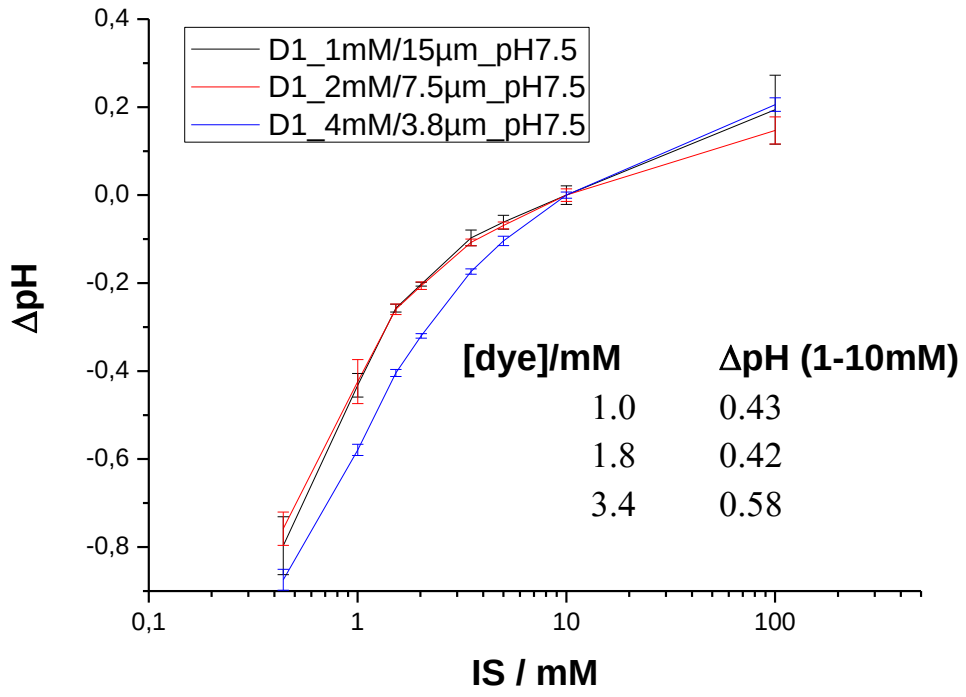

Figure 32: D1, pH7.5 – IS scanning experiments for all [dye].

For D1, strong shifts between 10 and 1 mM IS between 0.25 and 0.35 pH units in the titration measurements can be approved by the IS scanning experiments at pH 7.0. When it comes to pH 7.5 the deviation even gets higher by 0.1 pH units which would suggest a slight flattening of the curves which in turns can be approved by the dx values as they are all positive (meaning flattening). So, the found deviation is about a fivefold higher than it would be possible by theory in solution as fig. 21 suggests.

What else can be seen is that there seems to be no significant difference between a dye concentration of 1 and 2 mM. However, a dye concentration of 4 mM gives the worst results. Yet, significance of this influence could not be approved by the following experiments with hydrogels D4 and D7.

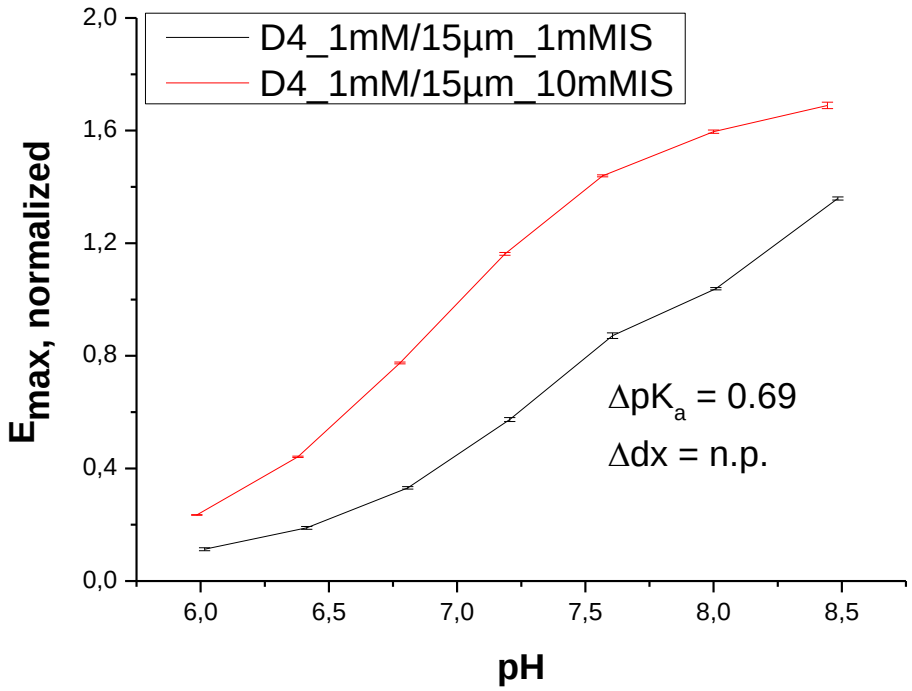

Figure 33: D4, 1 mM [dye] - titration measurements at 1 and 10 mM IS.

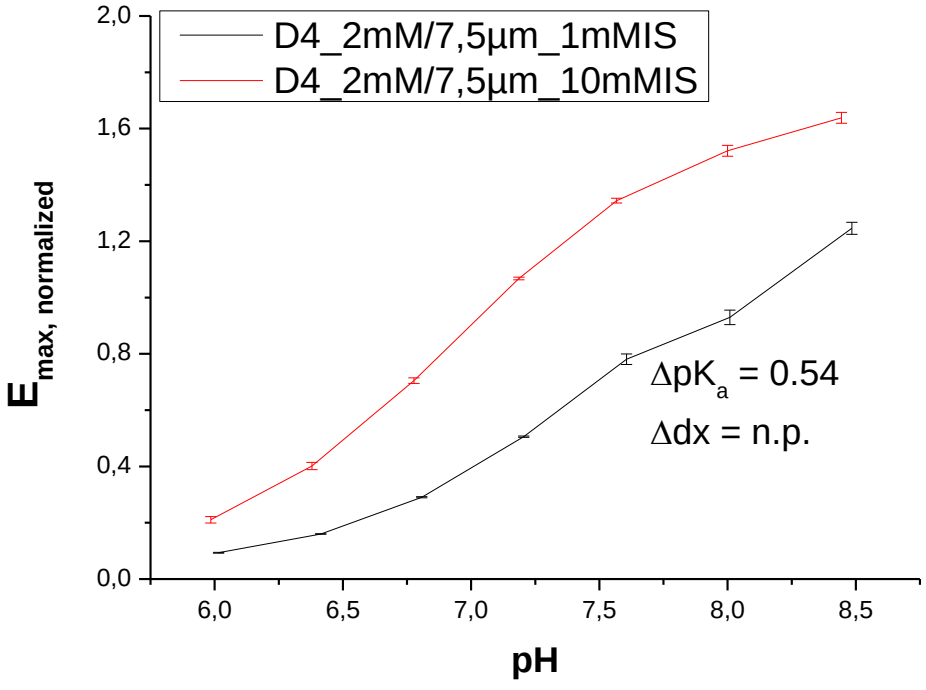

Figure 34: D4, 2 mM [dye] - titration measurements at 1 and 10 mM IS.

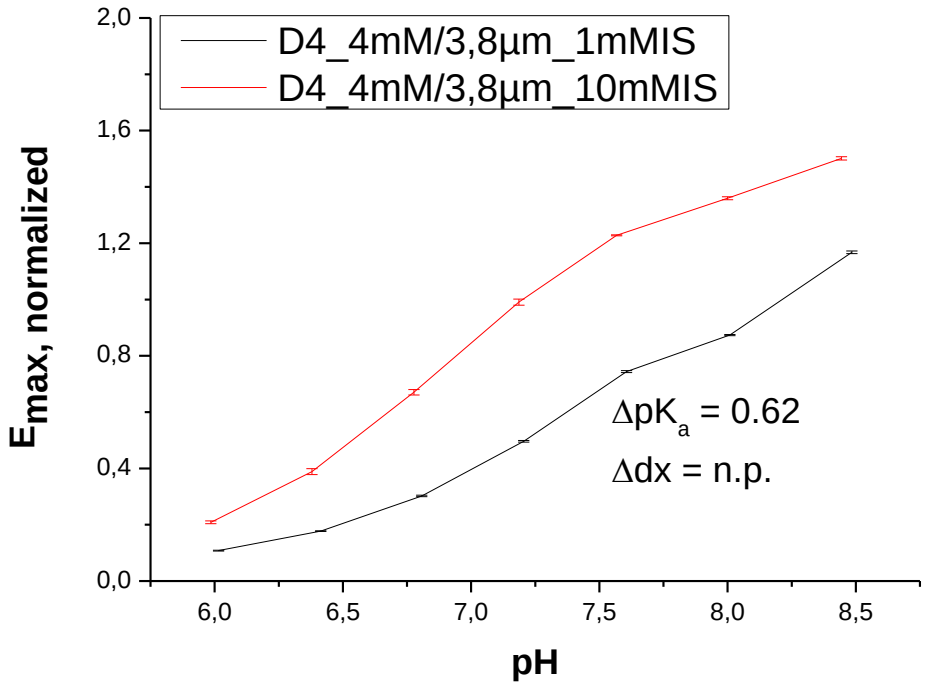

Figure 35: D4, 4 mM [dye] - titration measurements at 1 and 10 mM IS.

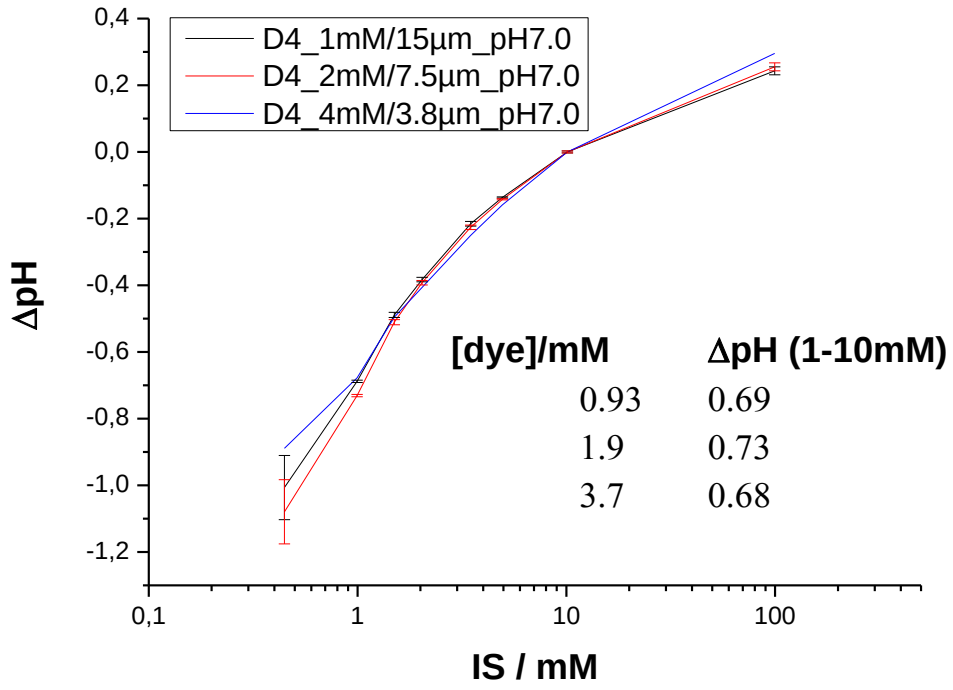

Figure 36: D4, pH7.0 – IS scanning experiments for all [dye].

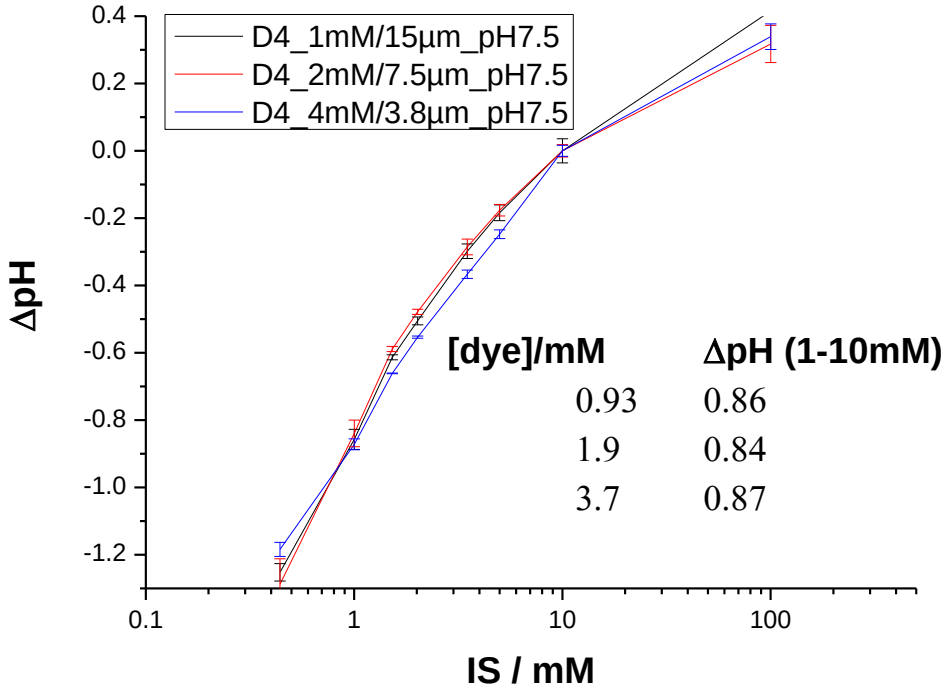

Figure 37: D4, pH7.5 – IS scanning experiments for all [dye].

Obviously, the pH range was not chosen broad enough for the 1 mM measurements of the D4 series. Thus, no values for Δdx can be given. The values for ΔpK_a from the curves in fig. 33, 34 and 35 go quite well together with the data from the IS scanning at pH 7.0 (fig. 36) being much higher than for D1 – around 0.7 units. As ΔpH at pH 7.5 gets even higher (up to around 0.85) than that for the IS scanning at pH 7.0 a flattening of the curve can be concluded again. Indeed, the graphs 33 to 35 would approve this. Obviously, none of the concentrations worked better than another one in the D4 hydrogel.

Jokic and coworkers found a very small pK_a shift in solution due to IS between 20 and 150 mM, namely 0.08 (37), yet it is clear that the effect gets much stronger when further decreasing IS. The pK_a values in the current experiments were all about 6.90 for 10 mM independent of the dye concentration. Jokic worked at about 4 mM dye concentration, so in the same concentration range, and found a pK_a of 6.73 in D4 for 20 mM IS. This shift of about 0.17 pH units quite well matches the current observations.

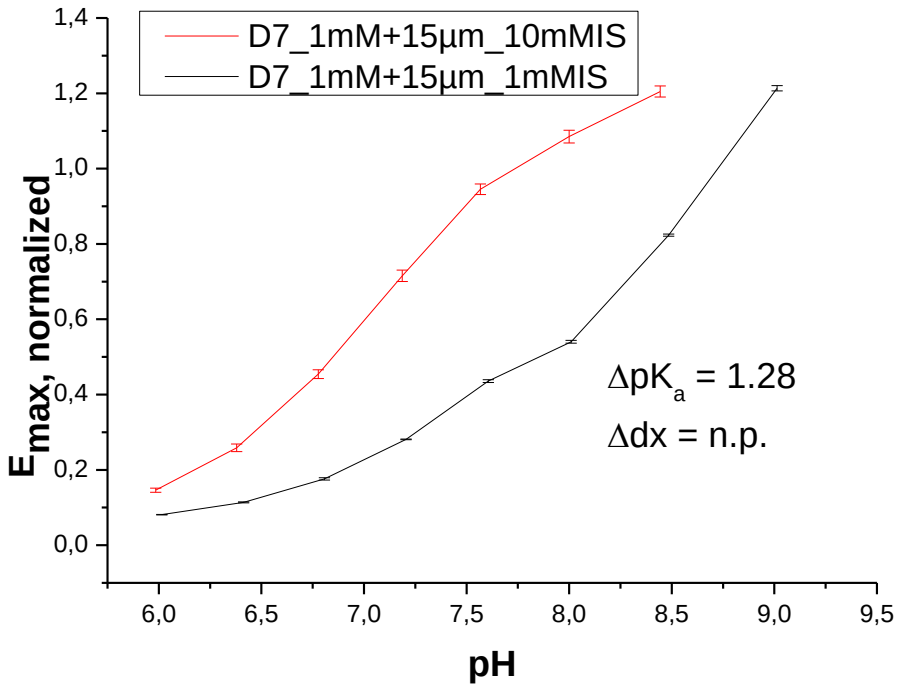

Figure 38: D7, 1 mM [dye] - titration measurements at 1 and 10 mM IS.

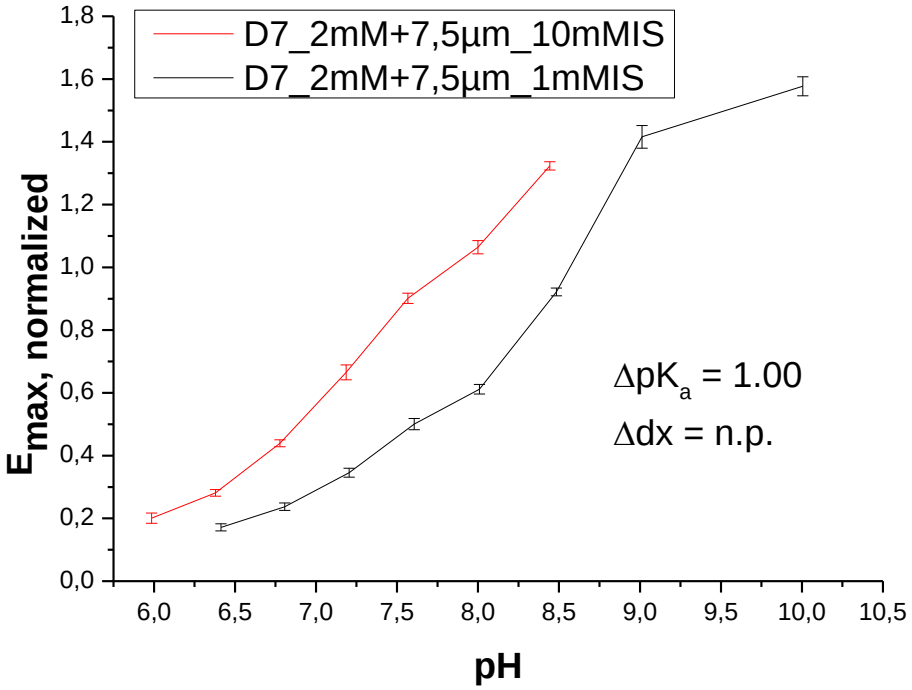

Figure 39: D7, 2 mM [dye] - titration measurements at 1 and 10 mM IS.

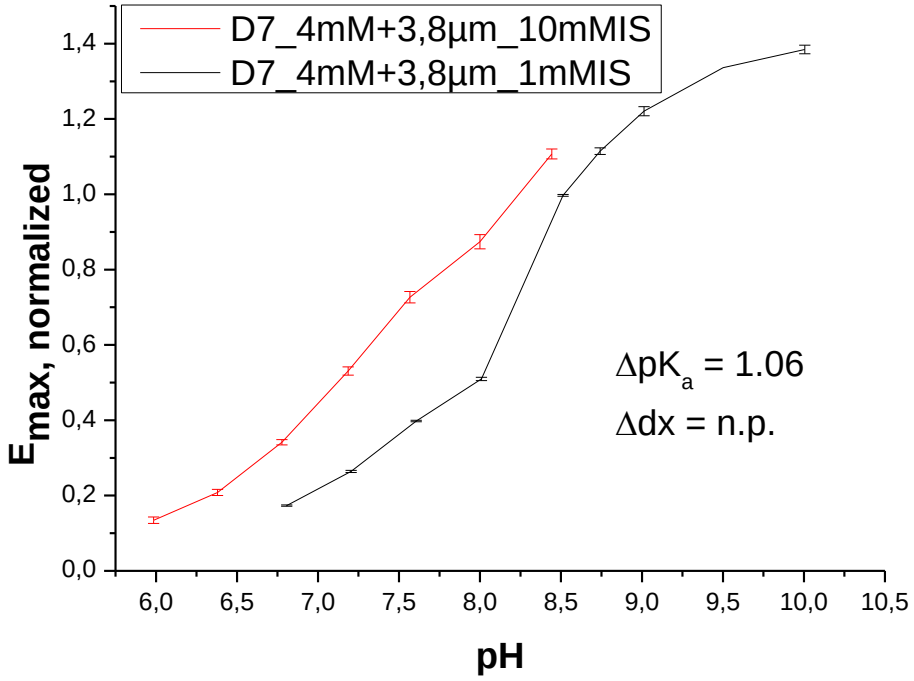

Figure 40: D7, 4 mM [dye] - titration measurements at 1 and 10 mM IS.

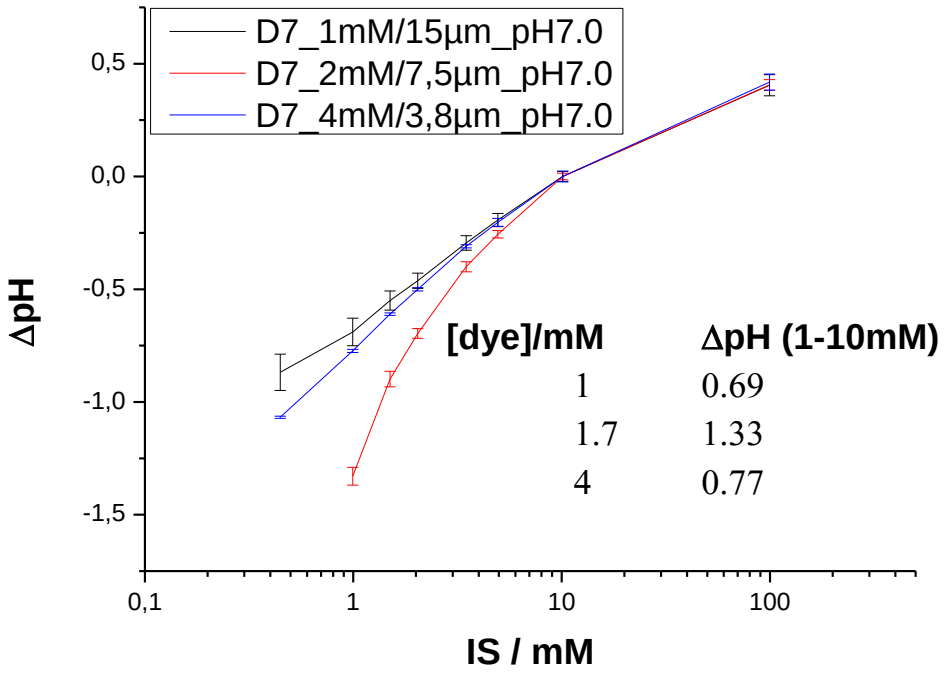

Figure 41: D7, pH7.0 – IS scanning experiments for all [dye].

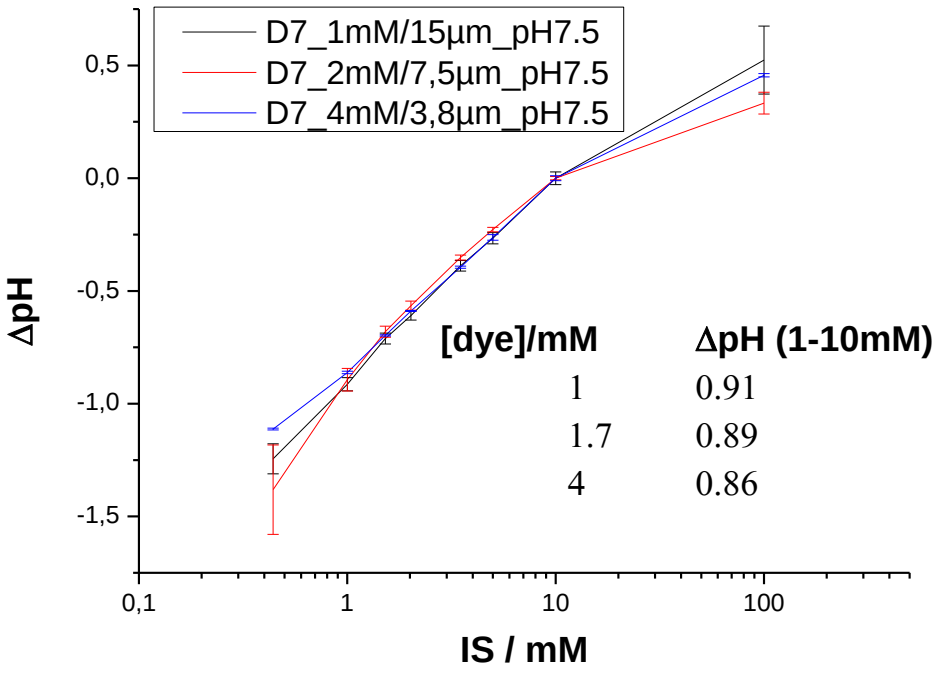

Figure 42: D7, pH7.5 – IS scanning experiments for all [dye].

The sensor with hydrogel D7 shows even greater deviations than the one with D4 when looking at the titration measurements. Yet, the problem of a too narrow pH range did not only occur for 1 but also for 10 mM IS. For 1 mM IS, it can be seen in the graphs that the very basic buffers (over 8.5) seem not to perfectely fit to the others (up to pH 8.5). The pK_a of the dye in D7 in 10 mM IS also lies further in the basic than it does in D4. So, all the values (except one) were recalculated with a fixed dx of 0.50. Also the calibration function for the IS scanning calculations works with recalculated values. Yet, the "raw" curves (fig. 38 to 40) alone already show extremely high big ΔpK_a shifts regardless of the calculated values – more than a whole pH unit. Yet, the values from the IS scanning experiments go together with the values for D4. The measurement at pH 7.0 for the sensor with 2 mM dye concentration does not fit to the other measurements at pH 7.0 for D7. Deviations get so high that the value for 0.5 mM could not even be calculated at all. On the other hand, the extreme deviation of more than a pH unit would fit to the values coming from the titration measurements. The values from the IS scanning experiments cannot even be compared directly: the curves at 1 and 10 mM IS rarely run parallelly. But the pH values are fixed to the same values for every sensor although every sensor exhibts a strongly different pK_a value (at least in different hydrogels). So, the distance between measurement pH and pK_a is not comparable. The most

important and unambiguous fact is that both hydrogels, D4 and D7 show exorbitantly large pK_a shifts and pH deviations, respectively.

The hydrogels of the D series are copolymers consisting of hydrophobic and hydrophilic domains. The ratio is determining the water uptake capabilities of the hydrogel. The water content decreases from D1 over D4 to D7 hypothesizing a connection to the behavior of the dyes embedded in them. The more water can be taken up, the higher the hydrogel's similarity to water. Consequently, the interface between solution and polymer, the surface, gets more diffuse resulting in a lower surface potential (see. equ. 34) and thus smaller IS dependent deviations. D4 and D7 take up less water than D1 leading to a more distinct surface, a higher surface potential and thus higher IS dependent pK_a shifts.

That no significant dependencies on the dye concentration could be found can have two reasons. On the one hand, the chosen concentrations are in the same range as the investigated IS range. On the other hand, the effective dye concentrations in the hydrogels are even higher. Local aggregation can be assumed in contrast to uniform distribution due to the hydrophobic domains of the polymers.

		10 mM IS			1 mM IS					ΔpH 1-10 mM	
	[dye] / mM	**pK_a**	**dx**	**correl.**	**pK_a**	**dx**	**correl.**	**ΔpK_a**	**Δdx**	**pH 7.0**	**pH 7.5**
D1	**1.0**	6.77	0.43	0.99994	7.02	0.47	0.99938	0.25	0.04	0.35	0.43
	1.8	6.79	0.45	0.99999	7.06	0.58	0.99958	0.28	0.13	0.27	0.42
	3.4	6.80	0.46	0.99997	7.14	0.53	0.99888	0.34	0.07	0.51	0.58
D4	**0.93**	6.90	0.43	0.99996	7.59*	0.50	-	0.69*	-	0.69	0.86
	1.9	6.95	0.47	0.99985	7.49	0.47	0,99889	0.54	0.00	0.73	0.84
	3.7	6.89	0.50	0.99754	7.51*	0.50	-	0.62*	-	0.68	0.87
D7	**1.0**	7.09	0.47	0.99944	8.37*	0.50	-	1.28*	-	0.69	0.91
	1.7	7.42*	0.50	-	8.42*	0.50	-	1.00*	-	1.33	0.89
	4.0	7.43*	0.50	-	8.49*	0.50	-	1.06*	-	0.77	0.86

Table 11: Summarized data for all absorption measurements. Values with asterisk are derived from recalculations with a dx value fixed at 0.50.

4.4 Fluorescence measurements (FM)

4.4.1 FM using a dye concentration of 0.1 mM in the D1 hydrogel

Measurements were performed over several days. The sensors were stored either in distilled water or in a buffer around pH 7.0 and 1 mM IS. It could be observed that the signal decreased over days. Dye leaching from D4 hydrogel was already observed by Jokic (37). There is no problem with the neutral form of the dye which is too hydrophobic to dissolve into water observably in the observed time. Yet, it happens to the charged form.

Fig. 43 (left graph) shows four pH curves recorded at 1 mM IS. Curve S2_B was recorded a day after the first one S2_A. The lowest curve S2_C was recorded another four days later. Yet, all the curves very well match regarding the values for pK_a and dx - even the two different sensors, S1 and S2, which states good reproducibility. Dye leaching is the best explanation for the signal decrease as photodegradation can be excluded. There was no illumination over the night and the weekend, respectively.

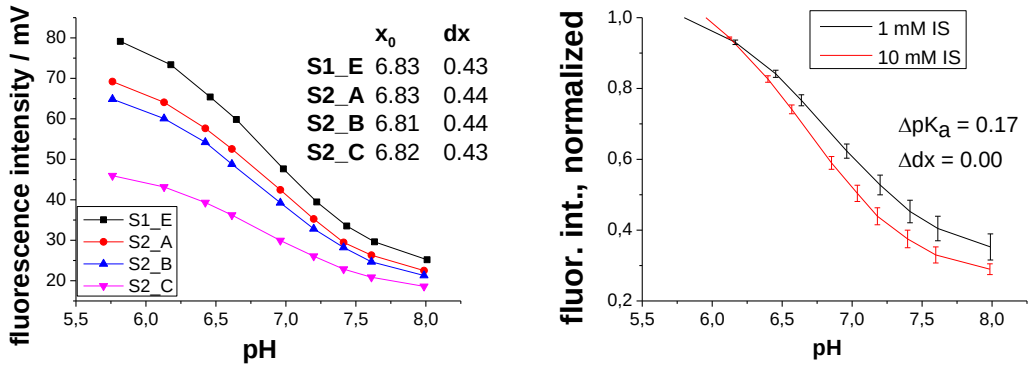

Figure 43: fiber sensor (D1, 0.1 mM [dye]); left: pH curves of two sensors at 1 mM IS with time lags of a day between S2_A and B and another four days to S2_C; right: Normalization of S2_A-B from the left side compared to the normalized curve related to 10 mM IS.

As all the parameters, above all x_0 and dx, were very close to each other for the curves, normalization was performed by the highest value. After that, averaging could be performed. Fig. 43 (right) also shows the normalized pH curves at 1 and 10 mM. The fits gave were good correlation coefficients (see table 12). ΔpK_a was 0.17 which is indeed lower than for all the other absorption measurements.

The further figures 44 and 45 for were already shown before. But here, they further contain the pH deviation curves which could be achieved at 0.1 Mm dye concentration. At pH 7.0, the single curves are given. No triple determination was performed but two repeat determinations for two different sensors showing good reproducibility although preparation by dip-coating was try-and-error handwork because of the low signals achieved. At pH 7.5, the measurements could just be performed with one of the sensors as the other sensor broke. Yet, a quadruple determination was performed here.

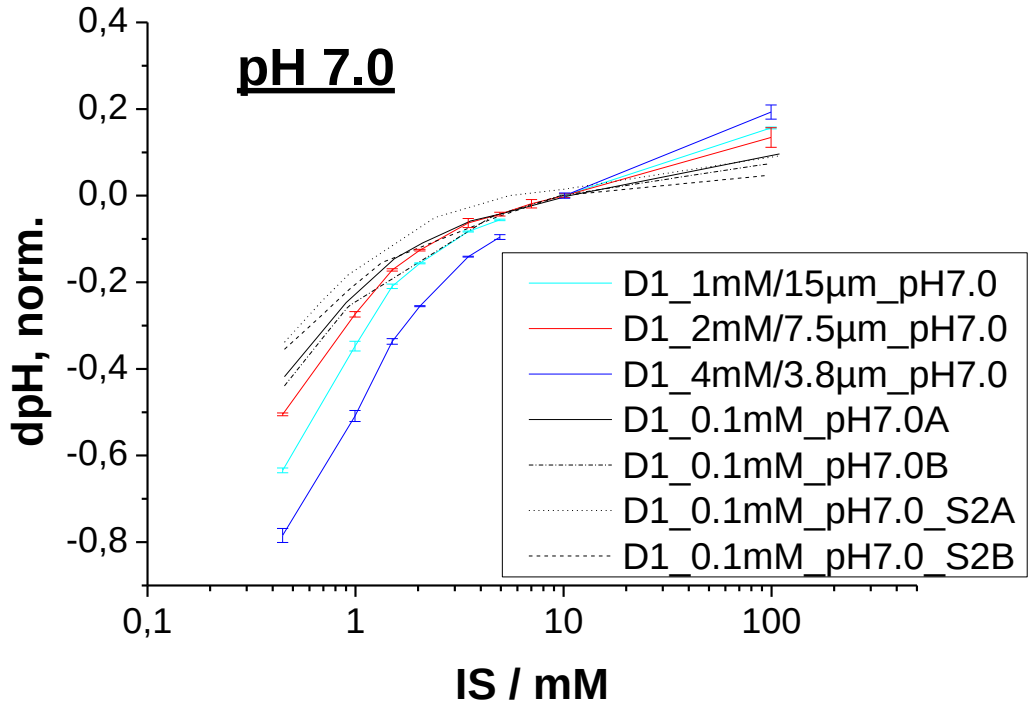

Figure 44: D1, pH7.0 – IS scanning experiments for all [dye] including 0.1 mM.

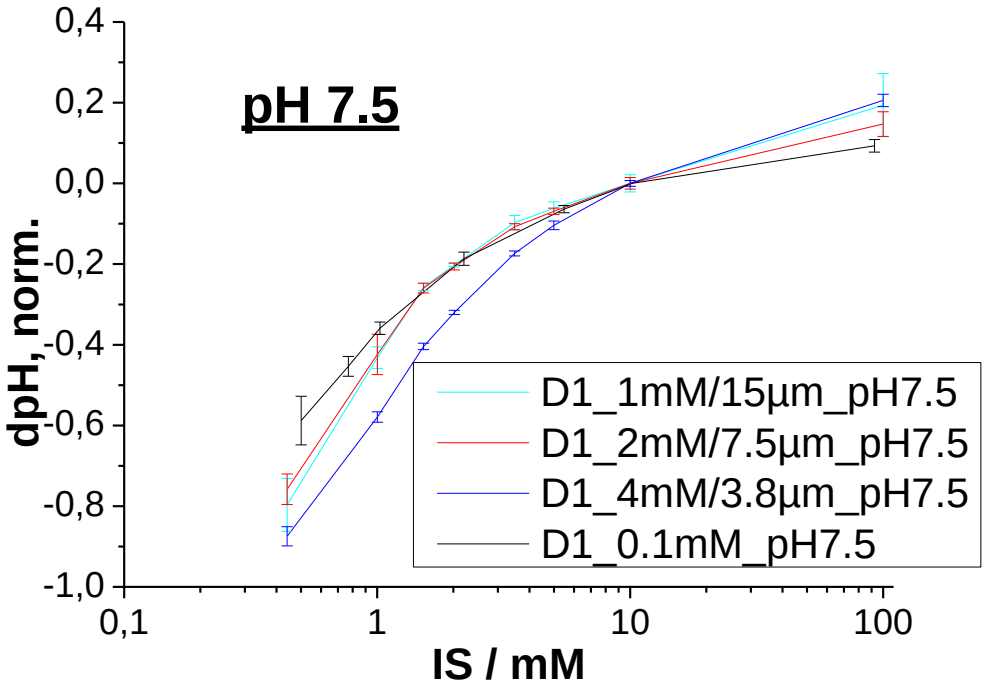

Figure 45: D1, pH7.5 – IS scanning experiments for all [dye] including 0.1 mM.

It can be seen that the results are better than in the absorption measurements, the pK_a shift gets smaller as well as the pH deviations. Yet, they are still not as low as 0.05 pH units between 1 and 10 mM which could be expected for an ideal system. Thus, the decrease in dye concentration is still not enough to optimize the system. Table 12 shows the collected data comparing it with the best results of the absorption measurements. ΔpK_a could be reduced from 0.25 to 0.17, ΔpH at pH 7.0 from 0.35 down to 0.23 and from 0.43 down to 0.35 at pH 7.5. A slight flattening of the curve could also be derived from the ΔpH values (in contrast to the ΔpK_a values). The worth of these better ΔpH values is even increased because two details have been ignored so far: a) the actual IS that was compared with 10 mM was 0.9 and not 1.0 mM and b) the pK_a slightly shifted to the acidic. Both of these facts actually have 'negative' influence: for 0.9 mM IS the deviation from 10 mM would be higher than for 1.0 mM; and as the pK_a is shifted to the acidic the deviation at the fixed pH values of 7.0 and 7.5 are also expected to be slightly higher than they would be in the same distance from the pK_a value. These additional facts increase the reliability of these values.

Jokic could observe a strong pK_a shift of 0.65 for the current dye when measuring pK_a via fluorescence and not absorption. This shift could be due to Förster resonance energy transfer (FRET) which is a concentration dependent effect. Thus, it could also be expected in the current experiments, which is indeed the case. Yet, the effect is just as small as 0.1 to 0.2 pH units. This, in turn, is because the dye concentrations (1.0 and 0.1 mM) are a manifold smaller than they were in Jokic's experiments (about 4mM). As just the acidic form of the dye is fluorescent, photoinduced proton transfer could also be a possible reason for lowering the apparent pK_a.

		10 mM IS			1 mM IS					ΔpH 1-10 mM	
	[dye] / mM	pK_a	dx	correl.	pK_a	dx	correl.	ΔpK_a	Δdx	pH 7.0	pH 7.5
D1	1	6.77	0.43	0.99994	7.02	0.47	0.99938	0.25	0.04	0.35	0.43
	0.1	6.66	0.40	0.99990	6.83	0.40	0.99984	0.17	0.00	0.23	0.35

Table 12: Collected data of the fiber optic fluorescence measurements with D1 hydrogel and a [dye] of 0.1 mM comparing it with the best results of the absorption measurements at 1 mM [dye].

4.4.2 FM using a dye concentration of 1.0 mM in polyacryloylmorpholine

The pH curves at 1 and 10 mM IS recorded with two different sensors simultaneously are shown in fig. 46. Both sensors represent the same measurement, the dotted curves the repeat measurements of each sensor.

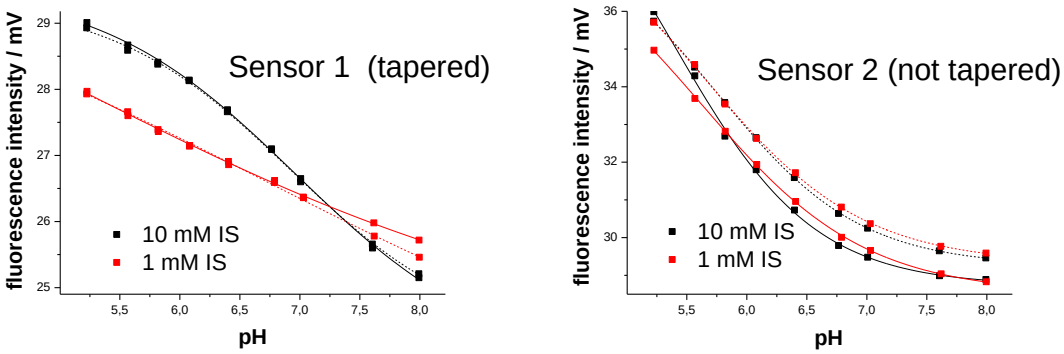

Figure 46: Titration measurements of two sensors at 1 and 10 mM IS. The continuous and the dotted lines just represent repeat measurements.

The sensors both showed good pH responses, these responses, however, differed drastically. Reproducibility lacked completely, which makes the measurements almost useless as both should actually give the same information. The non-tapered sensor (S2) is far from reaching a plateau in the measured pH range. As the same buffer substance had to be

used for the whole titration a decrease further than pH 5.2 was not possible. S2 would suggest a pK_a value between 5.4 and 5.8 which is much further in the acidic than it could be expected. For S1 (the tapered sensor), the suggested pK_a would be between 6.9 and 7.0 at 10 mM IS. At 1 mM IS, S1 showed almost linear behavior across the whole investigated pH range. For one of the repeat measurements, no reasonable pK_a could be calculated, for the other one it was 5.05, which is not really reasonable actually either. At which signal the curves started was decided each time anew. It was always the aim to await equilibrium in the form of a plateau. Yet, it did not take the same time for both sensors. S2 seemed to be quicker than S1. Yet, while waiting for a constant signal in S1 the signal of S2 once started to decrease again slightly. So, it was tried to find a good compromise in starting the measurements. The signals were still slightly decreasing when starting the measurement after waiting at least half an hour within all the measurements. After the single titration steps, the raw signals reached plateaus quite well. This was not always the case. When measurements were tried with S1 first, there always was a sensor drift upwards instead of a plateau. A similar effect was observed once in the fiber sensor using hydrogel D1. Thus, the sensors sometimes seem to need some conditioning time after being dipped into an aqueous solution for the first time for unknown reasons.

In any case, quite reproducible measurements could be performed with S1, with S2 too but with a signal offset. In S1, it seems that the main difference between the shapes of the curves due to different IS was the slope. The curve extremely flattened at 1 mM. For S2, this was not the case. Actually, this sensor seemed to work IS independent, which would actually be the desired aim. However, these sensors' behaviors have to be doubted due to their dissimilarity. A reason for that is tried to be given in the following passage.

Whether the fiber was tapered or not cannot result in such a huge difference. Actually, this should have no influence on the response but just on the signal intensity. Parallel measurements were done on the institute with the same matrix and this dye showing many problems. It can be concluded that the main problem for the sensor is the polymerization partly destroying the dye. The UV light is probably no problem as the dye is not affected by UV light regarding its absorption spectrum. Yet, the radical starter could attack the OH group of the dye and destroy its pH sensor capabilities. It is not known which derivatives and how many of those are built resulting in fluorescence that is disturbing the pH measurements but

which is not reproducible within polymerizations. There could be observed some IS dependency for the current two sensors for sure. Yet, results could not be used for any significant statement as no reliable statement can be derived even from these basic measurements.

5 Conclusion and outlook

For the special application of measuring sensor foils under air exclusion, a flow through system for measurements at controlled constant temperature has been developed. The system is easily accessible for further applications such as investigations of T dependency. The prototype-like flow rate control could be exchanged for a simpler setting of a constant flow rate. In the current case, the setup fulfilled its main purpose of excluding air. Flow rate control was possible but there were problems keeping it constant over time. Thus, automation was not fully possible which it basically should be according to theory. Several problems with the delivered software could be overcome.

The main application with which the measurement setup was tested were experiments to investigate IS dependency of different matrix dye concentration combinations. None of the nine combinations of the hydrogels D1, D4 and D7 with dye concentrations of about 1, 2 and 4 mM showed pH responses even close to what would be possible theoretically regarding the Debye-Hückel equation. Significant differences neither could be found between the hydrogels D4 and D7 nor between their dye contents. The pK_a shifts and the pH deviations at pH 7.0 and 7.5 range from 0.6 to 1.0 pH units. Smaller deviations can be achieved with the hydrogel D1 which contains the most hydrophilic domains as it can take up water up to 70 % of its own volume. Thus, D1 is the most ‘waterlike’ of the compared hydrogels leading to the smallest surface potential and consequently to the smallest deviation.

The reason that none of these polymers showed really good results is partly not due to the polymers itself but to the fact that the chosen concentrations – which were necessary to get reasonable absorption signals on the photometer – were within the IS range that actually should be investigated leading to distortion of the results. Besides, the hydrogels consist of chemically different domains, hydrophilic and hydrophobic ones leading to dye accumulation in the hydrophobic domains instead of uniform distribution. Thus, it can be assumed that the

local dye concentrations are higher than the intended 1, 2 or 4 mM. Further, distribution effects between the differently polar domains could occur upon (de)protonating the dye.

Another try was undertaken to decrease the dye concentration down to 0.1 mM, which was investigated in D1 hydrogel showing the best performance beforehand. Absorption measurements were not possible any more as the layer on a sensor foil could not be prepared that thick; besides response time would grow immensely. So, it was changed to measuring fluorescence intensity via a glass fiber sensor. The signals that could be reached by that were very low, still they could be used. The results were better than for the much higher concentration. ΔpK_a could be brought down from 0.25 (best result within the absorption measurements) to 0.17. However, about 0.05 should be possible according to theory.

The next step was trying another hydrogel where the dye could potentially be uniquely distributed. The polymer – a cross-linked polyacryloylmorpholine – does not consist of different domains so the whole polymer should take the dye and the whole polymer should swell in water at the same time. This should result in a waterlike surrounding for the dye suggested to be the best surrounding as the pK_a shift of 0.05 in previous experiments was measured in aqueous dye solutions and any surface potential could really be set zero as there should be no distinct surface any more.

Yet, the first problem was to get a signal high enough for reasonable measurements. This was not as easy as before where dip-coating could be applied to the same sensor tip more often repeatedly. In this case, the sensor matrix containing the dye was polymerized onto a silanised glass fiber tip. So, the used dye concentration was increased to 1 mM again. Finally, reasonable signals could be achieved and measurements were performed with two sensors parallelly. Both sensors of course showed pH sensing capabilities. Yet, their behaviors were highly apart from each other. None of both showed a shift as it was expected. The one sensor showed a drastic flattening, the other one actually no dependency of IS between 1 and 10 mM. Yet, these results cannot be used as the sensors should actually behave in the same way. Problems in the combination of polyacryloylmorpholino and the aza-bodipy dyes already arose in parallel experiments in the group. The hydroxyl group of the sensor dye is probably attacked by the radical starter during the polymerization resulting in an unknown and irreproducible mixture of pH sensitive dye and not pH sensitive derivatives finally ending

up in useless – irreproducible – pH curves. For avoiding that, the hydroxyl group must be protected before deprotecting it again in the final sensor. Still, parallel experiments show further problems concerning leaching and potential aggregation of the dye. It is supposed that aggregation events could be favored in the polymerization cocktail when the hydroxyl group is protected by an acetyl group as the dye thus gets even more hydrophobic.

Consequently, a way has to be found how the fiber sensor can be prepared reproducibly without any effects of aggregation, leaching and above all destruction of the dye. Protecting the OH group will have to be a part of this way. Leaching will be completely avoided when it will finally be possible to link the dye to the polymer matrix covalently.

A different way which was eventually not chosen for the current experiments would be the embedding of the dye in a hydrogel containing charges itself. So, a relatively high 'background IS' would be there in any case so that the response for all low IS solutions would be the same. This hydrogel must not be soluble in water still or covalently linked to a carrier. The indicator molecule would probably also have to be covalently linked/copolymerized then. The behavior of such a sensor either containing negative, positive or zwitterionic charges has to be investigated.

6 References

1. Janata J. Do optical sensors really measure pH? Anal. Chem. 1987;59(9):1351–6.

2. Rovati L, Fabbri P, Ferrari L, Pilati F. Plastic Optical Fiber pH Sensor Using a Sol-Gel Sensing Matrix. In: Yasin M, Herausgeber. Fiber Opt. Sensors [Internet]. InTech; 2012 [cited on june 10th, 2013]. URL: http://www.intechopen.com/books/fiber-optic-sensors/plastic-optical-fiber-ph-sensor-using-a-sol-gel-sensing-matrix

3. Gargas J. Aquarium pH adjustment apparatus. US Patent: US5529751A. 1997.

4. Cactus and Alkalinity [Internet]. [cited on june 10th, 2013]. Verfügbar unter: http://ralph.cs.cf.ac.uk/cacti/Cactus%20and%20Alkalinity.pdf

5. Narayanaswamy R, Wolfbeis OS. Optical Sensors: Industrial, Environmental and Diagnostic Applications. 2004. Springer.

6. Leiner MJP, Hartmann P. Theory and practice in optical pH sensing. Sensors Actuators B Chem. 1993;11(1–3):281–9.

7. Weidgans BM. New fluorescent optical pH sensors with minimal effects of ionic strength [Internet] [phd]. 2004 [cited on may 3rd, 2013]. URL: http://epub.uni-regensburg.de/10233/

8. Lin J. Recent development and applications of optical and fiber-optic pH sensors. Trac Trends Anal. Chem. 2000;19(9):541–52.

9. HACH [Internet]. [cited on april 23rd, 2013]. URL: http://www.hach.com/asset-get.download-en.jsa?code=62144

10. Thermoscientific [Internet]. [cited on may 10th, 2013]. URL: https://static.thermoscientific.com/images/D16873~.pdf

11. Cycle Chemistry pH Measurement [Internet]. [cited on may 3rd, 2013]. URL: http://www.snowpure.com/docs/thornton-high-purity-ph.pdf

12. High-Purity Water and pH [Internet]. [cited on april 22nd, 2013]. URL: http://www.millipore.com/references/files/pmc_url/$file/highpuritywater.pdf

13. Yuan S. Optimization of a Submersible Autonomous Spectrophotometric Sensor for PH Measurements in Low Ionic Strength Freshwater. University of Montana; 2006.

14. Opitz N, Lübbers DW. New fluorescence photometrical techniques for simultaneous and continuous measurements of ionic strength and hydrogen ion activities. Sensors Actuators. 1983;4:473–9.

15. Wolfbeis OS, Offenbacher H. Fluorescence sensor for monitoring ionic strength and physiological pH values. Sensors Actuators. 1986;9(1):85–91.

16. Weidgans BM, Krause C, Klimant I, Wolfbeis OS. Fluorescent pH sensors with negligible sensitivity to ionic strength. The Analyst. 2004;129(7):645.

17. Vishnoi G, Goel TC, Pillai PKC. pH optrode for the complete working range. 1999;319–25.

18. Korostynska O, Arshak K, Gill E, Arshak A. State Key Laboratory of Nonlinear Mechanics (LNM), Institute of Mechanics, Chinese Academy of Sciences, Beijing 100080, China. Sensors. 2007;7(12):3027–42.

19. Gründler P. Chemische Sensoren: Eine Einführung für Naturwissenschaftler und Ingenieure. 2004. Springer.

20. Hulanicki A, Glab S, Ingman F. Chemical sensors: definitions and classification. Pure Appl. Chem. 1991;63(9):1247–50.

21. Wolfbeis OS, Lukosz W, Kasche V, Ulrich R, Simon W, Morf WE, u. a. Symposium 6: Optodes and other new sensors in biochemical analysis. Fresenius J. Anal. Chem. 1990;337(1):23–7.

22. Sauerbrey G. Verwendung von Schwingquarzen zur Wägung dünner Schichten und zur Mikrowägung. Z. Für Phys. 1959;155(2):206–22.

23. Valeur B. Molecular Fluorescence: Principles and Applications: An Introduction. 1st edition. 2001. Wiley-VCH Verlag GmbH & Co. KGaA.

24. Atkins PW, Paula J de. Physikalische Chemie. 4th comp. rev. edition. 2006. Wiley-VCH Verlag GmbH & Co. KGaA.

25. Auzel F. Upconversion and Anti-Stokes Processes with f and d Ions in Solids. Chem. Rev. 2004;104(1):139–74.

26. Abella ID. Optical Double-Photon Absorption in Cesium Vapor. Phys. Rev. Lett. 1962;9(11):453–5.

27. Klimant I, Huber C, Liebsch G, Neurauter G, Stangelmayer A, Wolfbeis OS. Dual Lifetime Referencing (DLR) — a New Scheme for Converting Fluorescence Intensity into a Frequency-Domain or Time-Domain Information. In: Valeur B, Brochon J-C, Herausgeber. New Trends Fluoresc. Spectrosc. [Internet]. Berlin, Heidelberg: Springer Berlin Heidelberg; 2001 [cited on june 9th 2013]. S. 257–74. URL: http://link.springer.com/content/pdf/10.1007%2F978-3-642-56853-4_13.pdf

28. Borisov SM, Wolfbeis OS. Optical Biosensors. Chem. 2008;108(2):423–61.

29. Borisov SM, Mayr T, Karasyov AA, Klimant I, Chojnacki P, Moser C, u. a. New Plastic Microparticles and Nanoparticles for Fluorescent Sensing and Encoding. In: Berberan-Santos MN, Herausgeber. Fluoresc. Supermolecules Polym. Nanosyst. [Internet]. Springer Berlin Heidelberg; 2008 [cited on june 9th 2013]. S. 431–63. URL: http://link.springer.com/chapter/10.1007/4243_2007_013

30. Aqion [Internet]. [cited on may 3rd, 2013]. URL: http://www.aqion.de/site/44%20+%20DIN%2038404-C10R3

31. Riedel E, Janiak C. Anorganische Chemie. 6th edition. 2007. Gruyter.

32. Hütter LA. Wasser und Wasseruntersuchung. 1994. Diesterweg.

33. High-Purity Water and pH [Internet]. [cited on april 22nd, 2013]. URL: http://www.millipore.com/references/files/pmc_url/$file/highpuritywater.pdf

34. Beynon PR, Easterby J. Buffer Solutions. THE BASICS. 1996. Taylor & Francis.

35. Good NE, Winget GD, Winter W, Connolly TN, Izawa S, Singh RMM. Hydrogen Ion Buffers for Biological Research*. Biochemistry (Mosc.). 1966;5(2):467–77.

36. Green FJ. The Sigma-Aldrich Handbook of Stains, Dyes and Indicators. 1990. Aldrich Chem Co Library.

37. Jokic T, Borisov SM, Saf R, Nielsen DA, Kühl M, Klimant I. Highly Photostable Near-Infrared Fluorescent pH Indicators and Sensors Based on BF2-Chelated Tetraarylazadipyrromethene Dyes. Anal. Chem. 2012;84(15):6723–30.

38. Yari A, Dinarvand M. Sol-gel film doped with bromopyrogallol red as a highly sensitive sensing element for a new pH optical sensor. J. Iran. Chem. Soc. 2011;8(4):1091–7.

39. Hoffman AS. Hydrogels for biomedical applications. Adv. Drug Deliv. Rev. 2002;54(1):3–12.

40. Haesun Park, Kinam Park. Hydrogels in Bioapplications. Hydrogels Biodegrad. Polym. Bioapplications [Internet]. American Chemical Society; 1996 [cited on april 22nd, 2013]. S. 2–10. URL: http://dx.doi.org/10.1021/bk-1996-0627.ch001

41. Buffer calculator [Internet]. [cited on may 10th, 2013]. URL: http://www.liv.ac.uk/buffers/buffercalc.html

42. BioBuffer.pdf [Internet]. [cited on may 3rd, 2013]. URL: http://www.applichem.com/fileadmin/Broschueren/BioBuffer.pdf

43. Abel T, Sagmeister M, Lamprecht B, Kraker E, Köstler S, Ungerböck B, u. a. Filter-free integrated sensor array based on luminescence and absorbance measurements using ring-shaped organic photodiodes. Anal. Bioanal. Chem. 2012;404(10):2841–9.

44. HydroMed.pdf [Internet]. [cited on may 3rd, 2013]. URL: http://www.advbiomaterials.com/products/hydrophilic/HydroMed.pdf

45. Tian Y, Shumway BR, Cody Youngbull A, Li Y, Jen AK-Y, Johnson RH, u. a. Dually fluorescent sensing of pH and dissolved oxygen using a membrane made from polymerizable sensing monomers. Sensors Actuators B Chem. 2010;147(2):714–22.

8 Appendix

8.1 Further informations and data

8.1.1 Step-by-step instruction for the new measurement setup

The following steps had to be performed one after the other. Changing the order is partly but not generally possible as the flow and the flow rate, respectively, depend on more than just one handle. All these steps are necessary if dissolution of any gasses from the air into the measurement solution should be avoided.

1. Settings at the beginning in the flow order of the setup:
    - Start the computer and the thermostating bath and plug in the extra pump in the bath (= starting it)
    - Start the photometer software, the Firesting software and the selector software
    - Nitrogen main valve – closed
    - Nitrogen connection tube right before the pressure reduction valve – interrupted (tube clamp) – (just in case it is the only nitrogen connection available)
    - Nitrogen connection tube to the wash bottle – open – (just in case it is the only nitrogen connection available)
    - Pressure reduction manifold – any setting
    - Valve at the entrance of the valved distribution manifold – closed
    - Valves to the solution bottles – any setting
    - Rheodyne selector – remote control for operating via the computer, any position
    - Needle valve – closed (position as it is shown in fig. 12f)
    - 3-way valve – closed (open between waste and FTC)
    - Thermostatic bath – set to 24.1 °C (for measurements at 25.0 °C)
2. Buffer preparation:
    2.1. For buffer nitrogenation, the tubing coming from the wash bottle is inserted into the first buffer[7]
    2.2. A calibrated oxygen sensor connected to the Firesting is inserted into the first buffer.

[7] If another nitrogen line is closely available it is handier to use this and ignore the distribution in the setup. Thus, a slight overpressure could be applied to each bottle even during the connection to the system.

2.3. Nitrogen flow is started at a low grade and pressure is regulated till proper perfusion of the buffer is given (= so high that nothing splashes out of the bottle)

2.4. When the oxygen level has reached its plateau at about 0 % oxygen/air saturation the buffer can be inserted into the system. For that, the plug on the distinct position has to be lightly wetted.

2.5. After the nitrogen tube was wiped off to get no contamination into the next solution, steps 2.1 – 2.5 are repeated for the rest of the present solutions.

2.6. The tenth position where a last measurement solution could be inserted should be filled with an empty bottle (or containing a buffer that is just used in another experiment) if an automatic stop after an automated measurement is desired.

3. A foil[8] is inserted into the clip system of the FTC plug from the left to the right (handle down, clip system upwards) that the sensor layer does not get scratched.
4. The FTC plug can be inserted into the FTC to finally close the system. The O-ring of the plug must be greased lightly.
5. <u>Software:</u>

   5.1. The settings in the photometer software must be chosen. The baseline is either recorded anew now or it is loaded.

   5.2. If possible or desired the selector software – the order in which positions are selected in which interval – can be programmed. For automated stopping, a position (preferably 10) must be chosen where there is no pressure applied.

   5.3. The temperature offset must be inserted into the Firesting software each time anew. If wished, locking data to a file can already be started now.

6. <u>Settings right before the measurement</u> in the order of the setup:

   - Nitrogen main valve – open
   - Nitrogen connection tube in front of the pressure reduction valve – open
   - Nitrogen connection tube to the wash bottle – interrupted (tube clamp)
   - Pressure reduction manifold – desired pressure (see fig. 27)
   - Valve at the entrance of the valved distribution manifold – open
   - Valves to the solution bottles – open which are to be used, closed which will not be used
   - Rheodyne selector – at the position of the buffer which should enter the FTC first

[8] A blank foil at the first measurement of a series!

- Needle valve – open as far as it is desired (see. fig. 12)
- 3-way valve – closed (open between waste and FTC)

7. Starting the measurement:
   7.1. Make sure that the photometer software is ready to start recording. Consider when start is reasonable, probably when buffer will cover the sensor in the FTC for the first time if you wish not to get any spectra on air.
   7.2. Open 3-way valve by a 180° turn. Shortly after that, a few bubbles from the valve will run through the measurement. They do not disturb the measurements usually as they just run through the inner chamber.
8. Changing the measurement solutions is done via the selector either manually or remote by the inserted program. There will be bubbles running through the FTC after each change if it is the first measurement with this configuration as the capillaries between bottles and selector were empty before.
9. The measurement is either stopped manually by turning the 3-way valve or by the program when a position is chosen as the last one where there is no pressure applied. Just closing any valve on the pressure side of the system does not stop the flow immediately as there still is overpressure after closing it, of course.
10. After stopping a measurement, the main nitrogen valve should be closed.
11. Bottles can be removed. One should be aware that there was overpressure applied. So – as the system is supposed to be dense – opening the first bottle should be accompanied by a blop sound.
12. Before inserting the bottles for the next measurement and repeating the described steps, the system should be emptied. This works by connecting any syringe via any appropriate tube to the end of the system (the capillary going from the FTC to the waste) and pushing air through the system. It has to be emptied if the sensor has to be changed. Otherwise, emptying can be skipped if exchanging the residual solutions in the capillaries plus the remaining solution in the inner chamber just in the course of the measurement

does not virtually effect the measurements.[9] This can also be the way of choice if bubbles should generally be avoided. Then, measurement is not started via the 3-way valve (which should be open already) but via opening the needle valve or the selector (if it was at first set to a position e.g. 10 where there is no pressure applied).

8.1.2 Absorption measurements – performed raw data

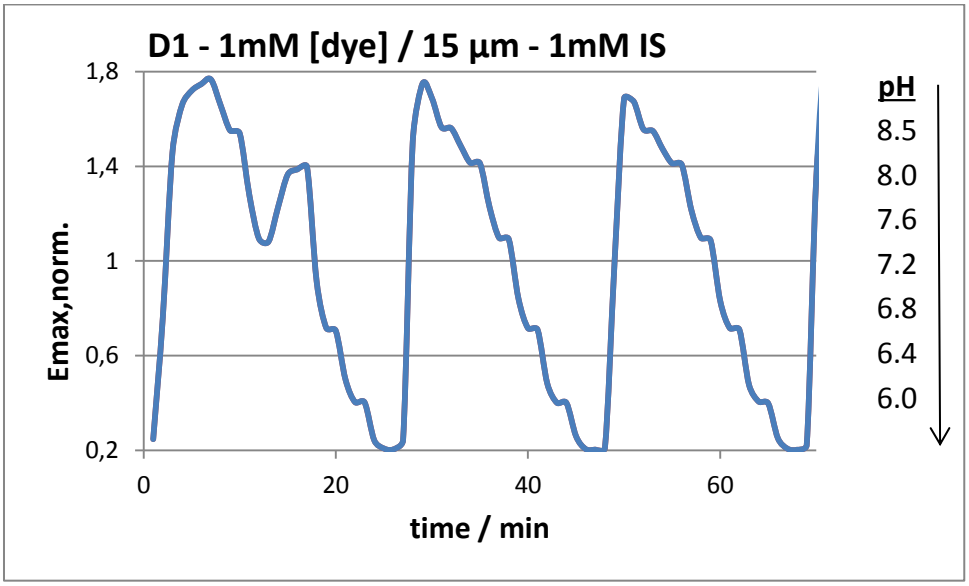

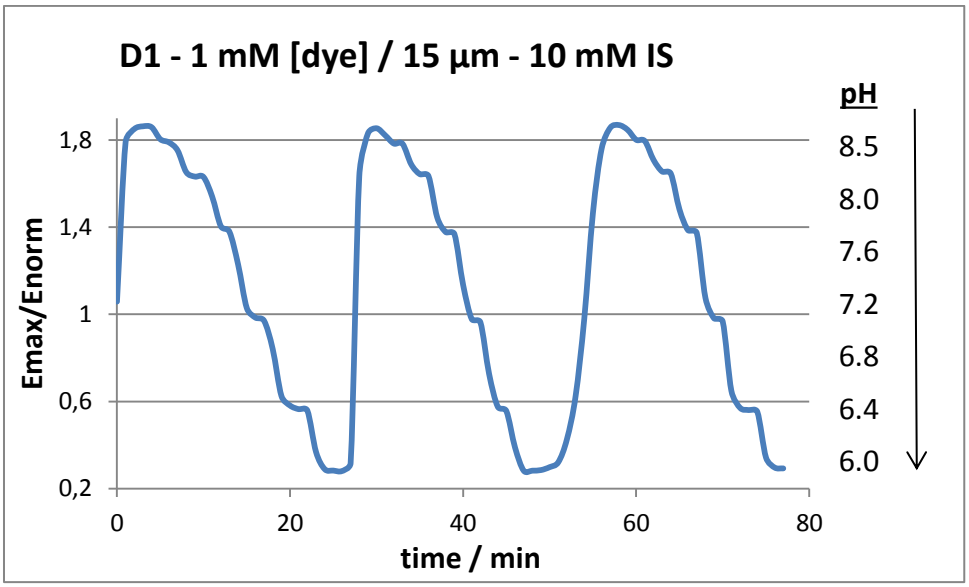

[9] It can lead to data (spectra) which cannot be explained by solely looking at the currently used solutions; e.g. signal decreases with each new buffer over time but right of the beginning of each buffer it slightly increases before the final decrease because of the old solutions in the capillaries. Yet this should not affect a plateau that should be reached.

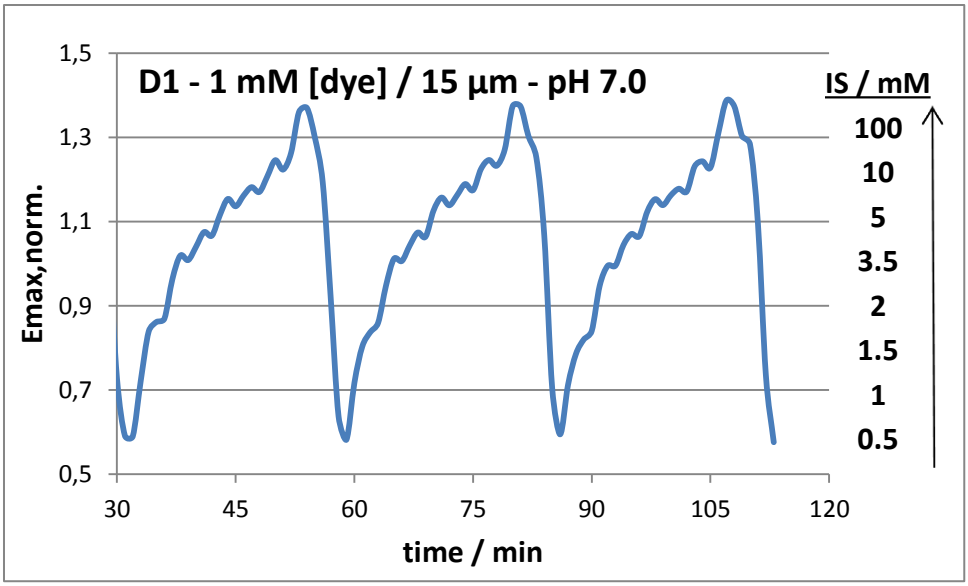
D1 - 1 mM [dye] / 15 µm - pH 7.0
Emax,norm.
1,5
1,3
1,1
0,9
0,7
0,5
30
45
60
75
90
105
120
time / min
IS / mM
100
10
5
3.5
2
1.5
1
0.5

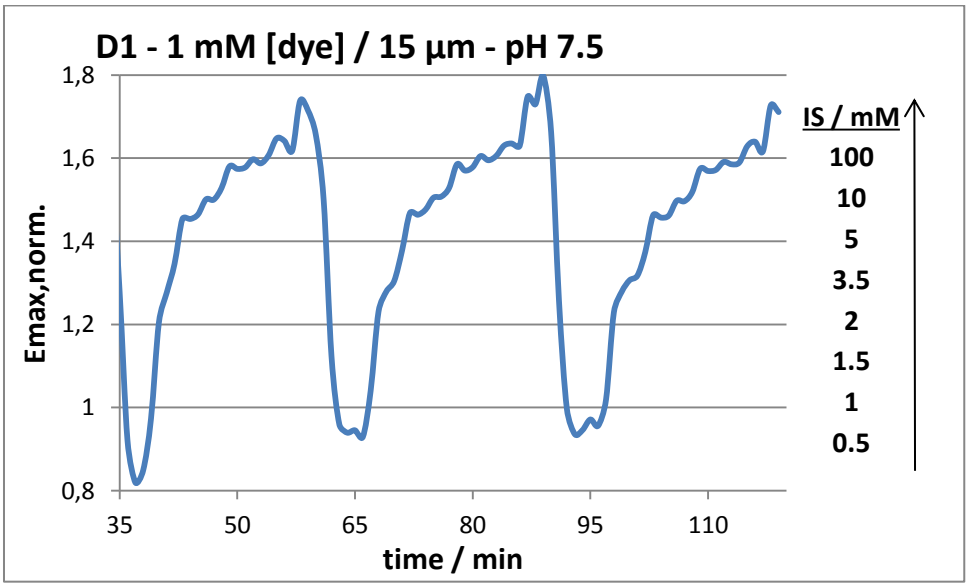
D1 - 1 mM [dye] / 15 µm - pH 7.5
Emax,norm.
1,8
1,6
1,4
1,2
1
0,8
35
50
65
80
95
110
time / min
IS / mM
100
10
5
3.5
2
1.5
1
0.5

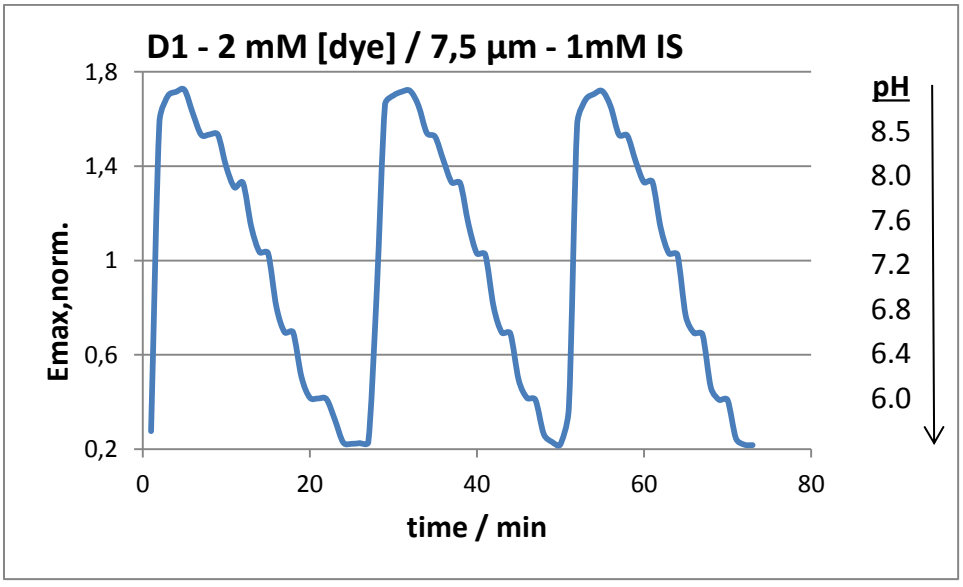
D1 - 2 mM [dye] / 7,5 µm - 1mM IS
Emax,norm.
1,8
1,4
1
0,6
0,2
0
20
40
60
80
time / min
pH
8.5
8.0
7.6
7.2
6.8
6.4
6.0

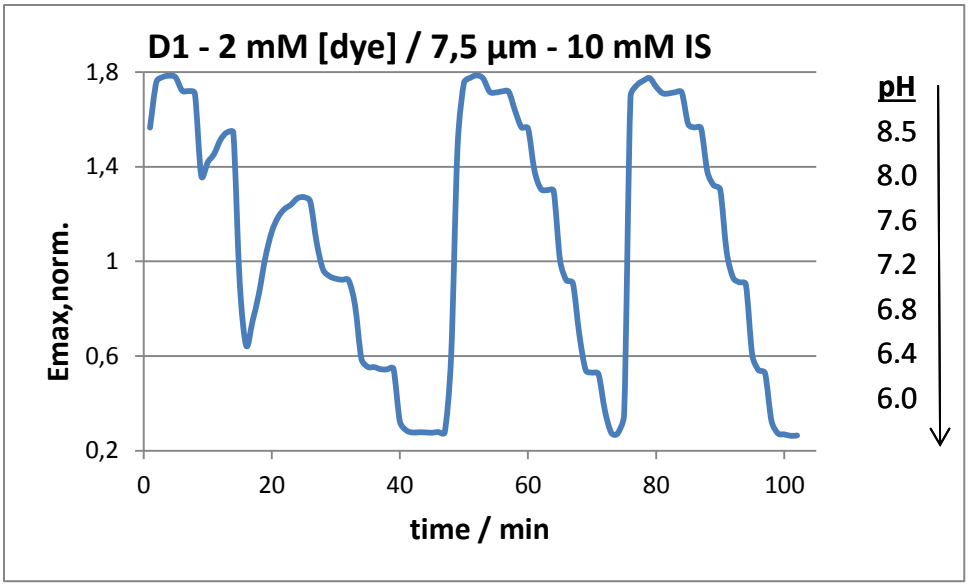
D1 - 2 mM [dye] / 7,5 µm - 10 mM IS
Emax,norm.
1,8
1,4
1
0,6
0,2
0
20
40
60
80
100
time / min
pH
8.5
8.0
7.6
7.2
6.8
6.4
6.0

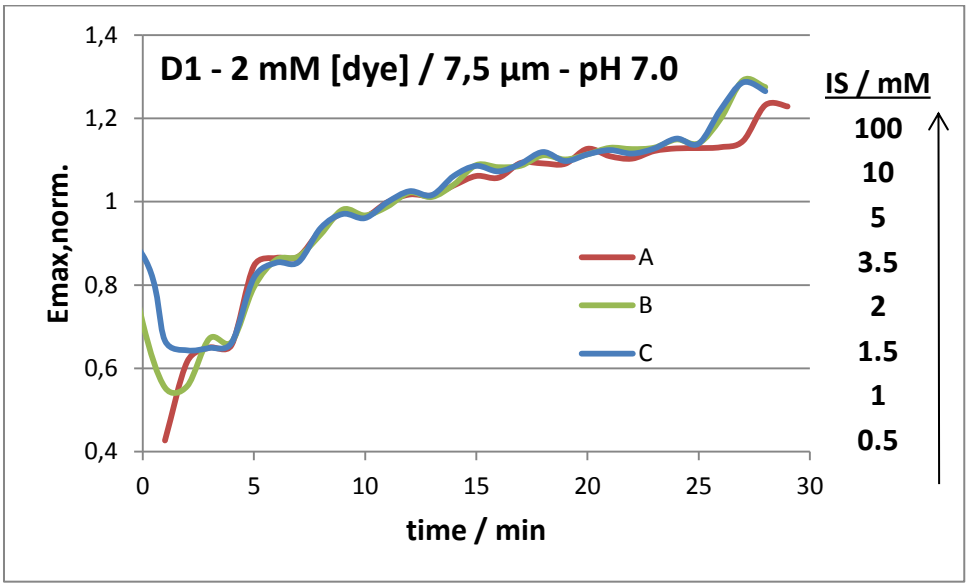
D1 - 2 mM [dye] / 7,5 µm - pH 7.0
Emax,norm.
1,4
1,2
1
0,8
0,6
0,4
0
5
10
15
20
25
30
time / min
A
B
C
IS / mM
100
10
5
3.5
2
1.5
1
0.5

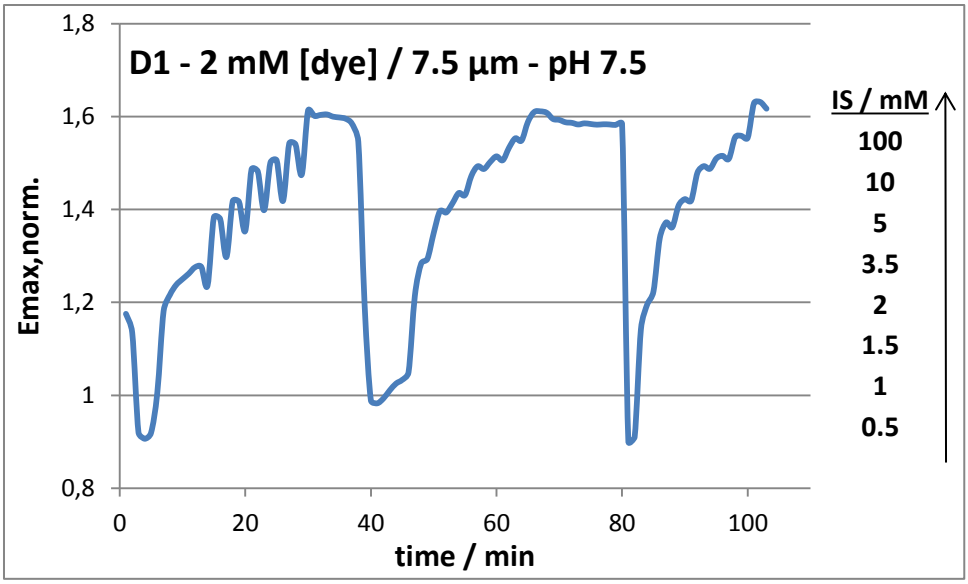

[10]

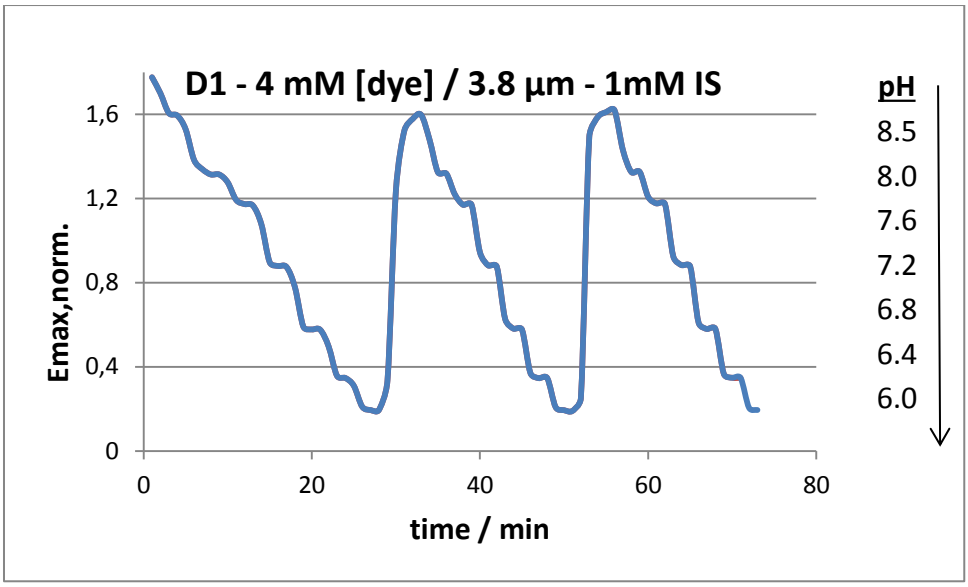

[10] Actually, the repeat determinations were not performed in a row but like it is shown for the same sensor for the measurement at pH 7.0. For clearness reasons data is presented in a row.

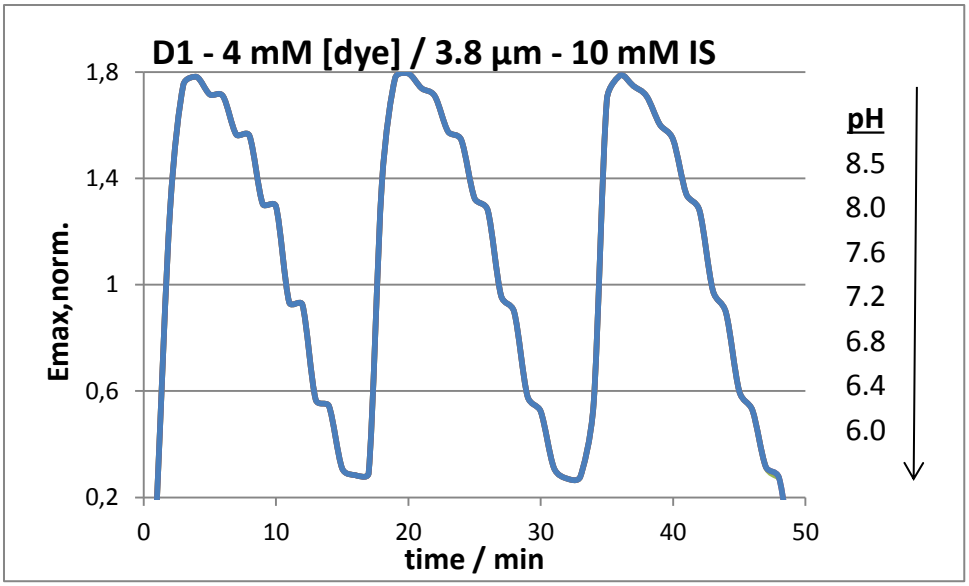
D1 - 4 mM [dye] / 3.8 µm - 10 mM IS
Emax,norm.
1,8
1,4
1
0,6
0,2
0
10
20
30
40
50
time / min
pH
8.5
8.0
7.6
7.2
6.8
6.4
6.0

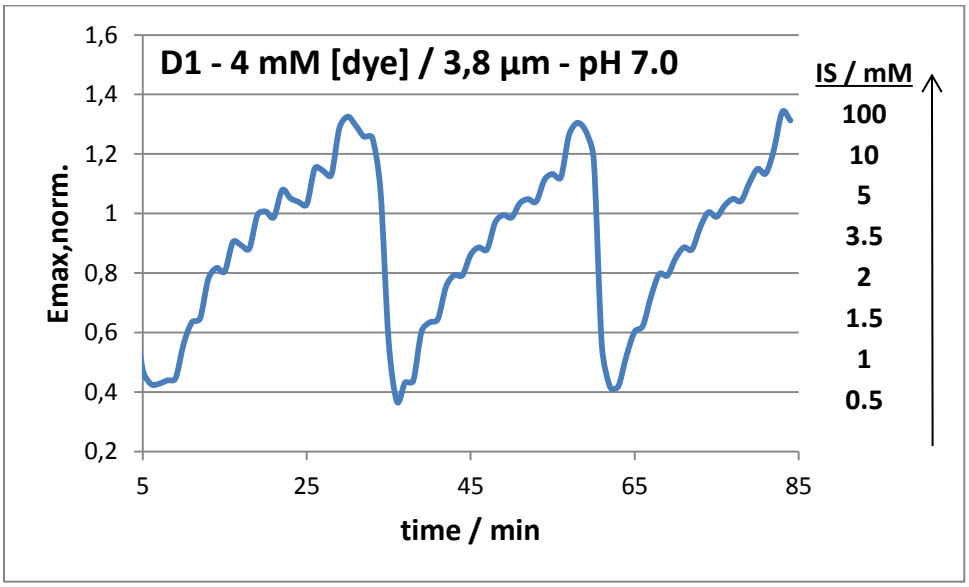
D1 - 4 mM [dye] / 3,8 µm - pH 7.0
Emax,norm.
1,6
1,4
1,2
1
0,8
0,6
0,4
0,2
5
25
45
65
85
time / min
IS / mM
100
10
5
3.5
2
1.5
1
0.5

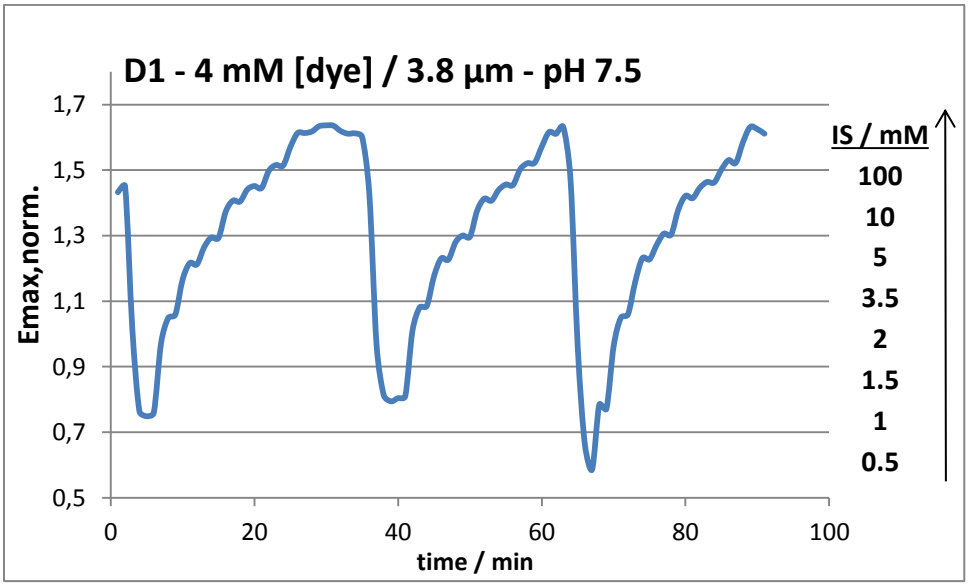
D1 - 4 mM [dye] / 3.8 µm - pH 7.5
Emax,norm.
1,7
1,5
1,3
1,1
0,9
0,7
0,5
0
20
40
60
80
100
time / min
IS / mM
100
10
5
3.5
2
1.5
1
0.5

8.1.3 Fluorescence measurements

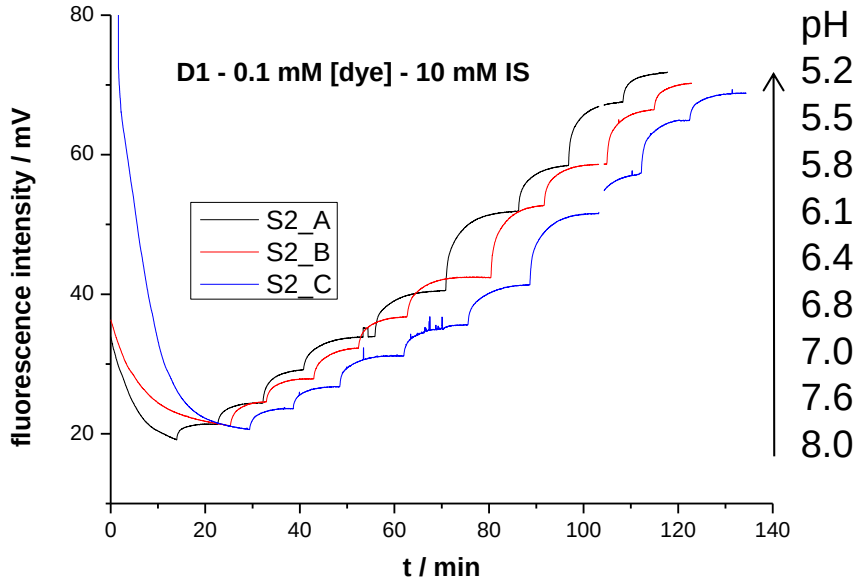

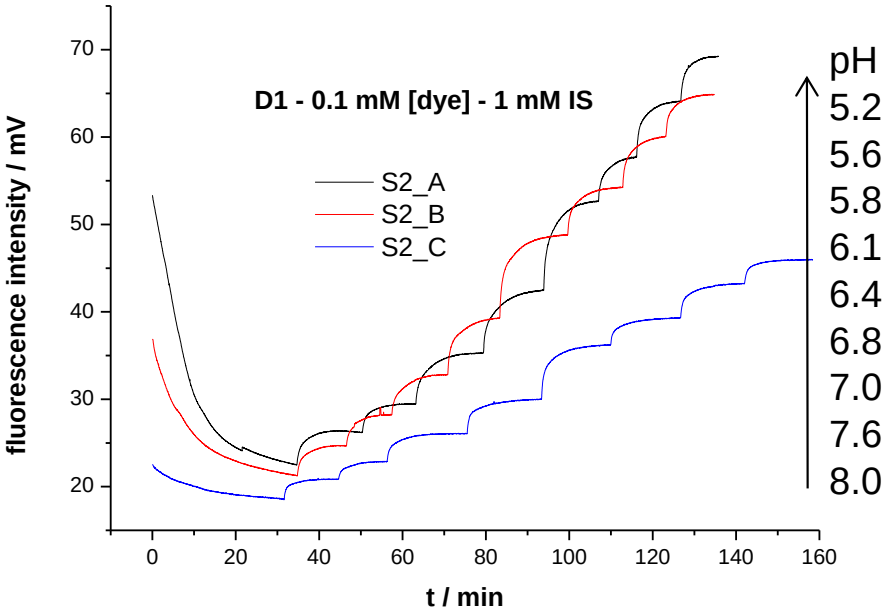

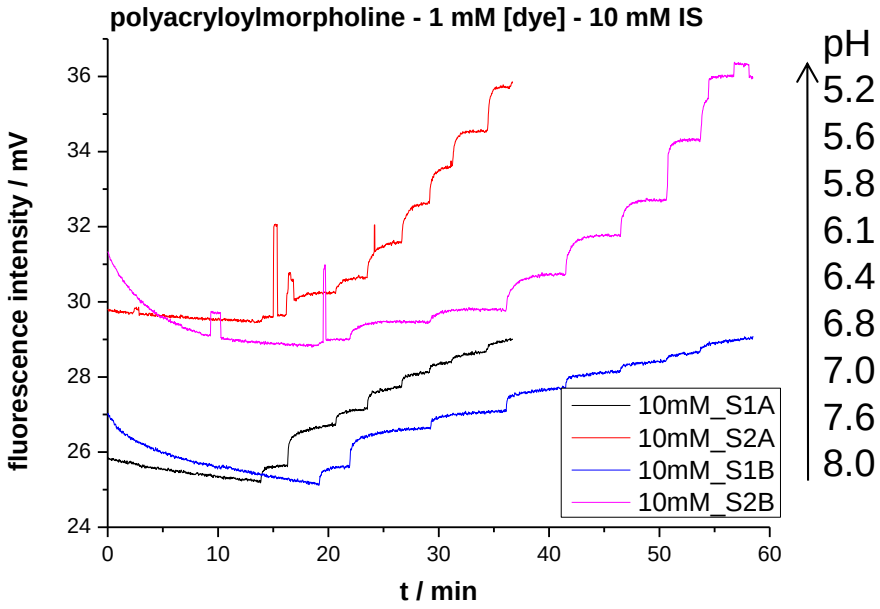
polyacryloylmorpholine - 1 mM [dye] - 10 mM IS
fluorescence intensity / mV
t / min
10mM_S1A
10mM_S2A
10mM_S1B
10mM_S2B
pH
5.2
5.6
5.8
6.1
6.4
6.8
7.0
7.6
8.0

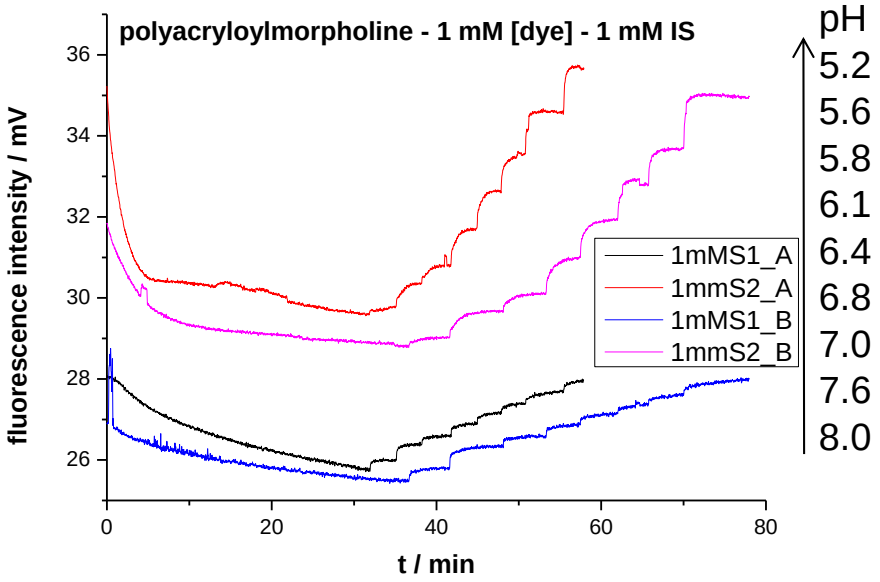
polyacryloylmorpholine - 1 mM [dye] - 1 mM IS
fluorescence intensity / mV
t / min
1mMS1_A
1mmS2_A
1mMS1_B
1mmS2_B
pH
5.2
5.6
5.8
6.1
6.4
6.8
7.0
7.6
8.0

8.1.4 Spiking solutions for the fluorescence measurements

Measurement	name	IS / mM	pH	[HA] / mM
titration at 1 mM IS	A	1,0	-[11]	2
	B	1,0	-	30
	C	1,0	-	99
titration at 10 mM IS	A	10	-	2
	B	10	-	30
	C	10	-	93
IS scanning at pH 7.0	A	12	7,02	-[12]
	B	95	7,09	-
	C	1670	7,50	-
IS scanning at pH 7.5	A	13	7,46	-
	B	96	7,52	-
	C	1673	7,88	-

8.2 Lists

8.2.1 List of chemicals

name	supplier
MOPSO	Roth, Karlsruhe, GER
TAPSO	Roth, Karlsruhe, GER
AMPSO	Roth, Karlsruhe, GER
mono-chloro-aza-BODIPY	in house synthesis
hydrogels D1, D4, D7	CardioTech Int. Inc., Wilmington, USA
4-acryloylmorpholine	Sigma-Aldrich Handels GmbH, Wien, AUT
N,N'-ethylenebisacrylamide	ABCR, Karlsruhe, GER
2-hydroxy-1-[4-(2-hydroxyethoxy)phenyl]-2-methylpropan-1-one	Sigma-Aldrich Handels GmbH, Wien, AUT
N_2 (99.999 % purity)	Air Liquide, Graz, Austria

[11] As there was no basic component weighed in, pH could not be calculated.
[12] Not given, as the pH values are the information of interest.

8.2.2 List of figures

8.2.3 List of tables